8-1961

Coulomb Excitation with Heavy Ions

Rogers Charles Ritter
University of Tennessee - Knoxville

To the Graduate Council:

I am submitting herewith a dissertation written by Rogers Charles Ritter entitled "Coulomb Excitation with Heavy Ions." I have examined the final electronic copy of this dissertation for form and content and recommend that it be accepted in partial fulfillment of the requirements for the degree of Doctor of Philosophy, with a major in Physics.

Robert W. Lide, Major Professor

We have read this dissertation and recommend its acceptance:

H. K. McGowan, Paul H. Stelson, William M. Bugy, D. A. Peasant, D. D. Lillian

Accepted for the Council:

Carolyn R. Hodges

Vice Provost and Dean of the Graduate School

(Original signatures are on file with official student records.)

33

August 2, 1961

To the Graduate Council:

I am submitting herewith a thesis written by Rogers Charles Ritter entitled "Coulomb Excitation with Heavy Ions." I recommend that it be accepted in partial fulfillment of the requirements for the degree of Doctor of Philosophy, with a major in Physics.

Robert W. Lide
Major Professor

We have read this thesis and recommend its acceptance:

H. K. McGowan

Paul H Stelson

Wm M Bugg

Dr Pearl

D. T. Lummen

Accepted for the Council:

J. E. Spivey
Dean of the Graduate School

COULOMB EXCITATION WITH HEAVY IONS

A Dissertation

Presented to

the Graduate Council of

the University of Tennessee

In Partial Fulfillment

of the Requirements for the Degree

Doctor of Philosophy

by

Rogers Charles Ritter

August 1961

ACKNOWLEDGEMENTS

It is a pleasure to acknowledge my gratitude to my research advisor, Dr. P. H. Stelson, and also to Dr. F. K. McGowan. In addition to the considerable contribution in the form of supervision and collaboration in this work, their example in research in the broader sense is appreciated. Dr. R. L. Robinson has also given welcome assistance during the course of this work.

Mrs. B. A. Denning has been particularly patient and helpful in the typing of the thesis.

The support of this research by the Oak Ridge Graduate Fellowship Program of the Oak Ridge Institute of Nuclear Studies, and by the facilities of the Physics Division of the Oak Ridge National Laboratory are primary contributions for which I am grateful.

TABLE OF CONTENTS

LIST OF TABLES

LIST OF FIGURES

FIGURE PAGE

CHAPTER I

INTRODUCTION

Coulomb excitation has been used since 1953 to provide information about nuclear structure. In this process low-lying states are excited in a target nucleus by the electrical shock from a passing charged projectile. Protons, deuterons and helium ions have been the most used projectiles in the past. Recently oxygen, nitrogen and neon have also been used in Coulomb excitation.

In the pure Coulomb excitation process only the electromagnetic interaction between the target and projectile nuclei is involved. This is a valuable property, because the dynamics of such an interaction have been accurately calculated. In contrast, analyses of nuclear force interactions are usually less accurate, as they depend on our incomplete knowledge of the nuclear force.

The electromagnetic excitation process most strongly excites the low-lying collective states in nuclei. It has been one of the foremost methods of studying collective nuclear motion. One studies the de-excitation gamma rays,[1] inelastically scattered projectiles[2] or internal conversion electrons[3] resulting from Coulomb excitation.

---

[1] See, e.g., the review paper by K. Alder, A. Bohr, T. Huus, B. Mottelson and A. Winther, Revs. Mod. Phys. 28, 432 (1956).

[2] B. Elbek and C. K. Bockelman, Phys. Rev. 105, 657 (1957).

[3] T. Huus, J. H. Bjerregard and B. Elbek, Dan. Mat. fys. Medd. 30, No. 17, (1956).

Observation of the gamma radiation is by far the most common of these methods of study, and was the one used in the present work. It can yield such information as level positions, level spins and relative parities, transition strengths, gamma ray multipolarity or multipole mixtures, and relative probabilities of various possible decay modes. This information bears on the relative importance of collective and individual particle aspects of nuclear motion in a given state, and on the general study of nuclear structure.

A nearly pure electromagnetic interaction can be achieved in nuclear bombardment, by taking advantage of the short range of the nuclear force and the relatively long range of the Coulomb force. If the projectile (kinetic) energy is kept well below the Coulomb barrier, a nuclear force interaction with the target is avoided.

At the same time, the projectile energy must be high enough for there to be a reasonable probability of electric excitation. The target nucleus must not experience such a slowly-changing electrical field from the projectile that it can readjust its motion without a transition. If it does the collision is termed "adiabatic."

The projectile and target nuclear charges, along with the projectile velocity, determine the operation between these upper and lower boundaries. In particular, heavy ions (high Z) are advantageous with light (low Z) targets. For a given target they can be used at higher energies than lighter projectiles. Thus, heavy ion projectiles can augment the operative range in Coulomb excitation.

In the work described here neon ions from 8 to 15 Mev, and nitrogen ions from 8 to 10 Mev, were used. Most of the targets were odd-A (nuclear mass number) in the range A = 47 to A = 75. Several advantages of such operation will be mentioned here. One is that oxide targets were used without the complicating oxygen reactions that accompany their use with lighter ions. Another is that it was much easier to avoid nuclear reactions with the target nuclei. Aside from these benefits there was the possibility that an unforseen effect might appear, providing an interesting adjunct to our existing knowledge of the process. This possibility was enhanced by the sporadic nature of the previously reported heavy ion Coulomb excitation work.

There were some disadvantages in using heavy ions. Stopping powers were only poorly known.* Also, target surface impurity layers in some cases resulted in greater yield errors than with light ions.

The Oak Ridge National Laboratory 5.5 Mv Van de Graaff accelerator was used in this research. Such accelerators have provided the bulk of the Coulomb excitation data in the past. Several of their features are important in this work. Among these, high energy stability, flexibility, beam position stability, and fine beam focussing are foremost.

Triply-charged ions were needed to reach 15 Mev in this Van de Graaff. But a usable amount of them was not provided by the conventional radio frequency ion source,[4] even though it was tested over a wide range

---

*See Appendix A.

[4] C. D. Moak, H. Reese and W. M. Good, Nucleonics 9, 18 (1951).

of operating conditions. Consequently, much of the work for this thesis involved the development of an improved ion source for triply-charged neon ions. This work was carried out on the ORNL Cockcroft-Walton accelerator. A PIG type (Phillips Ion Gauge) source was developed which was capable of putting 0.02 microamperes of triply-charged neon ions and about 2/3 microampere of doubly-charged neon ions at the target of the Van de Graaff. (Equivalent numbers of stripped 5^+ and 6^+ neon ions were actually obtained at the target.) Only doubly-charged nitrogen ions were available in usable quantities (defined as being enough to control the accelerator, usually greater than 0.005 microamperes).

The problem undertaken for this thesis can be stated now:

1) The development of a source of multiply-charged heavy ions suitable for use in the ORNL 5.5 Mv Van de Graaff accelerator.

2) Its use in studying, by Coulomb excitation, the low-lying states of some odd-A nuclei, primarily in the region A = 47 to A = 75.

The organization of this thesis is the following. Chapter II presents a background for the nuclear part of the research. In it the Coulomb excitation process is described, and pertinent nuclear models are briefly discussed. Chapter III is a discussion of the development of the heavy ion source. Also, some of the particular problems of operating it in the Van de Graaff are described. In Chapter IV the Coulomb excitation experimental arrangement, procedure, and gross results are given. Chapter V gives analyses of the results, in some cases interpreted in terms of a nuclear model. In Chapter VI a summary of the work is presented. Also this chapter mentions the possible usefulness of further work on the ion source, and on Coulomb excitation of the odd-A medium-light nuclei.

The history of heavy ion sources is a brief one. Jones and Zucker[5] first reported the use of an intense PIG-type discharge for this purpose. Anderson and Ehlers[6] used a pulsed PIG discharge to obtain various types of heavy ions. A number of large filament-type sources have been used for cyclotrons. These appeared to be completely unsuitable for the Van de Graaff, however. The r.f. source had been used on the ORNL 5.5 Mv Van de Graaff to produce doubly-charged neon ions.[7]

Both of the above PIG sources were in easily accessible locations. They used considerable power and pumping capacity, and had other features that were unsuitable for a Van de Graaff terminal. Also, the quantitative factors in the performance were not elaborated upon. A more general study of the PIG discharge was needed in this development.

The true PIG discharge was probably first reported by Penning[8] in 1937. Maxwell[9] had earlier (1931) used a similar geometry and magnetic field, but had included a filament. This greatly alters the characteristics. In the literature the true PIG discharge has also been called a "hollow anode" discharge and a "cold cathode" discharge. As used for an

---

[5] R. J. Jones and A. Zucker, Rev. Sci. Instr. 25, 562 (1954).

[6] C. E. Anderson and K. W. Ehlers, Rev. Sci. Instr. 27, 809 (1956).

[7] P. H. Stelson and F. K. McGowan, Nucl. Phys. 16, 92 (1960); P. H. Stelson and F. K. McGowan, Reactions Between Complex Nuclei (John Wiley and Sons, Inc., New York, London, 1960), p. 47.

[8] F. M. Penning, Physica 4, 71 (1937); F. M. Penning and J. H. A. Mobius, Physica 4, 1190 (1937).

[9] L. R. Maxwell, Rev. Sci. Instr. 2, 129 (1931).

ion source, this discharge has been discussed by Penning,[8] Backus,[10] Lorrain,[11] Kamke,[12] and many others. All of these discussions, however, only considered the hydrogen ion operation of the PIG source. In particular, the effects of multiple ionization and multiple charge exchange were missing.

The history of Coulomb excitation is more extensive. A comprehensive review of Coulomb excitation up to 1956 is given in reference 1. It will only be summarized here.

More than twenty years ago,[13] the possibility of producing nuclear excitations by electromagnetic interactions was considered. Then about ten years ago the theory of the process was developed considerably.[14] Also around 1950 a number of experimenters had suspected some such process from their reaction spectra, but the clear experimental identification of gamma rays from Coulomb excitation was not reported until 1953.[15]

---

[10] J. Backus, The Characteristics of Electrical Discharges in Magnetic Fields, (McGraw-Hill Book Company, Inc., New York, Toronto, London, 1949), p. 345.

[11] P. Lorrain, Can. J. Research, A25, 338 (1947).

[12] D. Kamke, Encyclopedia of Physics, XXXIII, (Springer-Verlag, Berlin, Gotingen, Heidelberg, 1956), p. 82.

[13] Rutherford, Chadwick and Ellis, Radiations from Radioactive Substances, (Cambridge University Press, Cambridge, England, 1930), p. 247; L. Landau, Physik Z. Sowjetunion 1, 88 (1932); V. F. Weisskopf, Phys. Rev. 53, 1018 (1938).

[14] See, e.g., K. A. Ter-Martirosyan, JETP (USSR) 22, 284 (1952) and C. J. Mullin and E. Guth, Phys. Rev. 82, 141 (1951).

[15] C. L. McClelland and C. Goodman, Phys. Rev. 91, 760 (1953); T. Huus and C. Zupancic, Dan. Mat. fys. Medd. 28, No. 1 (1953).

Since then, both the theory and experimentation have progressed rapidly. With the help of experimental stimulation,[16] the complete quantum mechanical treatment of the process has been done.[17] An important result of this is the accurate description of the angular distribution of the de-excitation gamma rays. In addition, a quantum mechanical calculation of the angular distribution of the inelastically scattered projectiles (for some special cases) was published.[18]

Experimental Coulomb excitation with heavy ions is more recent. In 1956[19] nitrogen ions in a cyclotron were used expressly for this purpose. Neon ions were used in a conventional Van de Graaff for Coulomb excitation,[7] and tandem Van de Graaff accelerators have accelerated oxygen ions up to 40 Mev for this purpose.[20] Additional work with the cyclotron has been reported[21] using neon, oxygen and nitrogen ions. Most of the work of references 7 and 19-21 has been similar to that done for this thesis.

---

[16] F. K. McGowan and P. H. Stelson, Phys. Rev. 99, 127 (1955).

[17] See, e.g., Biedenharn, McHale and Thaler, Phys. Rev. 100, 376 (1955) and K. Alder and A. Winther, Dan. Mat. fys. Medd. 29, No. 19 (1955).

[18] J. Bang, Dan. Mat. fys. Medd. 32, No. 5 (1960).

[19] D. G. Alkhazov, D. S. Andreyev, A. P. Greenberg and I. Kh. Lemberg, Nucl. Phys. 2, 65 (1956).

[20] H. E. Gove and C. Broude, Reactions Between Complex Nuclei, (John Wiley and Sons, Inc., New York, London, 1960), p. 57; B. M. Adams, D. Eccleshall and M. J. L. Yates, Reactions Between Complex Nuclei, (John Wiley and Sons, Inc., New York, London, 1960), p. 95.

[21] See, e.g., I. Kh. Lemberg, Reactions Between Complex Nuclei, (John Wiley and Sons, Inc., New York, London, 1960), p. 112; and D. G. Alkhazov, A. P. Grinberg, G. M. Gusinskii, K. I. Erokhina and I. Kh. Lemberg, Soviet Physics, JETP 37, 1086 (1960).

In a somewhat different region, linear accelerators have been used up to 200 Mev for heavy ion Coulomb excitation.[22] Heavy Nuclei were bombarded and the "multiple Coulomb excitation" process[23] was particularly of interest. Another interesting work with such high energy ions was the "Coulomb disintegration" of Li^6 projectiles.[24]

A list of nuclear structure information provided by Coulomb excitation would be very long.* Many new levels have been discovered by this process. It has determined many of their spins and lifetimes, and also the spins and lifetimes of many previously discovered levels. Possibly more than any other single nuclear process, Coulomb excitation has added to our understanding of nuclear collective motion. The information about low-lying levels in deformed nuclei applies directly to the rotational model.[25,26] Furthermore, Coulomb excitation has been foremost in

---

[22] B. Elbek, G. Igo, F. S. Stephens, Jr. and R. M. Diamond, Reactions Between Complex Nuclei, (John Wiley and Sons, Inc., New York, London, 1960), p. 102.

[23] K. Alder and A. Winther, Dan. Mat. fys. Medd. 32, No. 8 (1960).

[24] C. E. Anderson, Reactions Between Complex Nuclei, (John Wiley and Sons, Inc., New York, London, 1960), p. 67; R. L. Gluckstern and G. Breit, Reactions Between Complex Nuclei, (John Wiley and Sons, Inc., New York, London, 1960), p. 77.

* See, e.g., the long compilation of reference 1, p. 504.

[25] A. Bohr, Dan. Mat. fys. Medd. 26, No. 14 (1952); A. Bohr and B. Mottelson, Dan. Mat. fys. Medd. 27, No. 16 (1953).

[26] S. A. Moszkowski, Encyclopedia of Physics, XXXIX, (Springer-Verlag, Berlin, Gotingen, Heidelberg, 1957), p. 481.

nuclear vibration studies.[1,27] Coulomb excitation data has also been important in testing the Nilsson model,[28] which deals with the intrinsic structure of deformed nuclei.

But for odd-A nuclei in regions where the deformation is lacking, or questionable, there has been no accurate theoretical description of the collective aspects of the motion. Coulomb excitation has provided some data on these nuclei,[1,20,21,29] but a more intense study is needed.

Recent theoretical developments related to the theory of superconductivity have presented new approaches to the study of nuclear motion in general, and to the "difficult regions" in particular.* They provide added interest in the nuclei which are examined in this thesis.

---

[27] See, e.g., P. H. Stelson, Proceedings of the International Conference on Nuclear Structure, Kingston, Canada, (University of Toronto Press, Toronto, 1960), p. 787; and P. H. Stelson and F. K. McGowan, Phys. Rev. 121, 209 (1961).

[28] S. G. Nilsson, Dan. Mat. fys. Medd. 29, No. 16 (1955).

[29] See, e.g., G. M. Temmer and N. P. Heydenberg, Phys. Rev. 96, 426 (1954).

* A short description of the new models is given in Chapter II.

CHAPTER II

COULOMB EXCITATION AND NUCLEAR STRUCTURE

This chapter presents the properties of Coulomb excitation and nuclear models which are most pertinent to the present research. Section I provides information on the Coulomb excitation process. A summary of the classical derivation of the cross section is given. Also the results of angular distribution calculations are discussed. Section II describes several nuclear models which provide a basis for interpreting the nuclear information which is obtained. The nuclear shell model, the "unified model," and the pairing correlation theory are considered. Most of the discussion is about the latter two, which are not as well known as the shell model.

I. COULOMB EXCITATION

Criteria for the classical theory. The classical theory of Coulomb excitation provides an accurate cross section for the case of slow, heavy projectiles.[1] It is suitable for all of the calculations in this thesis. Quantitatively, the criterion is given by the size of the "Sommerfeld number"

$$\eta \equiv \frac{Z_1 Z_2 e^2}{\hbar v} , \qquad (1)$$

where $Z_1 e$ and $Z_2 e$ are the nuclear charges of the projectile and the

---

[1] K. Alder, A. Bohr, T. Huus, B. Mottelson, and A. Winther, Revs. Mod. Phys. 28, 432 (1956).

target, respectively, and v is the incident velocity of the projectile. The classical cross section is accurate when $\eta \gg 1$ (about 8 or greater). This follows from the fact that

$$\eta = \frac{a}{\lambda\!\!\!^{-}} \ , \tag{2}$$

where a is half the classical distance of closest approach for a head-on collision, and $\lambda\!\!\!^{-}$ is the de Broglie wavelength of the projectile. The formula for a is

$$a \equiv \frac{Z_1 Z_2 e^2}{\mu v^2} \ . \tag{3}$$

Here μ is the reduced mass of the projectile and the target nucleus. Only low-lying states are of interest here. In this case the classical hyperbolic projectile orbit is only slightly altered by the excitation of the target nucleus. Figure 1 illustrates such an orbit, for an infinitely massive target nucleus. The nonspherical target and projectile nuclei illustrate explicitly how the charge distributions can exert torques.

The classical cross section.[1] The classical differential cross section for Coulomb excitation can be written

$$d\sigma = P d\sigma_R \ , \tag{4}$$

where P is the probability of excitation during the scattering event, and the classical (Rutherford) differential scattering cross section is

$$d\sigma_R = \frac{a^2}{4} \frac{1}{\sin^4(\theta/2)} \, d\Omega \ . \tag{5}$$

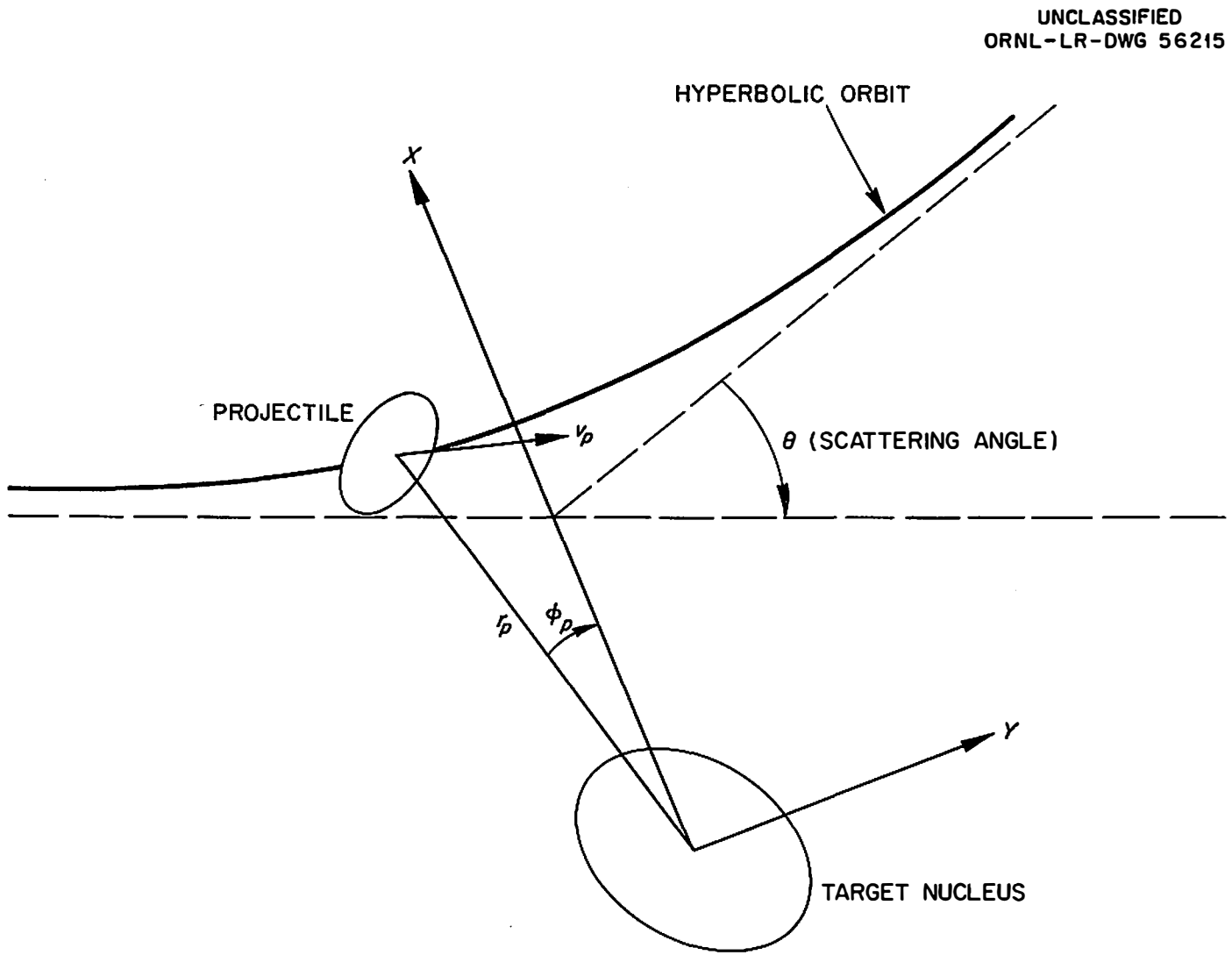

Fig. 1. Classical Picture of the Particle Orbit in the Coulomb Field of the Nucleus.

Here Θ is the scattering angle in the center-of-mass system. P can also depend on Θ.

The probability, P, of excitation of the target nucleus by a projectile scattered into the solid angle $d\Omega$ is written

$$P = \frac{1}{(2I_i + 1)} \sum_{M_i M_f} | b_{if} |^2 , \tag{6}$$

in terms of the amplitudes b_{if} for a transition of the target nucleus from an initial state i to a final state f. Here only unoriented nuclei are considered. Therefore the square of the amplitude is summed over all final magnetic substates M_f, and averaged over all initial substates M_i.

In all of the cases to be considered here, P is much smaller than unity. Thus first order perturbation theory is accurate[2] and one writes b_{if} in the conventional way

$$b_{if} = \frac{1}{i\hbar} \int_{-\infty}^{\infty} < f \mid H(t) \mid i > e^{i \frac{\Delta E t}{\hbar}} dt . \tag{7}$$

H(t) is the electromagnetic interaction term of the hamiltonian.

Only the electric interaction is significant in the majority of cases because of the slowness of the projectiles. For example, the M1 cross section in a typical case was calculated to be less than 10^{-5} of

---

[2] K. Alder and A. Winther, Dan. Mat. fys. Medd. 32, No. 8 (1960).

the E2 cross section. Furthermore E1 and E3 excitations are rare in the nuclear region of interest. It is nearly certain that only E2 excitation was involved in the present work.

The form of the electric interaction is the (quasi-) static one

$$H_E(t) = \int \rho_n(\vec{r})\ \phi\ (\vec{r},t)\ d\tau\ , \tag{8}$$

where $\rho_n(\vec{r})$ is the charge density in the nucleus which is being excited, and ϕ is the potential at the point $\vec{r}$ due to the projectile.

ϕ is written as a conventional multipole expansion and ρ is written in terms of point charge protons. These are inserted into (8), and then into (7). This gives the transition amplitude in a usable form. Using it in (4), (5) and (6) one obtains the result for the λ multipole component of the electric excitation differential cross section

$$d\sigma_{E\lambda} = \frac{4\pi^2 Z_1^2 e^2}{\hbar^2}\, a^2\, \frac{B(E\lambda)}{(2\lambda+1)^3}\, \frac{\sum_\mu |\ S_{E\lambda,\mu}\ |^2}{\sin^4(\theta/2)}\, d\Omega\ . \tag{9}$$

$S_{E\lambda,\mu}$ is an "orbital integral" in which μ is the projection quantum number of the electric multipole operator. $S_{E\lambda,\mu}$ contains the angular dependence of the excitation probability. $B(E\lambda)$ is the reduced transition probability

$$B(E\lambda; I_i \to I_f) \equiv \sum_{M_f,\mu} |\langle I_i M_i | \textstyle\sum_k e_k r_k^\lambda\ Y_\lambda^\mu(\theta_k,\phi_k) | I_f M_f\rangle|^2$$

$$= \frac{1}{2I_i+1}\, |\langle I_i || \textstyle\sum_k e_k r_k^\lambda\, Y_\lambda^0\ (\theta_k,\phi_k) || I_f\rangle|^2\ , \tag{10}$$

of the Eλ multipole operator. Here e_k and r_k are the charge and radial position of the k^{th} proton and Y_λ^μ is a spherical surface harmonic in which the angular position of the k^{th} nucleon is the argument. The final form uses the fact that the geometrical (substate) dependence of the matrix element is contained in a vector coupling coefficient (the Wigner-Eckart Theorem[3]).

An excitation of order λ is subject to the same parity and angular momentum selection rules as a radiative transition of this order. In particular, E2 excitation can only occur between like-parity states whose spins can, together with 2, form a triangle.

To complete the differential cross section calculation the orbital integral must be evaluated. This can be done in a parametric coordinate system. From reference 1, the result for E2 excitation is:

$$d\sigma_{E2} = \left(\frac{Z_1 e}{\hbar v} \right)^2 \frac{B(E2)}{a^2} \, df_{E2}(\Theta,\xi) \, , \tag{11}$$

where $df_{E2}(\Theta,\xi)$ can be called a "differential excitation function," which depends on the scattering angle Θ, and on the important "adiabatic parameter" ξ:

$$\xi \approx \frac{Z_1 Z_2 e^2}{\hbar v_i} \cdot \frac{\Delta E}{2E} = \eta_i \frac{\Delta E}{2E} \, . \tag{12}$$

---

[3] M. E. Rose, Elementary Theory of Angular Momentum, (John Wiley and Sons, Inc., New York, 1957) p. 85.

Here η_i is the Sommerfeld number for the incident velocity v_i. Commonly "symmetrized" forms,

$$\xi = \eta_i - \eta_f \text{ , and } a = \frac{Z_1 Z_2 e^2}{\mu v_i v_f} \tag{13}$$

are used, which more correctly accounts for the energy exchange in the collision. It can be shown that[1]

$$\epsilon\xi \approx \frac{\text{collision time}}{\text{nuclear period}} \text{ ,} \tag{14}$$

where ϵ is the orbit eccentricity

$$\epsilon = \frac{1}{\sin (\theta/2)} \text{ .} \tag{15}$$

The total cross section is of interest in this thesis. For this, (11) is integrated over θ with the result:

$$\sigma_{E2} = \left(\frac{Z_1 e}{\hbar v_i} \right)^2 \frac{B(E2)}{a^2} f_{E2}(\xi) \text{ .} \tag{16}$$

Here $f_{E2}(\xi)$ is the "excitation function" and is plotted in Figure 2. For ξ greater than about 0.8, $f(\xi)$ decreases rapidly. This is the main factor in the energy dependence of the cross section. The quantum mechanical calculation gives the same form for the cross section, but the excitation function f_{E2} depends on η_i. When $\eta_i = \infty$, the two results agree.

Equation (16) is the basic one for interpreting measured Coulomb excitation yields in terms of the B(E2) values. In Chapter IV, equation (16) is given in numerical form and is incorporated into the thick target yield formula.

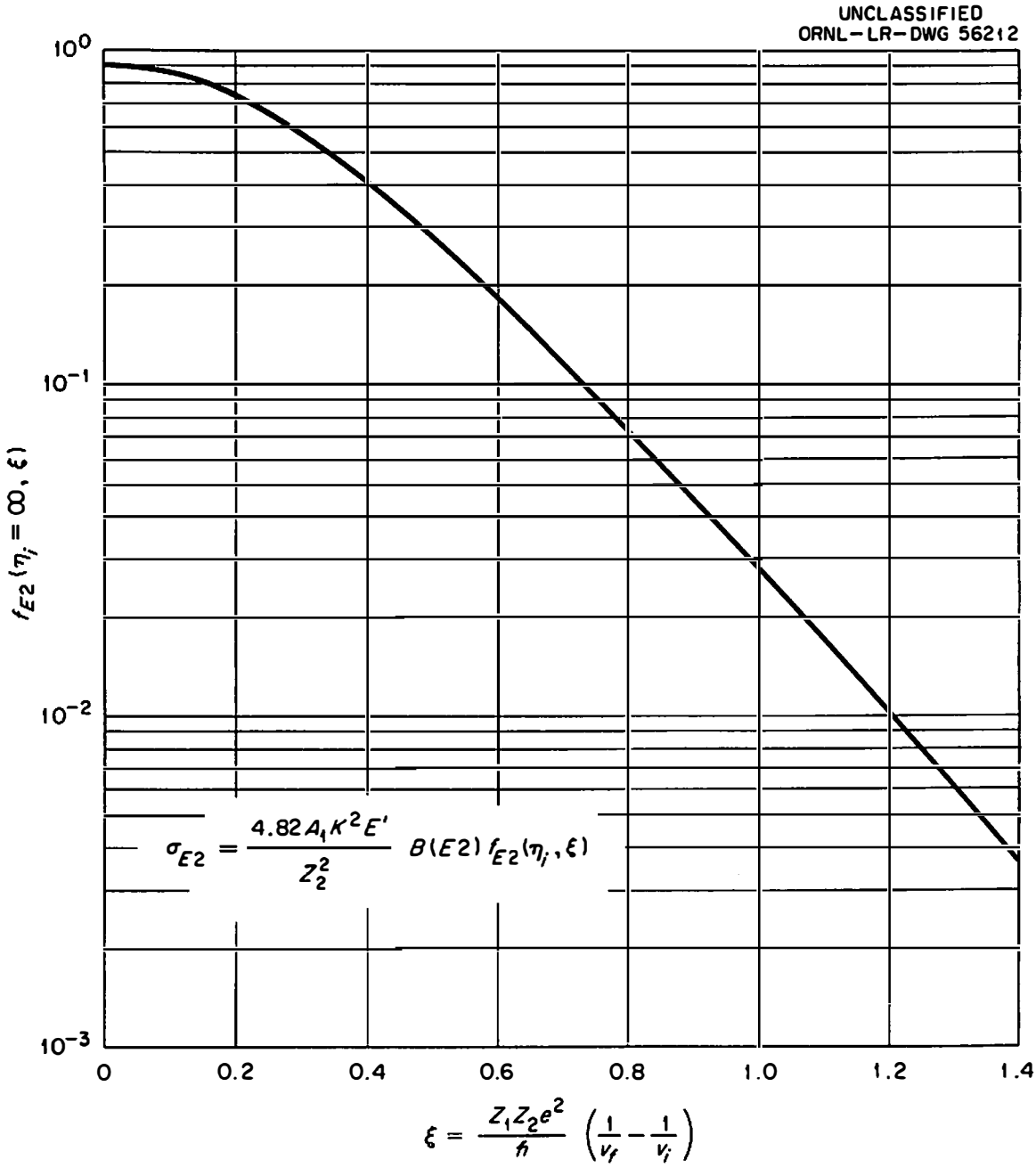

Fig. 2. E2 Coulomb Excitation Function for "Classical" Projectiles ($\eta_i = \infty$).

Angular distribution of the de-excitation gamma rays. The semi-classical calculation of the gamma ray angular distribution is not always accurate.[1,4] As a result, the more difficult quantum mechanical calculations have been made.[1,5] However, in the cases considered here, the classical limit is accurate, and has been used.

What is called the angular distribution of the de-excitation gamma rays is actually a correlation with the incident direction of the projectiles. This is very similar to the type of correlation in which the first of two cascade gamma rays provides an axis of quantization with respect to which the angular distribution of the second has meaning. In fact, the multipolarity of the Coulomb excitation plays the same role as the multipolarity of the first gamma ray of a two-gamma-ray cascade. Figure 3 depicts this analogy. The situation of correlated gamma rays has been well studied theoretically[6] and experimentally.

One can consider the excitation process as one that can preferentially populate certain magnetic sublevels of the excited nucleus, according to the multipolarity of the excitation process. Conveniently, the beam direction can be taken as the quantization axis for the substates.

---

[4] F. K. McGowan and P. H. Stelson, Phys. Rev. 99, 127 (1955).

[5] See, e.g., L. C. Biedenharn and M. E. Rose, ORNL report 1789 (1954); Breit, Ebel and Russell, Phys. Rev. 101, 1504 (1956).

[6] See, e.g., L. C. Biedenharn and M. E. Rose, Revs. Mod. Phys. 25, 729 (1953); L. C. Biedenharn, Nuclear Spectroscopy, B (Academic Press, New York and London, 1960), p. 732.

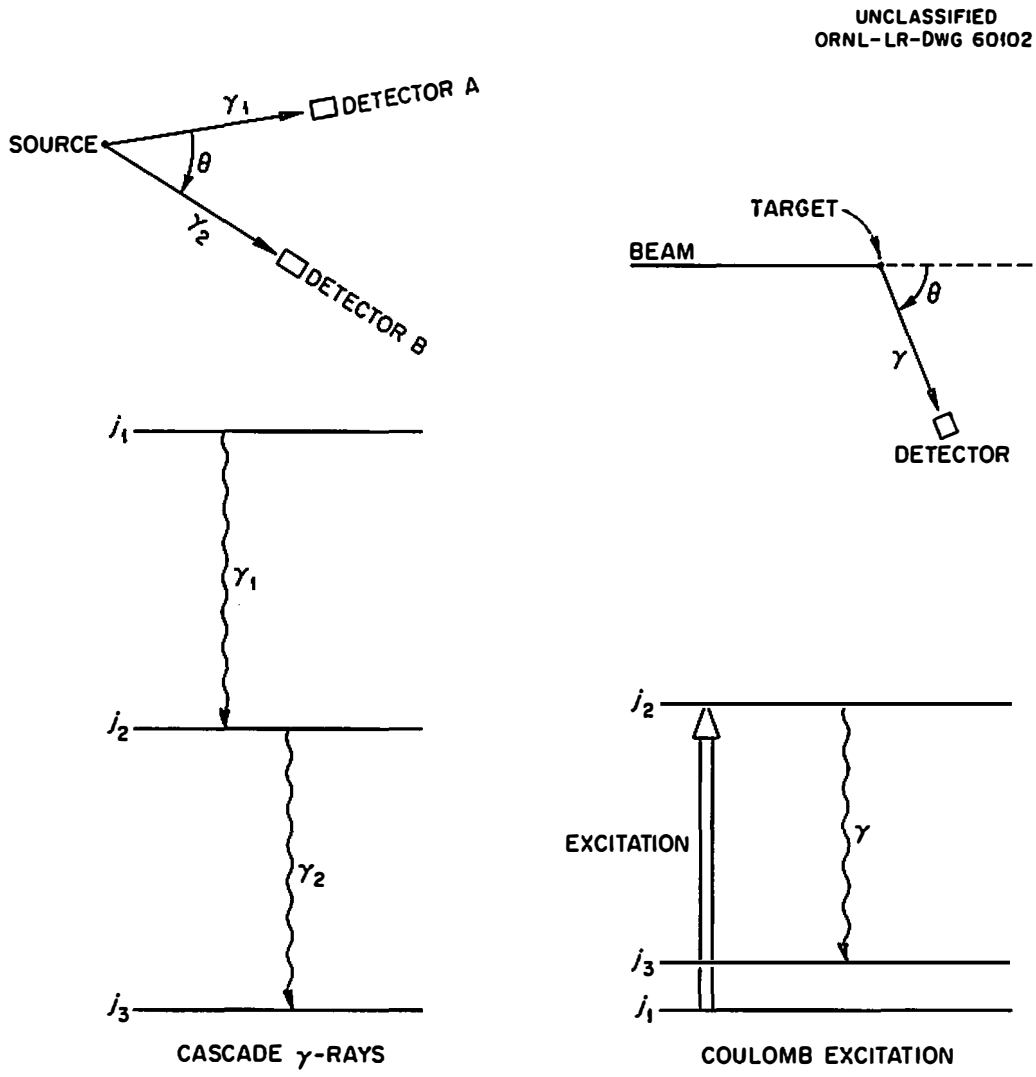

Fig. 3. Analogy Between Cascade γ-Ray and Coulomb Excitation Angular Distributions.

The weighted sum of the radiation patterns of the various sublevel de-excitations (which are not measurably separated in energy) gives the measured angular distribution.

Conventionally, measured and calculated angular distributions are written as series of even order Legendre polynomials. Theoretically, the term coefficients have values depending on all of the level spins and gamma ray multipolarities involved. In the use of this, the coefficients of experimental distributions are statistically determined from the data. Then, for unmixed transitions (those in which only one multipole is involved in each transition), the level spins and gamma ray multipolarities are in principle unambiguously determined by comparing the experimental coefficients with the theoretical ones. Even in more general cases this is sometimes possible, as will be shown.

The cascade gamma ray distribution is written

$$W(\Theta) = \sum_{\nu} A_{\nu} P_{\nu} (\cos \Theta), \qquad (17)$$

where Θ is the angle between the first and second gamma rays.

In the case of E2 Coulomb excitation one must write the distribution

$$W(\Theta) = 1 + a_2 A_2 P_2 (\cos \Theta) + a_4 A_4 P_4 (\cos \Theta) , \qquad (18)$$

where A_2 and A_4 are the same as above, and have been tabulated many places (see, e.g. reference 6). However, a_2 and a_4 are "particle parameters" which depend upon the excitation parameter ξ and η_i. Figure 4 shows the classical theoretical value of a_2 vs. ξ, for $\eta_i = \infty$.

One of the especially useful features of Coulomb excitation angular distributions is that the excitation of a given level is unmixed,

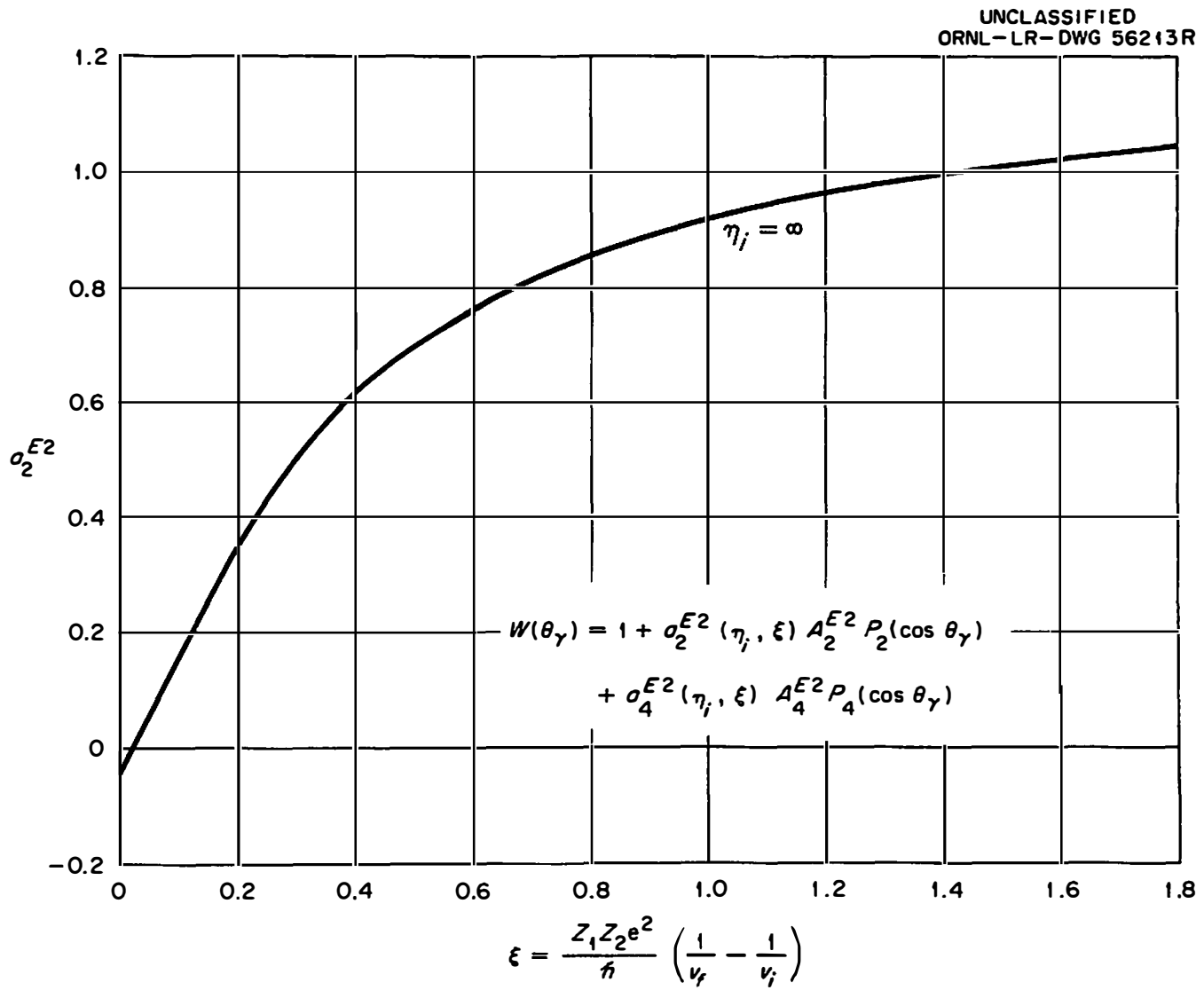

Fig. 4. Particle Parameter for γ-Ray Angular Distributions Following E2 Coulomb Excitation.

i.e., is E2 (in the cases considered here). In general, the selection rules permitting, the de-excitation gamma rays can be mixed E2 and M1 (or conceivably other mixtures if the decay is not back to the ground state). In such cases A_2 and A_4 are functions of the spins, the multipolarities, and the E2/M1 amplitude ratio, called δ.[6] This limits the number of cases in which unique spin assignments can be obtained. Several such cases, however, appeared in this research, and will be taken up in Chapter V. Also, in that chapter, the correction for finite detector size, and the attenuation by extranuclear fields, will be considered.

II. NUCLEAR MODELS

In approximately the last decade a great deal of progress has been made in the study of nuclear models for describing the low energy aspects of nuclear structure. In particular, the nuclear shell model, the unified model, and the nuclear pairing correlation theory have led to an increased understanding of many of the nuclear properties of interest here. A number of clever and useful hybrids of these models, with special applications, have also been developed. But many nuclei, e.g. the medium-light nuclei, are still difficult to represent by any model.

The current models of nuclear structure are able to consider three important low-energy effects of the nuclear force. The main part of the interaction is represented by a static, spherical, self-consistent

potential well,[7] in which each nucleon moves independently. In addition to this, long-range and short-range residual effects of the interaction are considered. The long-range residual interactions are responsible for certain coherent nucleon motions which result in non-spherical surface deformations, either permanent or vibratory. Somewhat opposing this is the short-range part of the residual interaction. It gives rise to a "pairing effect" which favors spherical symmetry.

The historical development of the models represents successive efforts to accommodate these essential features. Following the shell model, the unified model[8,9] incorporated a non-spherical part of the nucleon interaction into the self-consistent field. The well was assumed to be time-dependent, in that it could either rotate or vibrate. Some of the collective nuclear properties, such as enhanced quadrupole moments, enhanced transition strengths, and rotational spectra, of certain nuclei were explained. In addition Nilsson,[10] using a deformed

---

[7]See, e.g. M. G. Mayer and J. H. Jensen, Elementary Theory of Nuclear Shell Structure, (John Wiley and Sons, Inc., New York, 1955) p. 105; and J. P. Elliot and A. M. Lane, Encyclopedia of Physics XXXIX (Springer-Verlag, Berlin, Gottingen, Heidelberg, 1957) p. 241.

[8]A. Bohr, Dan. Mat. fys. Medd. 26, No. 14 (1952); A. Bohr and B. Mottelson, Dan. Mat. fys. Medd. 27, No. 16 (1953).

[9]S. A. Moszkowski, Encyclopedia of Physics, XXXIX, (Springer-Verlag, Berlin, Gottingen, Heidelberg, 1957) p. 476.

[10]S. G. Nilsson, Dan. Mat. fys. Medd., 29, No. 16 (1955).

diffuse-edge well, introduced a model which is able to explain the individual-particle spectra in many highly-deformed odd-A nuclei. The main successes of these models were achieved without the explicit consideration of pairing effects.

Racah[11] introduced the seniority concept into the shell model, in an effort to explain some of the observed pairing effects. The decreased binding energy of the last nucleon in odd-A nuclei, over the average in neighboring even-A nuclei, had been observed for some time. For example, it had been considered in the semi-empirical mass formula.[12] But a mathematical way to even approximately treat the pairing effect among many nucleons has only recently been developed.

The theory of superconductivity of metals[13] provided the technique for a many-body treatment of the pairing effect. After its introduction in that field, the analogy and possible application to nuclear structure was soon suggested.[14] By now a number of additional authors have contributed to the formalism which is used for treating this aspect of

---

[11] See, e.g., G. Racah, Proceedings of the Rehovoth Conference on Nuclear Structure, (North-Holland Publishing Company, Amsterdam, 1958) p. 155; also see reference 7.

[12] See, e.g., Mayer and Jensen, reference 7.

[13] J. Bardeen, L. N. Cooper, and J. K. Schrieffer, Phys. Rev. 108, 1175 (1957).

[14] A. Bohr, B. Mottelson, and D. Pines, Phys. Rev. 110, 936 (1958); A. Bohr, Comptes Rendus du Congres International de Physique Nucleaire, (Dunod, Paris, 1959) p. 203.

nuclear structure.[15,16,17] One of the best known successes of the theory is the prediction, in even-even nuclei, of an energy gap in the intrinsic states, of about 1 to 3 Mev above the ground state. This is in agreement with experiment.

The following three sub-sections discuss a recently broadened explanation of nuclear collective motion, the pairing correlation theory, and some aspects of the unified model.

Nuclear collective motion. One interpretation[18] of nuclear collective motion assumes that its main features depend on two somewhat opposing types of nucleon correlations. The first is the tendency of a given nucleon to adjust its orbit to the self-consistent field of all the other nucleons. This has been called the "aligned coupling" scheme.[18,19] For example, in the doubly-magic nucleus Pb^{208}, the field and the nucleon density distribution are approximately spherical. If one nucleon is removed, or added, its (shell-model) density

---

[15] See, e.g., N. N. Bogolyubov, JETP, USSR 34, 58 and 73 (1958); N. N. Bogolyubov, Nuovo Cimento, 7, 794 (1958); and J. G. Valatin, Nuovo Cimento, 7, 843 (1958).

[16] S. T. Belyaev, Dan. Mat. fys. Medd., 31, No. 11 (1959).

[17] L. S. Kisslinger and R. A. Sorensen, Dan. Mat. fys. Medd., 32, No. 9 (1960).

[18] See, e.g., the review by B. Mottelson, Proceedings of the International Conference on Nuclear Structure, Kingston, Canada (University of Toronto Press, Toronto, 1960) p. 525.

[19] B. R. Mottelson, The Many Body Problem, (John Wiley and Sons, Inc., New York, 1959) p. 283.

distribution is removed from or added to that of the remaining nucleons. This is predominantly at certain regions of the nucleus, and the field is thereby slightly deformed. The removal or addition of still more nucleons tends to increase the aligning field and the nuclear shape distortion.

The short range effect of the residual force, on the other hand, favors spherical symmetry. The attractive short range part of the residual force contributes primarily to pairing effects. (More than two like nucleons cannot be very close together because of the Pauli principle.) The optimum correlation (energetically favored) is with nucleons paired in orbits with a total spin of zero. It is believed, for example, that the ground states are spin zero for all known even-even nuclei.[20]

Thus a nucleon pair couples to spin zero and has a spherical density distribution as its optimum configuration. There is a coherent effect among pairs outside closed shells which is in general only partly achieved. In a very deformed field, the pairing correlations can be quite poor.

Which of the two types of correlation will dominate in a given nucleus depends roughly on the number of nucleons, n, outside closed shells. The gain in binding energy due to the two types of correlations, (for n $\ll$ the maximum number of particles in the shell) is given approximately as[18]

---

[20]Mayer and Jensen, reference 7, p. 65.

$$\text{B.E.} \sim n\Delta \tag{19}$$

for the pairing effect, and

$$\text{B.E.} \sim 1/2[n(n-1)F] \, , \tag{20}$$

for the aligning effect. Δ is one-half the binding energy per pair, and F is the strength of the aligned field produced by one nucleon. With increasing n, (20) becomes dominant, and for large enough n the nucleus is permanently deformed.

In spherical nuclei, where there are relatively few particles outside closed shells and the pairing scheme dominates, collective motion can still exist. These nuclei are of particular interest here, and a microscopic description[18] of that effect will be given.

Neglecting the aligning effect, each nucleon pair would have a spherical density distribution. For each pair of orbits there would be small time-dependent fluctuations which would, however, average to zero deviation from spherical symmetry. But during a fluctuation the temporary non-spherical distribution, considering now the long range part of the force, is experienced by other pairs. These tend to correlate their fluctuations to this field because of the aligning effect, and thus in turn act back on the first pair. The net effect is that the fluctuations are increased in size and they are slowed from the characteristic frequency corresponding to the binding energy ($\sim \frac{\Delta}{\hbar}$). These slower, larger fluctuations are the collective nuclear vibrations.

For nuclei which have large permanent deformations, the pairing effect is less prominent, but it is not absent. A number of collective

effects have been satisfactorily treated by the unified model, without considering pairing correlations. But certain aspects of the motion, particularly the experimental values for the rotational moments of inertia, were not explained without assuming significant residual interactions.[21] Recently, the inclusion of pairing correlations in the calculation[16,22] has given good agreement with experimental values for the moment of inertia. A number of other collective properties of highly deformed nuclei are known, but they will be taken up under the unified model.

Vibration effects were also studied before the development of the pairing correlation theory. These will also be discussed with the unified model.

The pairing correlation theory. Two applications of the pairing correlation theory will be considered here. The one by Belyaev[16] uses some idealized assumptions and is fairly general. Some of the experimental facts which the model predicts are:[16] "(1) the stability of the spherical shape of nuclei near the closed shells; (2) the sharp transition between spherical and deformed nuclei; (3) the significant reduction of the moment of inertia from the value for rigid rotation; and (4) the existence of low-energy vibrations in spherical nuclei near

---

[21]A. Bohr and B. Mottelson, Dan. Mat. fys. Medd. 30, No. 1 (1955).

[22]See, e.g., A. B. Migdal, JETP, USSR, 37, 249 (1959) and Nucl. Phys. 13, 655 (1959).

the bound of instability." The model also predicts the existence of the energy gap and the observed increase in single-particle level density just above the gap.

The model of Kisslinger and Sorensen,[17*] on the other hand, has given specific results for a number of nuclei. However, it has thus far been restricted primarily to single-closed-shell nuclei (S.C.S). It thus avoids consideration of the short range neutron-proton interaction, which is a difficult problem. Furthermore, in S.C.S. nuclei the pairing force is generally dominant enough that the long range part of the residual interaction can be treated as a perturbation.

An abbreviated description of the technique for applying the pairing correlation theory is as follows.[23] A transformation is made from the real pair-correlated particles to non-interacting "quasi-particles" which can be treated as independent particles via the shell model. A significant aspect of the transformation is the particular form assumed for the "pairing force." The pairing force is assumed to act only between particles in conjugate states $| j,m >$, $| j,-m >$. For the nucleon pairs (1, 2) and (3, 4) the pairing interaction is written (in terms of only the magnetic substates) as[14]

$$< m_1,m_2 \mid V \mid m_3,m_4 > = - G \, \delta_{m_1+m_2,0} \, \delta_{m_3+m_4,0} \qquad (21)$$

---

*This will be referred to here as the K.S. model.

[23]An application of this theory without considering the long range residual force was given by N. K. Glendenning, Phys. Rev. 119, 213 (1960).

where G is a constant. This simplified interaction, although it is probably not the most accurate that can be devised to represent the short range force, is one that can be used in the theory.

To supply the basic set of levels to which the theory is applied, a single-particle well is approximated in the best way possible for each set of S.C.S. nuclei. For example, the single-particle spectrum of Pb^{207} describes the neutron hole well for the lead isotopes. With the use of this well for the other isotopes, the effect of a changing A on the well is ignored, but at least the effect on the well of particle correlations is minimized.

The spectrum of the single-particle well is used to find the quasi-particle levels (e.g. for the other lead isotopes) by means of the "Bardeen Solutions."[17] In these one finds for each isotope, the "chemical potential," λ, and the "energy gap," Δ, as a simultaneous solution of the equations

$$\frac{G}{2} \sum_j \frac{\Omega_j}{[\epsilon_j-\lambda)^2 + \Delta^2]^{1/2}} = 1 \qquad (22)$$

and

$$\sum_j \Omega_j \left\{1 - \frac{\epsilon_j - \lambda}{[(\epsilon_j-\lambda)^2 + \Delta^2]^{1/2}}\right\} = N . \qquad (23)$$

The sum over j is over the single-particle states, ϵ_j, which were obtained from the well. G is the strength of the pairing force (assumed to be about 19/A Mev for the Ni isotopes and for the 28 neutron S.C.S.

nuclei) and N is the number of nucleons occupying the levels outside the closed shells (e.g. 5 in Ni^{61}). Ω_j is the pair degeneracy, $(\frac{2j+1}{2})$, of the j level.

The λ and Δ obtained, for a given nucleus, are used to find the quasi-particle energies

$$E_j = \left[(\epsilon_j - \lambda)^2 + \Delta^2\right]^{1/2} . \qquad (24)$$

The spectra of the quasi-particle states are found from the E_j. In an odd-A nucleus, the lowest single quasi-particle level (that is, the lowest E_j) is the ground state. Higher E_j's are the excited states. In an even-even nucleus the ground state is a quasi-vacuum, and the excited states are the two, four, etc. quasi-particle states. These correspond to two, four, etc. elementary excitations, and are obtained as the sum of two, four, etc. E_j's. The existence of a gap of at least 2Δ for the lowest excited (two) quasi-particle state follows from (24). In addition to the quasi-particle excited states there are collective ones, to be discussed later. But first, the treatment of the effect of long range residual interactions on the quasi-particle states will be mentioned.

In the K.S. model, the long range part of the residual force is assumed to have an angular dependence given by P_2 (cos Θ_{ij}). (The angular dependence is the important part, and the low multipole components of the force between particles i and j are associated with the long range part). This force can provide an explanation for quadrupole vibration spectra and for permanent quadrupole deformations.

The long range residual force is applied to the N quasi-particles, using perturbation theory. The resulting spectrum is the one which is to be compared with experimental single-particle levels.

Collective levels are treated differently. It is assumed that the main part of the long range force is better represented by the interaction of each particle with a total nuclear quadrupole field. Using this assumption, the model is able to give estimates of the mass and stiffness vibration parameters, collective state energy levels, and collective transition strengths, for a number of S.C.S. nuclei. The method has a similarity to the approach of the (vibrational) unified model, but some pairing effects are included. One difference from the Bohr-Mottelson results[8] for a single particle coupled to a vibrator is that a quasi-particle near the Fermi surface ($E = \lambda$) is more weakly coupled to the oscillation, while one farther from the Fermi surface is coupled more strongly.

An important result, which is similar to the unified model, is the prediction of a low-lying collective first excited 2^+ state for even-even nuclei, which is well below the quasi-particle states. That is, it is in the gap. There is good agreement with the experimental energies for levels of this type.

For odd-A nuclei collective effects are possible, but specific results were not given in reference 17, as the authors felt that there was not yet experimental evidence for these states in S.C.S. odd-A nuclei. Chapter V will discuss several possible examples of such states.

The unified model. In the conventional unified model, permanent or vibratory deformations have been included in the self-consistent field. Nuclei with large permanent deformations are identified by their "rotational" spectra. They have been found at approximately A = 25, A = 150 to A = 190, and A > 222.[24] Certain even-even nuclei have near-harmonic low-energy spectra, and they have been called "vibrational." Several regions where they have been identified[9] are approximately at A = 60 to A = 150 and A = 190 to A = 220.

Also, vibrations of the permanently deformed nuclei have been considered. These usually have been interpreted as being of one or two volume-conserving types which also retain equatorial symmetry. Vibrations which flatten the nucleus azimuthally have been called γ vibrations, while those which preserve axial symmetry have been called β vibrations.

The interpretation of spectra of deformed nuclei therefore, in general, involves a number of rotational bands. Each rotational band belongs to either a different intrinsic configuration,[24,25] or to a different member of a vibrational spectrum.[26] Figure 5 depicts a simple example of this.

---

[24] B. R. Mottelson and S. G. Nilsson, Dan. Mat. fys. Skrifter, 1, No. 8 (1959).

[25] D. A. Bromley, Proceedings of the Rehovoth Conference on Nuclear Structure, (North Holland Publishing Company, Amsterdam, 1958) p. 108.

[26] See, e.g. reference 1, p. 540.

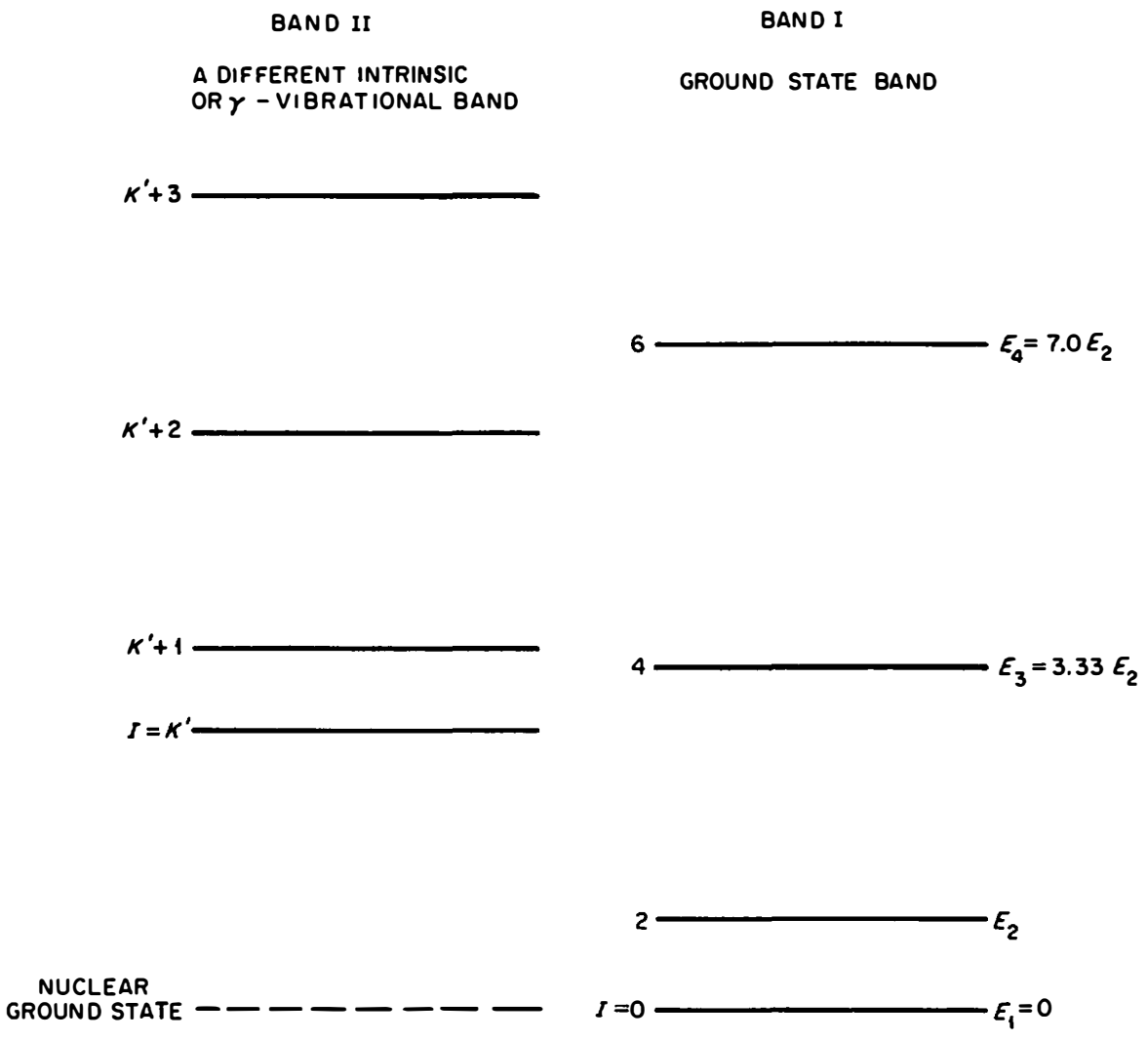

Fig. 5. Lowest Energy Levels of an Even-Even Nucleus With Two Rotational Bands.

The spectrum of each rotational band has the form

$$E_I = \frac{\hbar^2}{2\mathcal{I}} [I(I+1) - I_o(I_o+1)] , \qquad (25)$$

where $\mathcal{I}$ is the effective moment of inertia of the rotation, I is the spin of the level in question, and I_o is the ground state spin. (A special case occurs when the ground state spin is 1/2; then (25) does not apply.[27])

The predicted spin sequence is I_o, $I_o + 2$, $I_o + 4$, ... for the members of a rotational band in even-even nuclei (except where the band is part of a γ-vibrational spectrum). In odd-A nuclei the predicted sequence is I_o, $I_o + 1$, $I_o + 2$, ...

Quadrupole transitions between members of a rotational band (in which the nucleus does not significantly change shape) are enhanced over an estimated single-particle transition, by amounts from about 10 up to more than 100. Generalized single-particle estimates for this comparison have been reported, and will be discussed at the end of this sub-section.

There have been a number of different individual models proposed[28] for "vibrational nuclei." Thus far, however, it has not been possible to obtain as accurate a description as for rotational nuclei. One of the earliest models treats the surface motion as vibrations of spin-2

---

[27] For a consideration of this case, see, e.g. reference 9 or 24.

[28] See, e.g. the review of P. H. Stelson, Proceedings of the International Conference on Nuclear Structure, Kingston, Canada (University of Toronto Press, Toronto, 1960) p. 787.

phonons.[8,29] Another model deals with anharmonic β-vibrations of these spherical or nearly spherical nuclei.[30] The model of Davydov and Filippov, in the original form,[31] assumes that it is not vibrations, but rather rotations of a flattened ellipsoid, which are responsible for the observed spectra and other collective properties. There are still other models which deal with these nuclei.

These models differ, among other things, in some of the spins and degeneracies of their predicted spectra. As yet the experimental evidence allows no clear choice among them. Consequently, the geometrical aspects of vibrational nuclei are still an unsettled question.

However, vibratory parameters such as stiffness, effective mass, and deformation amplitude are obtainable from experimental data if one interprets the collective motion as phonon vibrations. The energy of the first excited state, and the B(E2) of the transition from this state to the ground state are used to calculate these parameters for a given nucleus.[28,32] On the average, the mass parameter obtained in this way is about 10 times the value which would be predicted under the assumption of irrotational flow.

---

[29] G. Scharff-Goldhaber and J. Weneser, Phys. Rev. 98, 212 (1955).

[30] L. Wilets and M. Jean, Phys. Rev. 102, 788 (1956).

[31] A. S. Davydov and G. F. Filippov, Nucl. Phys. 8, 237 (1958). See also F. K. McGowan and P. H. Stelson, Phys. Rev. 122, 1274 (1961).

[32] G. M. Temmer and N. P. Heydenberg, Phys. Rev. 104, 967 (1956).

The vibrational nuclei also predict enhanced quadrupole transitions. The transport of a quadrupole component of charge is responsible for the B(E2) which is measured, for example, in Coulomb excitation. Both rotational and vibrational collective transitions involve enhanced amounts of such charge transport. A general formula for the B(E2) has been given[33] in terms of the r.m.s. value of the deformation parameter, β, whether it be permanent or vibratory.

$$B(E2) \approx \left[\frac{3}{4\pi} ZeR_o^2\right]^2 \overline{\beta^2} \quad . \tag{26}$$

This strong experimental link with the collective aspect of the transition still is subject to some difficulty. This arises from the practice of exhibiting an experimental transition rate, $B(E2)_{exp}$, as some factor times a predicted single-particle rate, $B(E2)_{s.p.}$. This factor, called the "enhancement" of the transition, is to some extent a measure of the collective character of the state.

A general estimate of $B(E2)_{s.p.}$ has been made[34] which has been useful. However there is some question about the wave functions and spins which should be assumed for such an imaginary transition. Moszkowski has given an estimate[35] which includes a "statistical weight factor," which is often used.

---

[33] See, e.g., Reference 28, Figure 5, and Reference 9, p. 520.

[34] One of the early estimates is given by V. F. Weisskopf, Phys. Rev. 83, 1073 (1951).

[35] S. A. Moszkowski, Beta- and Gamma-Ray Spectroscopy, ed. K. Siegbahn, (North Holland Publishing Co., Amsterdam, 1955) p. 373; also Phys. Rev. 89, 474 (1953).

A short discussion of this question has been given.[36] In spite of some arguments to the contrary, the statistical factor is used in the work of this thesis. At least, for nuclei fairly near closed shells, the use of actual spins in the statistical factor will not be too unrealistic. The single-particle estimate used in Chapter V is

$$B(E2)_{s.p.} = \frac{1}{4\pi} (3/5\ R_o^2)^2\ c(j>, j<) \frac{2j_f + 1}{2j_< + 1}. \qquad (27)$$

Here $R_o = 1.2\ A^{1/3} \times 10^{-13}$ cm., and the statistical factor $c(j_>, j_<) \left(\frac{2j_f + 1}{2j_< + 1}\right)$ is in the compact form given in reference 8.[37]

Recently, a member of collective E3 and E4 transitions have been reported. However, they will not be discussed here.

---

[36] D. H. Wilkinson, Nuclear Spectroscopy, B, ed. Ajzenberg-Selove, (Academic Press, New York, 1960) p. 861.

[37] Bohr and Mottelson, p. 104.

CHAPTER III

ION SOURCE DEVELOPMENT

A radio frequency (r.f.) type ion source is normally used in the ORNL 5.5 Mv Van de Graaff accelerator. With this system neon gas had been accelerated,[1] but usable quantities of triply charged neon ions had not been found in the analyzed beam.

The design of the r.f. source had reached a relatively high degree of refinement for hydrogen ion production. This familiarity favored some additional studies of its performance with multiply charged heavy ions, even though the principle of operation did not appear to be the most favorable for that purpose.

The ORNL 200 kv Cockcroft-Walton accelerator was available for the ion source testing, and it was much more suitable than the Van de Graaff for the initial studies. The terminal was easily accessible and operating time was not so much at a premium.

In the Cockcroft-Walton tests of the r.f. source, the largest multiply charged components that were measured were 1.2 microamperes of doubly charged neon ions (Ne^{2+}) and 0.028 microamperes of triply charged neon ions (Ne^{3+}). Furthermore, the lifetime of the source was short (of the order of an hour) in the operational mode which provided the largest multiple charge currents.

---

[1] P. H. Stelson and F. K. McGowan, Reactions Between Complex Nuclei, (John Wiley and Sons, Inc., New York, 1960), p. 47.

The PIG type ion source was expected, in principle, to be a more efficient producer of multiply charged ions, but its adaptation to a Van de Graaff for that purpose had not been reported. In two entirely different environments[2,3] the PIG source had supplied relatively large fractions of multiply charged ions for a number of different gases.

Therefore, for this work a PIG source was designed which would be suitable for the Van de Graaff. It was tested first on the Cockcroft-Walton where it provided up to 2.4 microamperes of Ne^{2+} ions and 0.17 microamperes of Ne^{3+} ions to a Faraday cup. The Ne^{3+} component, particularly, was larger than had been measured for the r.f. source. The PIG source was installed in the Van de Graaff accelerator. The multiple charge components measured at the target, though reduced from the Cockcroft-Walton values, were strong enough to be used for Coulomb excitation.

This chapter has the following arrangement. Section I describes the test arrangement on the Cockcroft-Walton accelerator. In Section II, the principle of operation of the PIG source is discussed and also the present design. Section III gives the performance characteristics and pertinent test results for operation in the dc mode. In Section IV the operation of the source with ac and pulsed power supplies is described.

---

[2]C. E. Anderson and K. W. Ehlers, Rev. Sci. Instr. 27, 809 (1956).

[3]R. J. Jones and A. Zucker, Rev. Sci. Instr. 25, 562 (1954).

Section V considers the adaptation and operation of the PIG source on the Van de Graaff. Section VI briefly describes the Cockcroft-Walton tests of the r.f. source.

I. THE COCKCROFT-WALTON TEST ARRANGEMENT

The ion source test arrangement on the ORNL 200 kv Cockcroft-Walton is shown schematically in Figure 6. Isolating transformers provided up to 5 kw of electrical power to the ion source. An electrometer-microammeter read the current collected in the Faraday cup.

Both neon and argon gases were used in the testing of the r.f. and PIG sources. The Cockcroft-Walton voltage was set at 70 kv for argon ions and 100 kv for neon ions. At these voltages all of the multiple charge components of interest in the beam could be bent and separated with the analyzing magnet.

The resolution of the system was largely determined by the diaphragm at the exit of the magnet. It had a 1/4 inch diameter hole. The resolution was high enough for the present work, as the mass 20, 21 and 22 peaks of neon were well separated.

Usually there were many more peaks (of the order of 30) in the analyzed beam spectrum than just those expected from the various charge components. Part of these were caused by contaminants such as oxygen, nitrogen and aluminum (from aluminum cathodes when they were used). But also the charge exchange in the beam created new peaks. As a result of a gain or loss of charge by gas collisions between the base of the

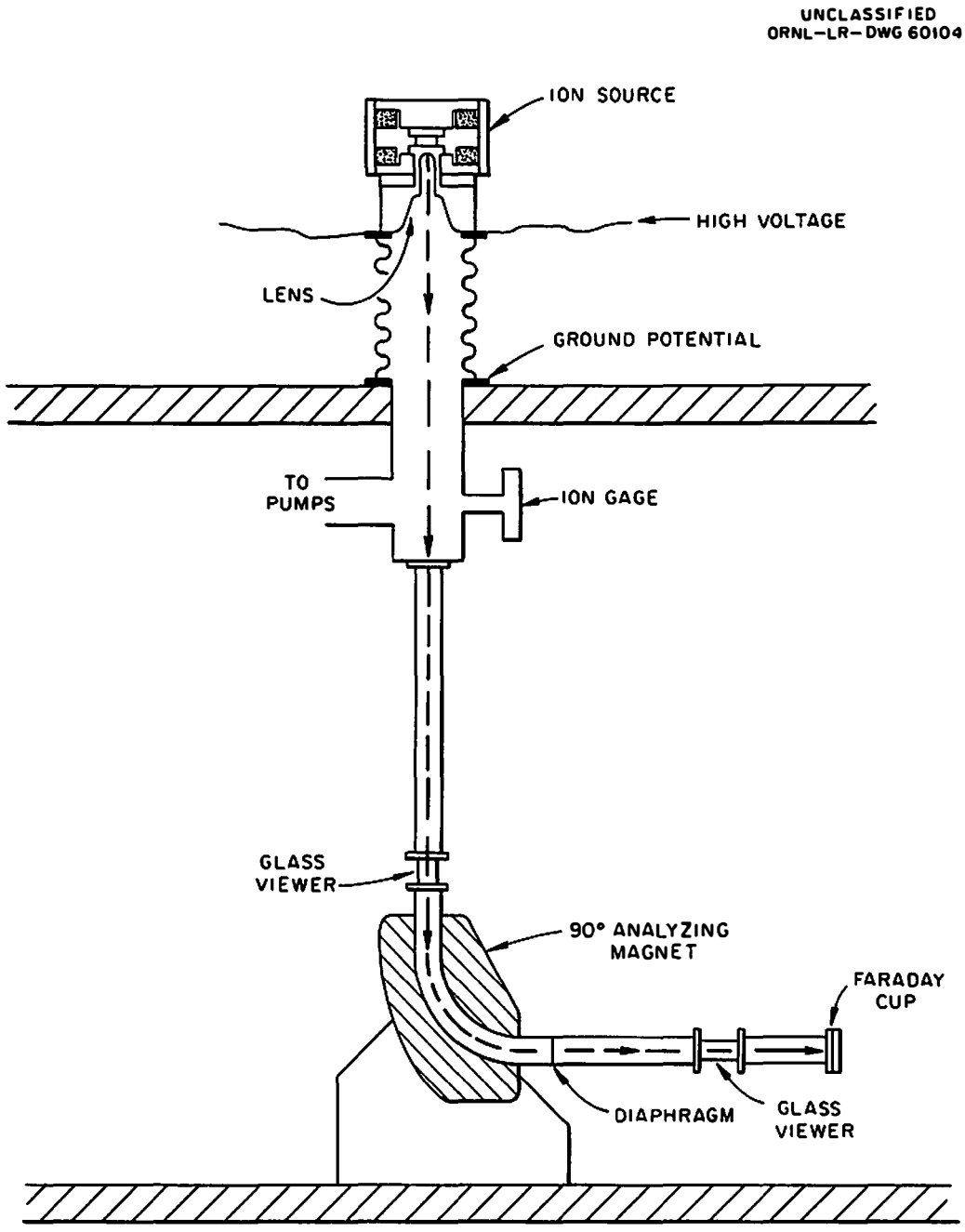

Fig. 6. Experimental Arrangement for the Ion Source on the Cockcroft-Walton Accelerator.

accelerating tube and the top of the magnet, some of the ions were bent differently in the magnet.

The appearance of the additional peaks was not in itself serious. Along with the analyzing magnet calibration, the 10 per cent natural abundance of neon-22 provided an identification of the neon peaks. The 10:1 mass 20 and mass 22 peaks could be readily identified at each charge state.

A more serious consequence of charge exchange was the alteration of the quantities of ions collected in the Faraday cup. The charge exchange cross sections of neon and argon are known to be large.[4] Particularly with large gas flows and the attendant poor vacuum, the currents read in the Faraday cup were inaccurate measures of the absolute and relative magnitudes of the various components in the output of the ion source. In the limit of equilibrium charge exchange conditions (which may have been reached at times with argon), there would be no relationship between the source output and the currents measured in the Faraday cup.

In both of the types of ion sources the measured output depended strongly on the gas pressure in the discharge. Individual pressure determinations could only be deduced indirectly, from calculations using the gas flow and the flow conductance of the ion source exit canals. The gas flow was measured, after a calibration, by the ion gauge in the accelerator system. (It is expected that the pumping speed of the two

---

[4] P. R. Jones, F. P. Ziemba, H. A. Moses and E. Everhart, Phys. Rev. 113, 182 (1959).

CVC MGH-180 mercury diffusion pumps[5] was nearly constant in the pressure range of interest.)

II. THE PIG SOURCE OPERATION AND DESIGN

Principle of operation. The arrangement of a simple PIG type discharge is illustrated in Figure 7. A conducting cylinder forms the anode. At both ends are the cathodes which are electrically connected together. These are placed in a magnetic field which is parallel to the axis of the anode. When the arrangement is used as an ion source, the ions can be removed through a hole either in the anode or in one cathode.

A unique feature of this discharge is its high impedance. This arises from the efficient electron trap which the configuration forms. The magnetic field prevents the easy radial movement of the electrons to the anode. This also explains why, without a heated cathode, a sufficient number of electrons can be accumulated to maintain the discharge at low pressure in a small volume.

In principle, the PIG discharge should be a relatively efficient producer of multiply charged ions. With the high impedance, a high discharge voltage, E_D, can be applied without an excessive dissipation of power. The electrons can gain relatively high energies in falling through this potential.

---

[5] H. D. Stromberg, University of California Radiation Laboratory report, UCRL-5119, (1959).

UNCLASSIFIED
ORNL-LR-DWG 56211

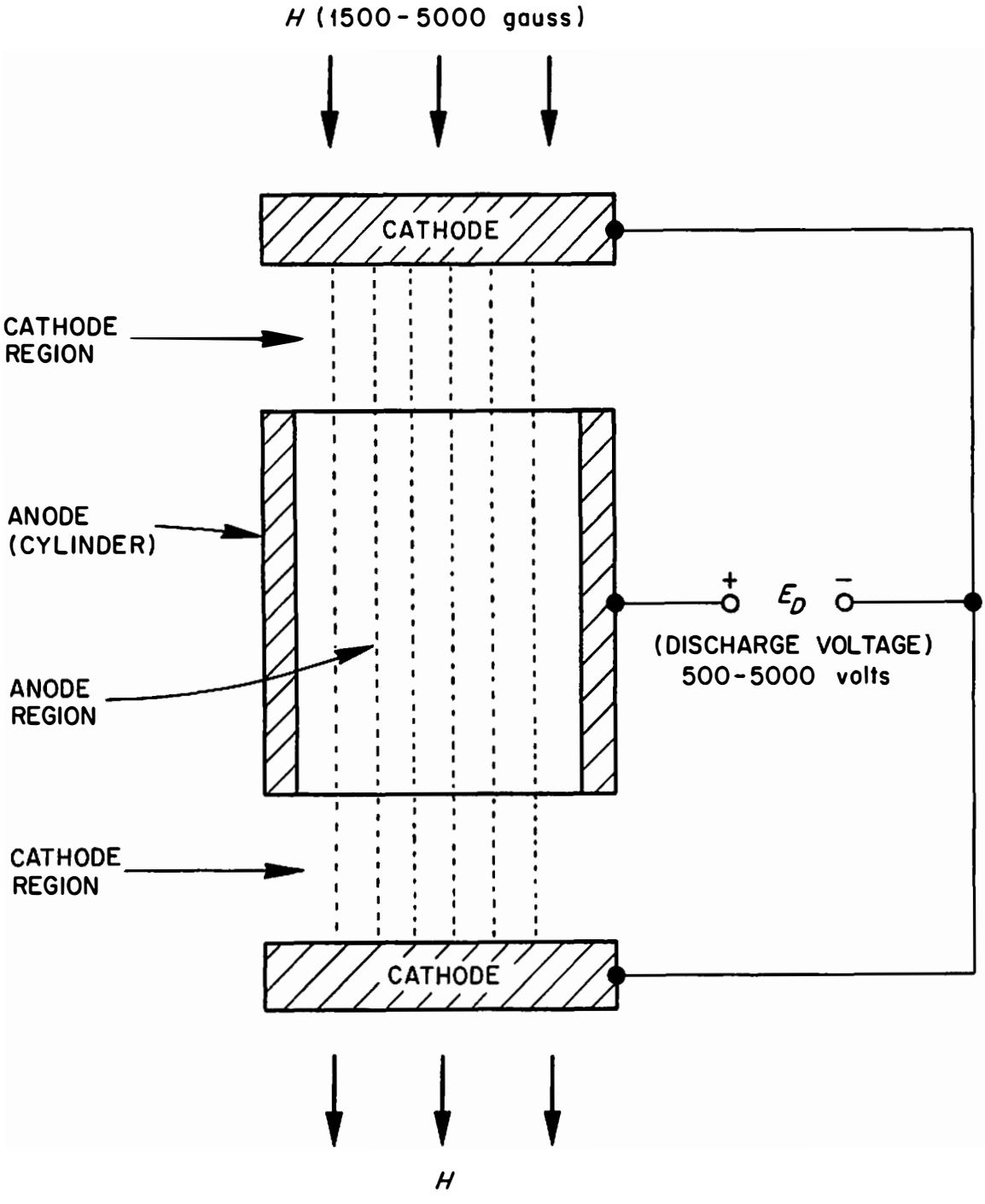

Fig. 7. Simple PIG Type Discharge.

The mechanism for electron travel to the anode is not yet completely understood. It is known that the PIG plasma has oscillations[6] which result in random electric fields with the largest component perpendicular to the magnetic field. These fields cause a small radial drain velocity across the magnetic field at 10^8 E/H centimeters per second, where E is the (random) electric field in volts per centimeter and H is in gauss. This is called the "Hall current."[7] An additional small radial drain of electrons is caused by collisions in the plasma.

It is possible to present a qualitative explanation of some of the observed PIG characteristics. With reference to Figure 7, the longitudinal potential gradient is strong in the cathode regions and weak in the anode region. This is the case, to varying degrees, whether there is plasma or a vacuum in the source.[8]

Free electrons are produced by electron-gas atom collisions within the plasma* and as secondary electrons from ions colliding with the cathodes. To a lesser extent other processes may be present. Measurements of secondary electrons produced by kilovolt ion bombardment of

---

[6] J. Backus, Characteristics of Electrical Discharges in Magnetic Fields, ed. A. Guthrie and R. K. Wakerling, (McGraw-Hill Book Company, New York, 1949), p. 361.

[7] H. Alfven, Cosmical Electrodynamics, (Oxford University Press, London, 1950), p. 49.

[8] F. Salz, R. G. Meyerand, Jr., E. C. Lary, and A. P. Walch, Phys. Rev. Letters 6, 523 (1961).

*Electrons freed directly by collisions within the plasma will be called "direct electrons."

metals[9] suggest that there should be less than an order of magnitude difference in the numbers of secondary and direct electrons in the discharge.[10]

It is expected that most of the faster electrons are in the anode region, where they have fallen through at least part of the discharge potential, E_D. These would originate mainly at the cathodes or in the cathode regions. The actual distribution of velocities should depend on the relative sizes of the anode and cathode regions.

The relative probability of multiple ionization from a single electron-gas atom collision increases with energy.[11] Figure 8 shows most of the available data for this with neon gas. Unfortunately, information is missing for electron energies in excess of 400 to 600 ev. Another important lack of data is that for multiple-step ionizing processes. The probability of additional ionization by further electron collisions would be expected to increase with electron energy.

Thus one cannot directly predict the quantitative importance of multiple-step ionization on the relative charge states of the PIG source. However, there are implications from the data of references

---

[9] P. F. Little, Encyclopedia of Physics, XXI, (Springer-Verlag, Berlin, Gottingen, Heidelberg, 1956), p. 638.

[10] See also reference 6, p. 349, where measurements indicated about 1/3 as much secondary electron current as ionic current.

[11] W. Bleakney, Phys. Rev. 36, 1303 (1930); H. S. W. Massey and E. H. S. Burhop, Electronic and Ionic Impact Phenomena, (Oxford University Press, London, 1952), p. 38.

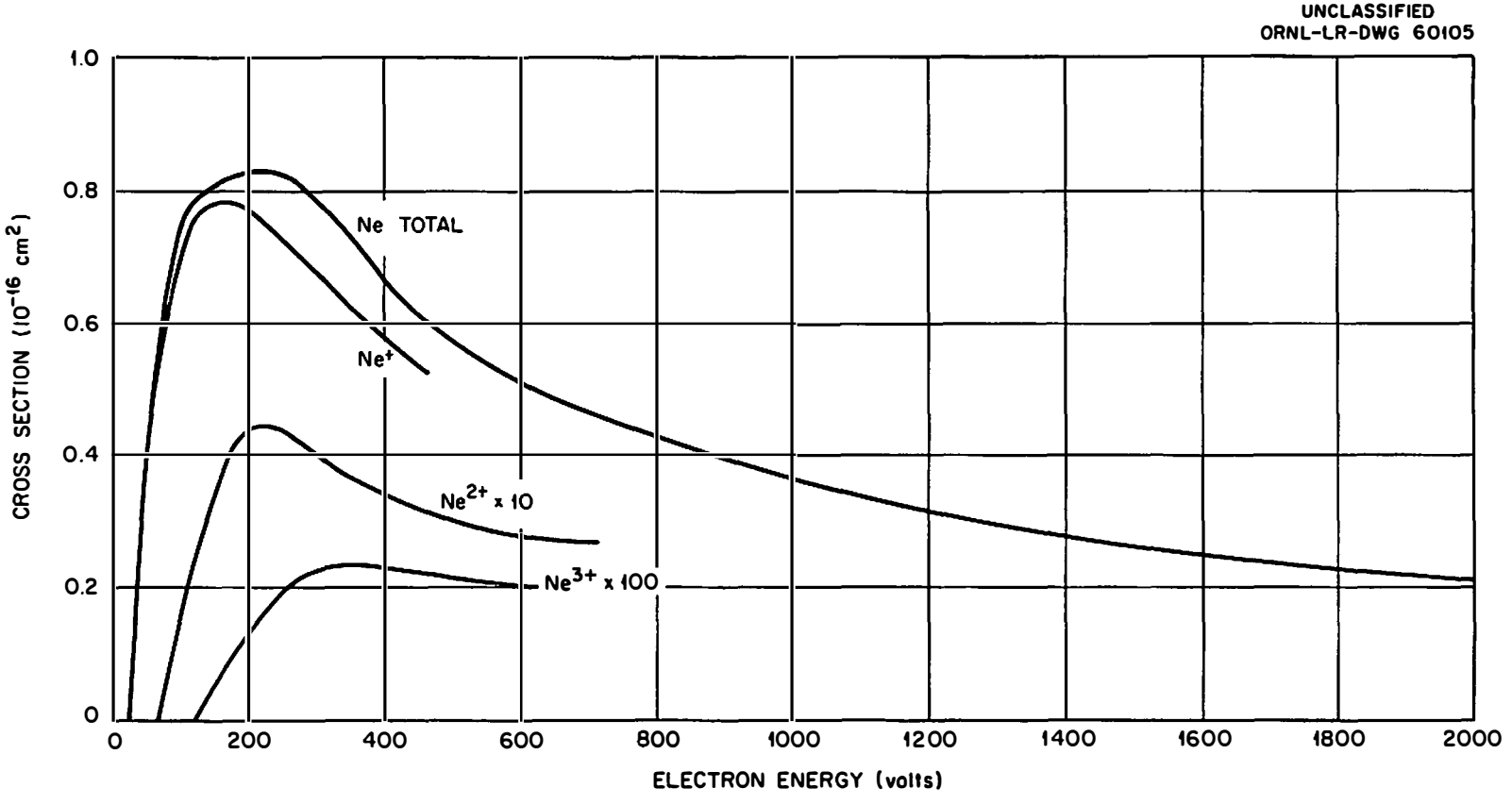

Fig. 8. Cross Section for the Ionization of a Neon Atom in a Single Collision by an Electron.

2 and 3 that such collisions are important. At E_D = 600 volts the Jones-Zucker source produced N^{2+} and N^{3+} currents greater than the N^+ current, and an N^{4+} current 1/3 as great as the N^+ component. Cross section data similar to that in Figure 8 is not available for nitrogen, but it appears unlikely that single collisions could produce such large multiple charge fractions. (In the present tests nitrogen produced much poorer multiple charge fractions than neon.) Similarly, the data for neon and other gases in the Anderson-Ehlers source (at higher voltages) appear to confirm the importance of multiple step ionization. One factor which might affect the conclusions in this argument is the possibility of selective extraction.

It appears that, in principle, extraction from the anode would be preferable, as the probability of electron recombination in the interval between ion formation and removal would be minimized. (Most of the fast electrons, and hence the multiple charge ionization, should be in the anode region.) The cross sections for electron recombination charge exchange are expected to be particularly high for low energy multiply charged heavy ions. This is true at one hundred kev,[4,12] and it is probably also true at six to fifteen kev. The importance of extraction on ion source performance has been studied by several authors,[13] but mainly with respect to hydrogen ions.

---

[12] P. M. Stier, C. F. Barnett, and G. E. Evans, Phys. Rev. 96, 973 (1954).

[13] See, e.g., J. Kistemaker, Nucl. Instr. and Methods 11, 179 (1961).

The choice of extraction methods. Two practical difficulties stood in the way of the present use of anode extraction. First, to be efficient, it would require a large thin extraction aperture, so that the extraction field could "reach into" the plasma. But this requires a high pumping capacity in the accelerator. Whereas Jones and Zucker had used two 20 inch diffusion pumps and Anderson and Ehlers had used one 14 inch diffusion pump, there was much less capacity on the two accelerators to be used in the present work. Two four inch diffusion pumps provided an estimated 165 liters per second pumping speed at the base of the Cockcroft-Walton. The pumping speed at the top of the Van de Graaff accelerator tube was estimated to be about 25 liters per second.

Secondly, anode extraction requires that the beam travel across the magnetic field. Unless the magnetic field could be kept extremely constant, beam movement would cause trouble in the relatively inaccessible Van de Graaff terminal. (Neither of the referenced installations were in pressurized systems.) Even without such a difficulty, beam wandering was very likely a significant factor in the minimum errors of the angular distribution work reported in Chapter IV.

Cathode extraction, with a small exit canal, was chosen for the present ion source. The cathodes were small and simple, so that a variety of canal sizes could be tested. Sputtering wear rates put a limit, however, on the minimum length (about 1/8 inch) that would be practical for the exit canal. This is in contrast to the thin apertures that could be used with an anode extraction system.

The ion source design. Figure 9 is an exploded view of the ion source without the magnet. The brass housing at the top has the gas entrance, the insulated high voltage lead, and one cathode. Boron nitride insulators support a sand-blasted stainless steel anode. The exit canal screws into a plate, which also forms the top element of the main focussing lens. This plate fastens to a flange. Aluminum gaskets provide the seal between the brass housing and the flange, and between the flange and the magnet pole piece (not shown).

This assembly fits between the pole pieces of the magnet. They are four inches in diameter, and have a two inch gap. The bottom pole face is hollow, to accept the combination lens-extractor electrode from below. Figure 10 shows the assembly mounted on a head which sits atop the Van de Graaff accelerator tube. The lens is inside. A different mount was used on the Cockcroft-Walton, but the magnet was the same. The thermal switch mounted on the iron prevents overheating of the coils.

The two coils of the magnet are in parallel. Each consists of No. 16 enamelled wire and has a cross section of two inches by three inches. The iron is Armco, and the four legs of the magnet, each with a 3/4 inch by 4 inch cross section, have a total cross sectional area about equal to that of the pole faces. Calibration with a flip coil showed that the magnetization was very linear in the usable range, and that the field was 5000 gauss at about 9.2 amperes. Heat dissipation limited the operation to about 8 amperes, even when a blower was used.

The parallel resistance of the magnet coils was about 9 ohms cold, and 11 ohms hot. A 100 volt, 10 ampere magnet power supply was

UNCLASSIFIED
PHOTO 52505

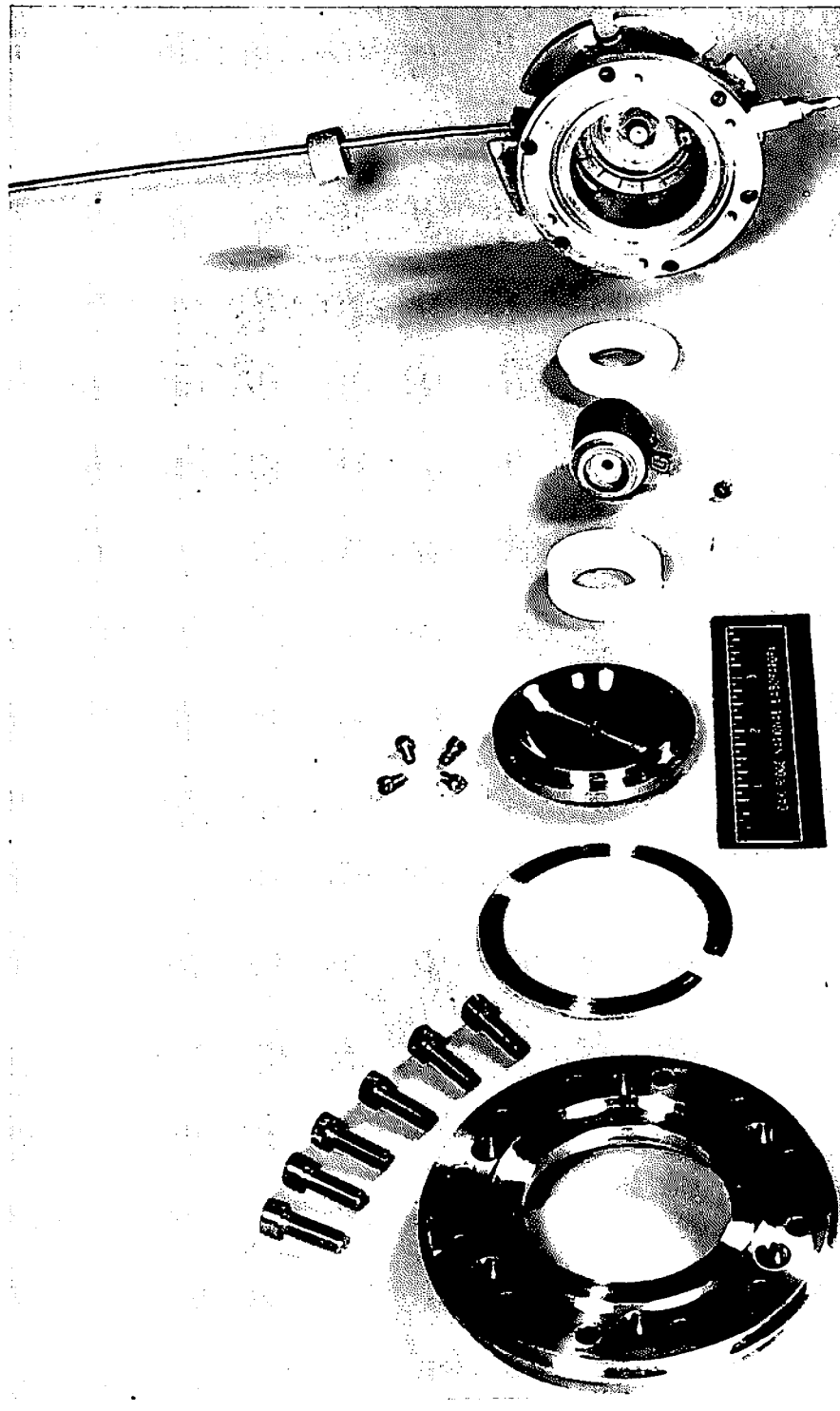

Fig. 9. Heavy Ion PIG Source, Exploded View.

UNCLASSIFIED
PHOTO 53059

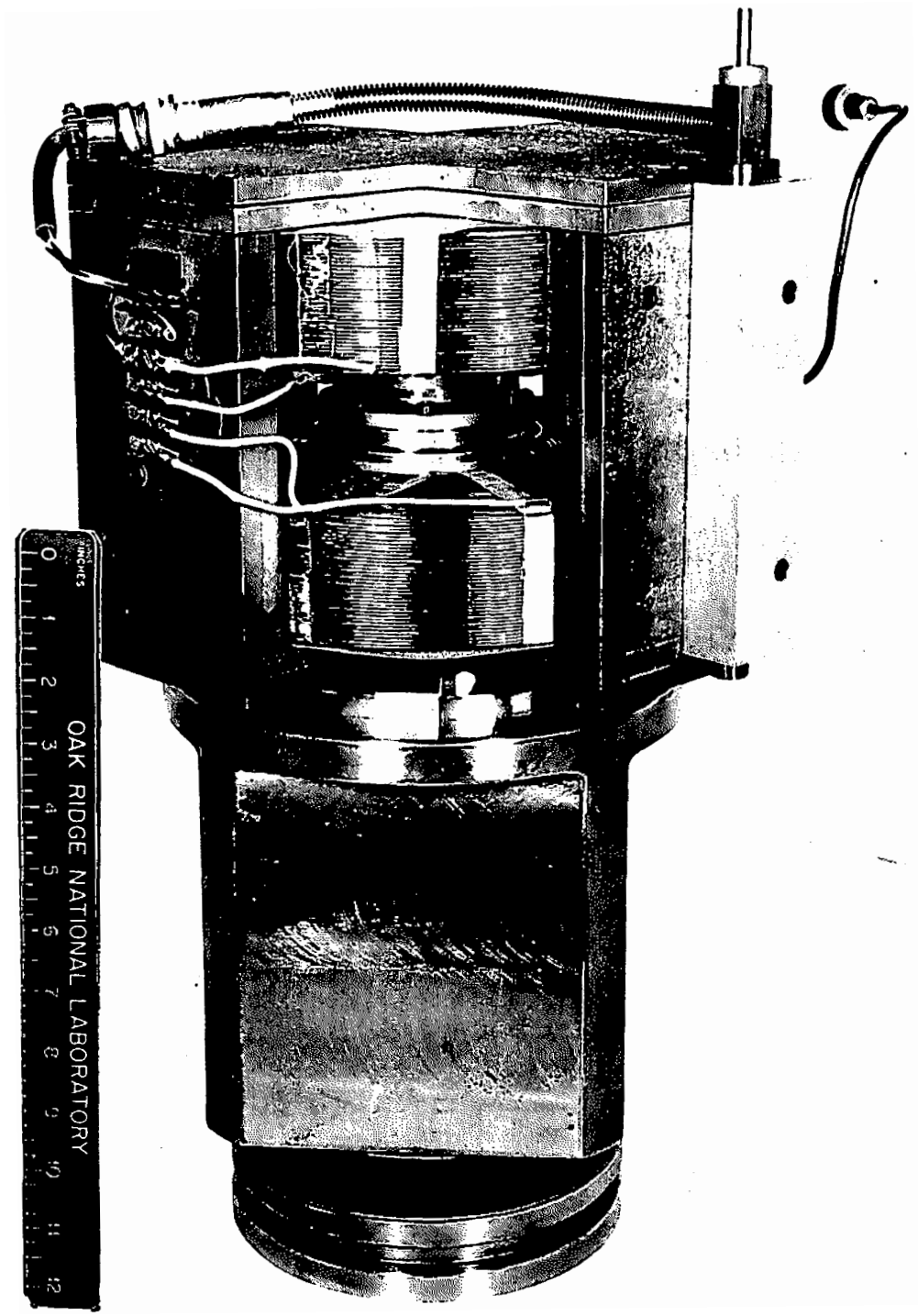

Fig. 10. Heavy Ion PIG Source and Lens Mount Assembly.

built. Silicon diode rectifiers were used in this supply on the Cockcroft-Walton, but they could not stand the occasional sparking in the Van de Graaff. They were replaced by selenium rectifiers, which had been proven in that service.

A 0-3500 volt, 350 ma. discharge voltage supply was built for the initial testing of the PIG source. This was able to provide operation in a fairly intense mode. For the Van de Graaff operation a smaller 6000 volt, 30 ma. supply replaced the heavy one, as only low-intensity operation was used.

The gas leak was an Ideal-Aerosmith, Inc. No. 52-2-11 sensitive needle valve. A one-foot lever arm was fastened to the handle, and was operated against a spring. A 40:1 gear reduction box helped in obtaining the sensitive flow control that is needed.

Figure 11 shows the power supplies, gas bottle, 80 kilovolt lens supply, and auxiliary parts that comprised the electronic terminal plate which was used with the PIG source in the Van de Graaff.

Several detailed features of the Anderson-Ehlers source[2] were included in the present design. The shape of the anode was such that the insulators were shielded from metal sputtered off the cathodes. At first lavite insulators and a carbon anode were used. Later, as part of an effort to reduce the high temperature outgassing, they were replaced by boron nitride and stainless steel,* respectively.

---

*This was privately suggested by C. E. Anderson.

UNCLASSIFIED
PHOTO 53060

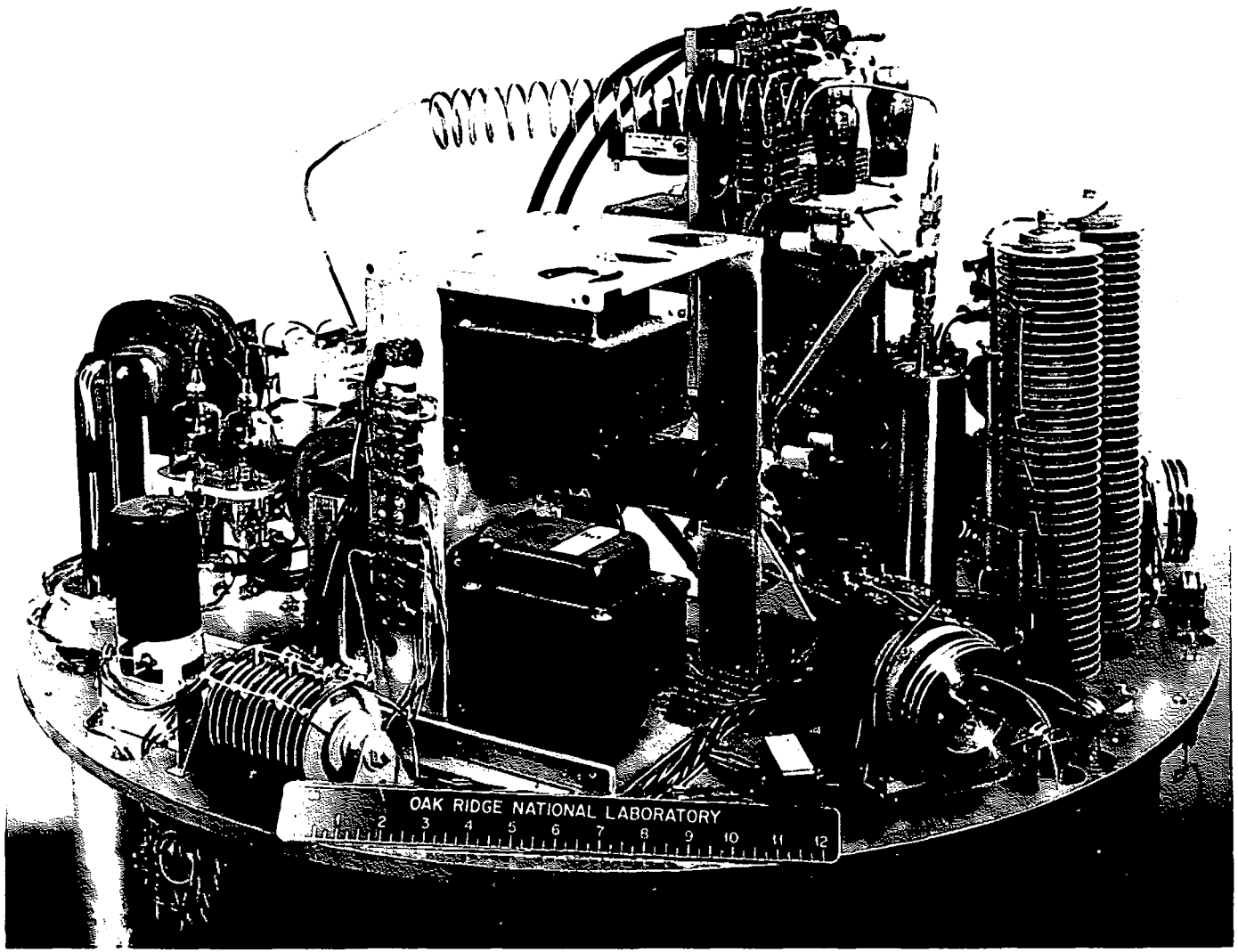

Fig. 11. Terminal for the PIG Source in the 5.5 Mv Van de Graaff.

Cathode materials of tantalum, titanium, zirconium and aluminum were tested. On the Cockcroft-Walton, titanium seemed to be the preferable material because of its low sputtering rate and high secondary emission. But with the sustained low intensity operation in the Van de Graaff, fine leaves of titanium would flake off the anode and short the source. Because of this flaking it was necessary to remove the pressure tank three times in one week. It was not feasible to study this effect extensively to circumvent the trouble with titanium. Tantalum was found not to flake seriously in this operation. Even though it slightly reduced the Ne^{3+} output, tantalum was more practical for the Van de Graaff.

The discharge region, formed by the anode and cathodes, was a cylinder 1/4 inch diameter by 1-1/16 inches long. The anode region was 3/4 inch long and was centered between the cathodes. For some of the low intensity operation the discharge region was reduced to 1/8 inch diameter, with a different anode. There was no noticeable change in performance, which supports the report[14] that the low intensity discharge column is very narrow.

The exit canal design had a significance besides the effect on extraction efficiency. For a given source pressure, it controlled the gas flow rate, and probably to some extent the beam focussing. The gas flow affects the gas loading of the accelerator as well as several internal aspects of the discharge, which will be discussed in following Sections. The final cathode design, as used in the Van de Graaff, is shown in Figure 12.

---

[14] P. Lorrain, Can. Jour. Research 25A, 338 (1947).

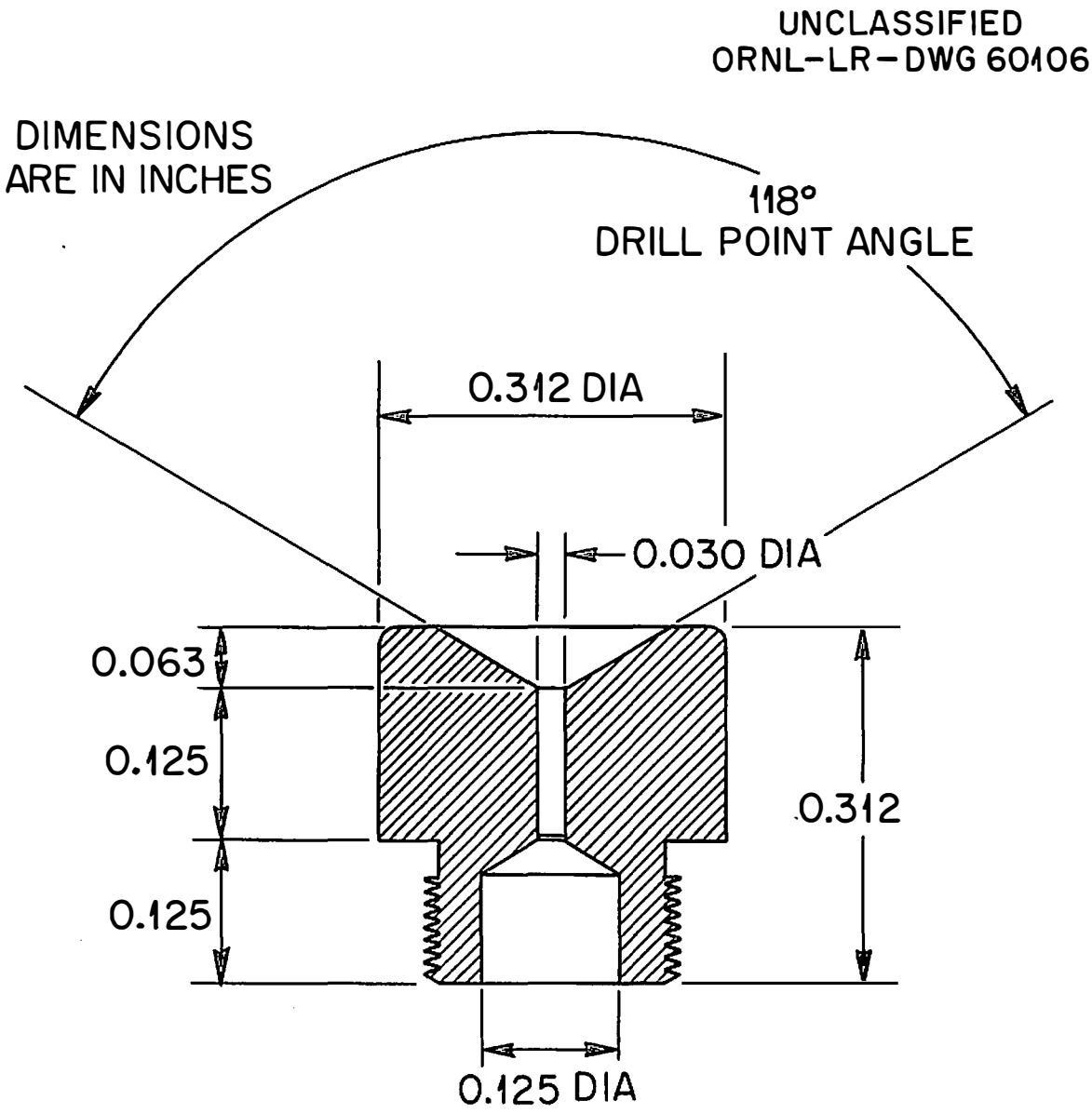

Fig. 12. Exit Cathode for the Heavy Ion PIG Source.

Water cooling tubes were originally soldered to the brass housing. They were removed when it was found that even the most intense mode was unaffected by cooling.

III. DC PIG SOURCE PERFORMANCE

There were two (arbitrarily defined) modes of operation of the PIG source. The low intensity mode (taken here to be that for a discharge current of 20 ma. or less) provided the highest measured total beam. However, the output characteristics of the high intensity mode probably were not accurately measured because the mode generally required higher gas flows. The resultant poorer vacuum and high charge exchange almost certainly reduced the triply charged component seriously, and possibly also the other components.

The pressure in the discharge. The use of the accelerator ion gauge as a reference for the ion source pressure introduced some uncertainties. Such an indirect method was needed, nevertheless, because the discharge volume could not be sampled directly. It was desirable to minimize the outgassing surfaces in the ion source.

An absolute flow calibration for the accelerator ion gauge and pumping system was made, with the assumption of constant pumping speed. The gas was allowed to flow overnight at a setting for typical operation. (The source was turned off.) The decrease in the gas bottle pressure was noted. With the knowledge of the gas bottle volume and the elapsed time an average gas flow was determined.

Several such determinations were made. The one taken as a standard calibration for the Cockcroft-Walton work is the following. Corresponding to typical operation with a 0.040 inch diameter by 1/8 inch long exit canal, there was a measured neon gas flow of about 1.3 micron-liters per second. At this flow the ion gauge reading was 3.5×10^{-6} mm Hg above the residual value. A source pressure of about 30 microns was calculated for these conditions. Similarly, in the Van de Graaff an 0.020 inch diameter by 1/8 inch long exit canal provided typical operation with a neon gas flow of about 0.25 micron-liters per second. The calculated source pressure was about 40 microns.

Room temperature was assumed for the source pressure calculations. There was no reasonable way to estimate the operating gas temperature. Furthermore the pumping effect of the sputtered cathode material[15] could not be estimated. These factors complicate the calculation of a reference source operating pressure.

It seems unlikely that the ion source operating pressure under the above conditions was actually less than 30 microns. This is higher than that quoted for most PIG type ion sources,[16] but the operation was near the low end of the pressure range of the present source. The small size of the discharge volume may partly explain this.

---

[15] Some commercial pumps are based on the PIG discharge. See, e.g., L. D. Hall, Rev. Sci. Instr. 29, 367 (1958).

[16] See, e.g., references 2, 6, and 13.

The relative values of the ion source operating pressure, under different conditions, were similarly subject to uncertainties. To the extent that gas temperature and PIG pumping were variables, the flow measurements failed to give correct relative indications of the source pressure. An occasionally significant variable was the outgassing of surfaces struck by the beam. As the (stray) bombardment of these surfaces changed with beam size and dispersion the ion gauge reading also varied. For a given gas leak setting, it was sometimes possible to double the ion gauge reading by changing other ion source parameters. Variations in the accelerator pumping speed would also alter the relative pressures.

Nevertheless, there was a discernible relation between the ion gauge reading and ion source performance. Also, there was usually just a small change in the ion gauge reading when the ion source voltage was turned on, at a given gas leak setting. Therefore the above "standard" calibration will arbitrarily be used in the present discussions. Where necessary, correction for the relative sensitivity of the VG-1A ion gauge[17] to other gases is made. The flow calibration point was probably repeatable to about $\pm$ 25 per cent.

The discharge characteristic. Before the installation on the Cockcroft-Walton, the PIG source was briefly studied on a simple test

---

[17] S. Dushman, Vacuum Technique, (John Wiley and Sons, Inc., New York, 1955), p. 350.

arrangement. The discharge characteristics and the total beam could be measured, but not the beam components. Argon gas was used. There was no absolute pressure calibration.

It was found that a 5000 to 100,000 ohm resistor had to be put in series with the power supply to prevent blowing one ampere fuses in the output circuit. This indicates the size of the initial current surge. Such an initial surge is characteristic of this ion source.

Figures 13a and b show the measured output and discharge characteristics of the ion source at a pressure near the lower end of the operating range. The three curves represent different magnetic field strengths. Several features of the curves of Figure 13b were observed again on the Cockcroft-Walton. At voltages above 2500 and with a low gas pressure, an increased magnetic field usually raised the discharge current (but not the output current). Also, when the source could be operated at an especially low pressure, there was usually a voltage above which the dynamic resistance (slope of the curve) became negative.

The higher pressure, more conventional performance, with argon ions is illustrated in a different type of plot in Figure 14. These data were taken on the Cockcroft-Walton, where the pressure measurements had significance. The curves show simultaneously that the measured voltage was approximately independent of both pressure and current. The different intensities were accomplished with relatively small changes in voltage, as the ratios of the curve ordinates are approximately proportional to the currents.

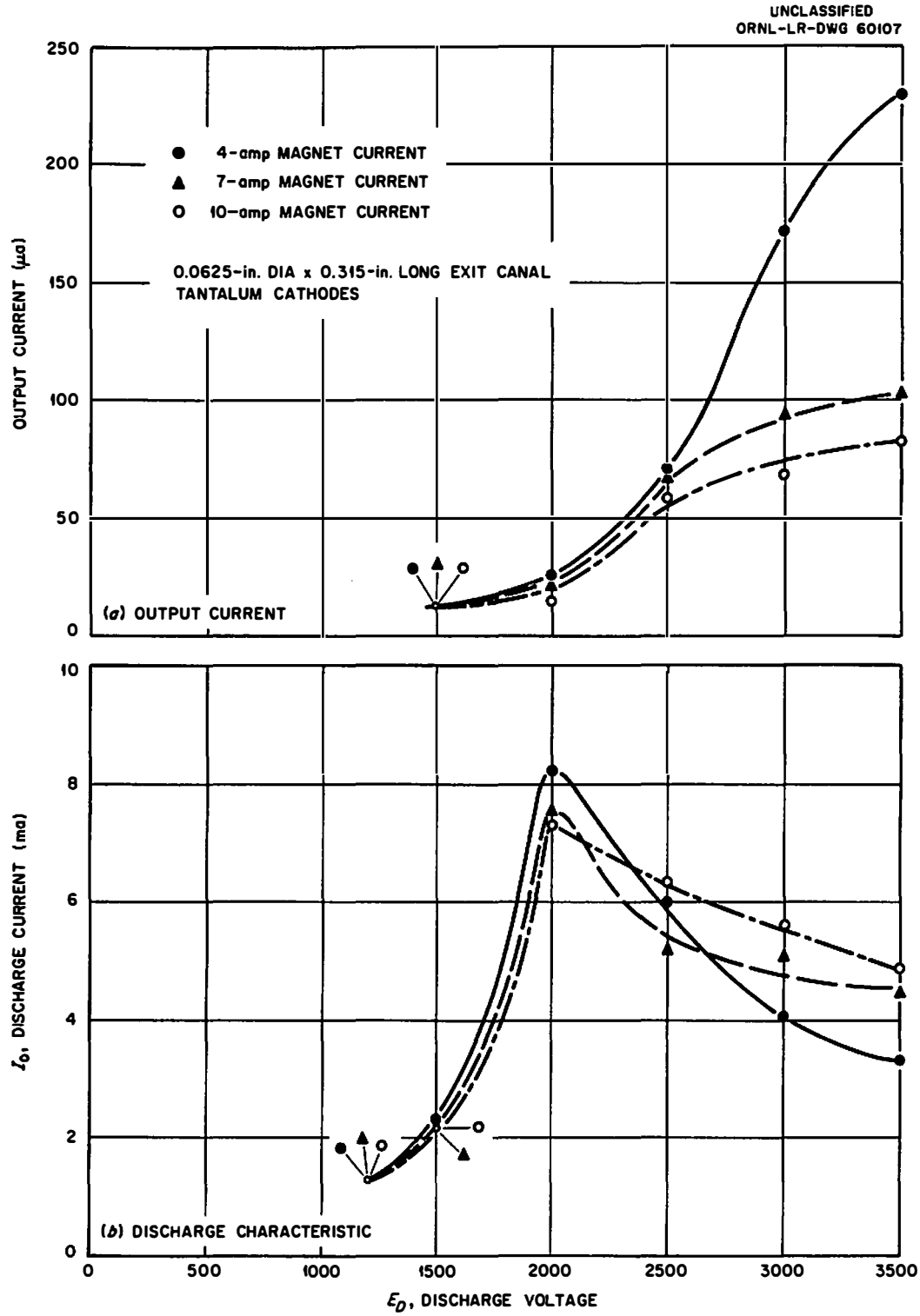

Fig. 13. Discharge Characteristic and Output Current With Argon Gas at Low Pressure.

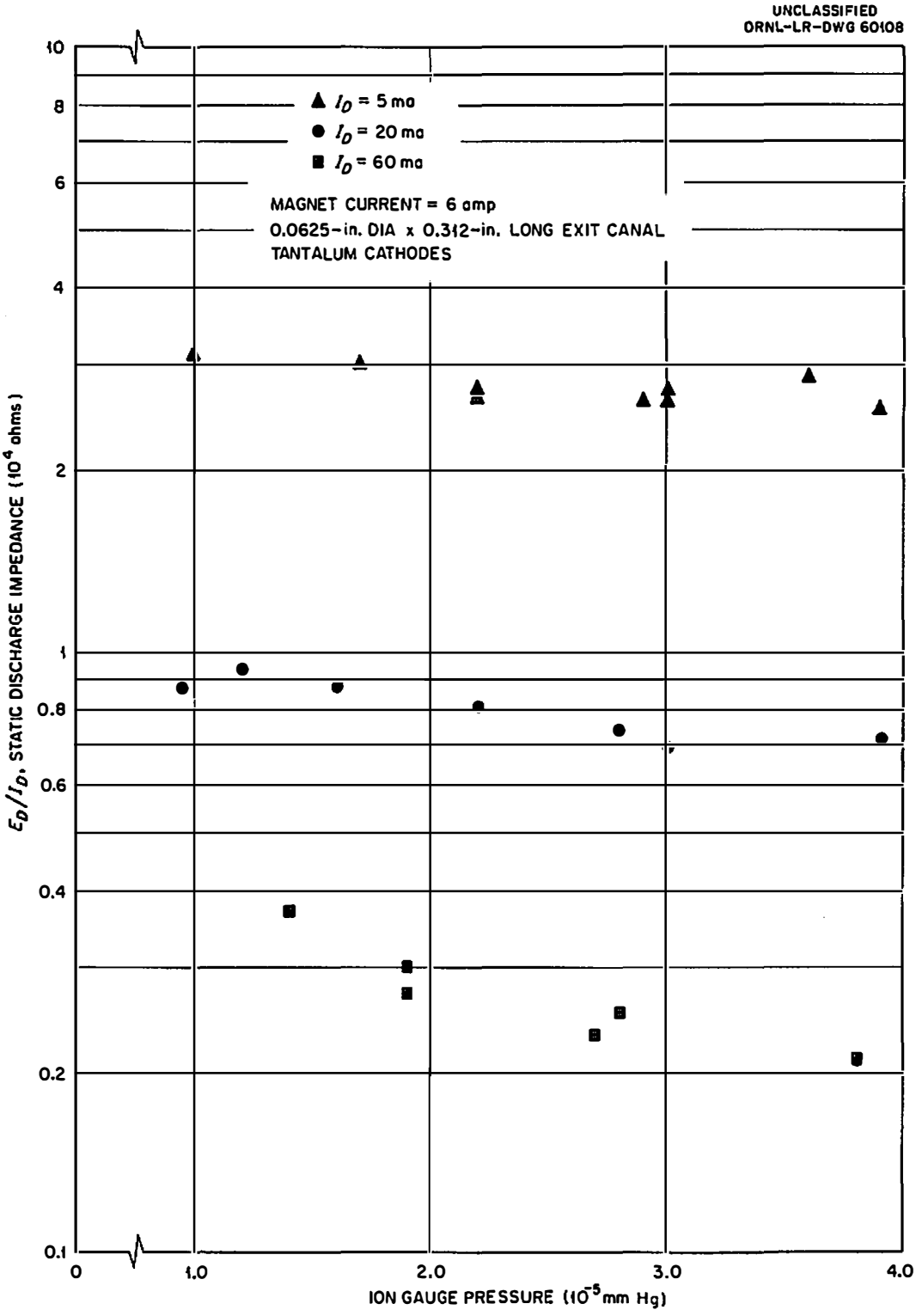

Fig. 14. Discharge Impedance Vs. Pressure of Argon Gas.

The neon gas discharge properties were not as smooth. Part of this may have been due to changes in the discharge character as a result of the higher ionization potentials of neon. Also, smaller exit canals were generally used with neon. The increased importance of outgassing could have such an effect. It was observed with neon that there was an hour or so of unsteady operation after the system was exposed to atmosphere. This is believed to be caused by outgassing. The occasional appearance of black deposits in the ion source, even with a stainless steel anode, increased the belief that outgassing was occurring.

Output characteristic. Some typical component beam currents which were collected in the Faraday cup are plotted as a function of pressure in Figure 15 for argon, and Figure 16 for neon. In addition to charge exchange the geometrical collection efficiency reduced the sum of these currents by 1/2 to 1/4 from the total current measured above the magnet. For example, the total neon beam measured above the magnet was typically 150 to 200 microamperes, whereas the peak Ne^+ component in the Faraday cup was typically 50 to 70 microamperes. A search at other accelerator voltages did not produce evidence of other large beam components. For this type of loss the fractional reduction of current is expected to be approximately uniform for the various components.

The curves of Figures 15 and 16 represent a combination of the ion source output characteristics and subsequent charge exchange in the

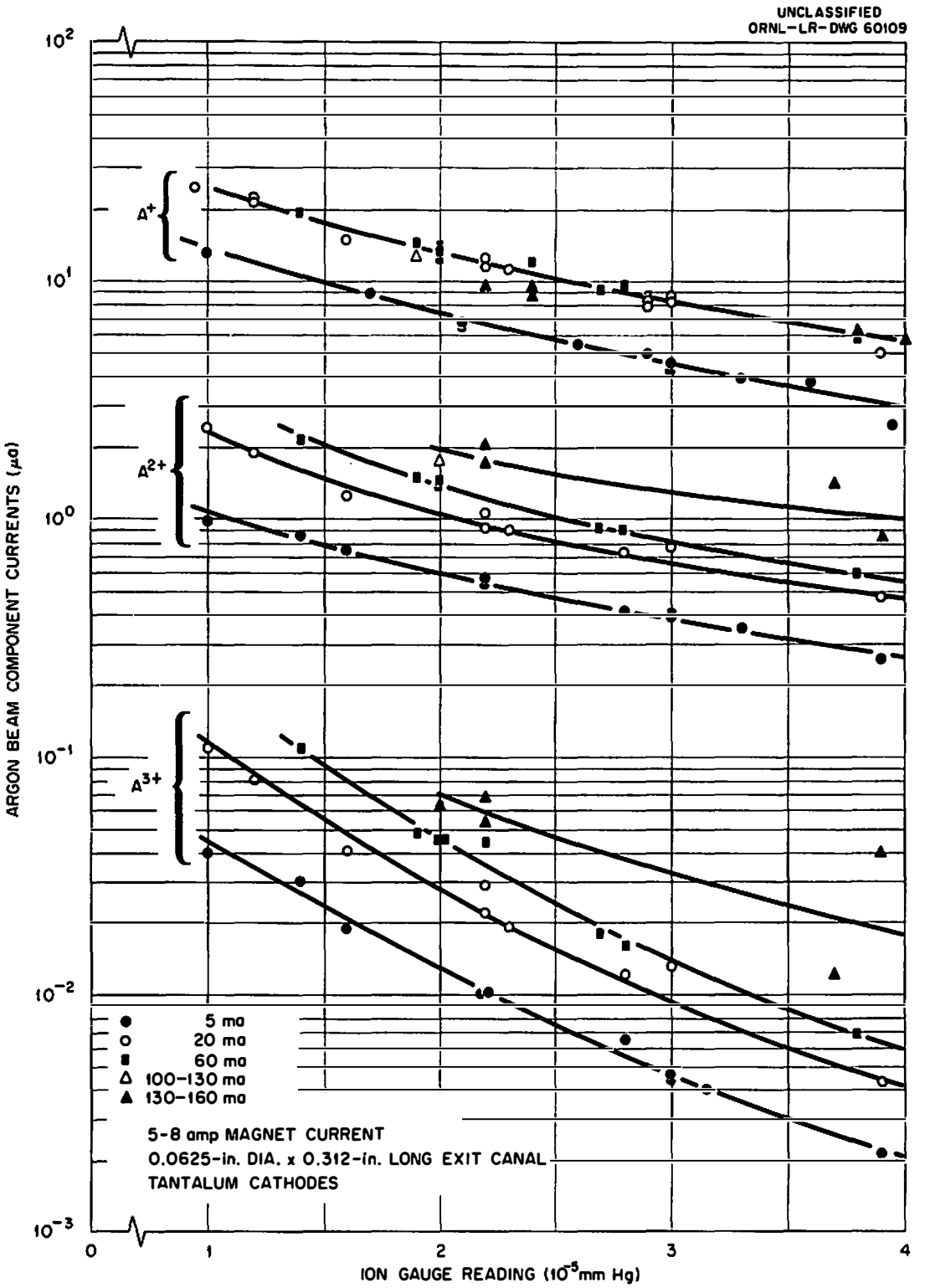

Fig. 15. Argon Output Components in the PIG Source.

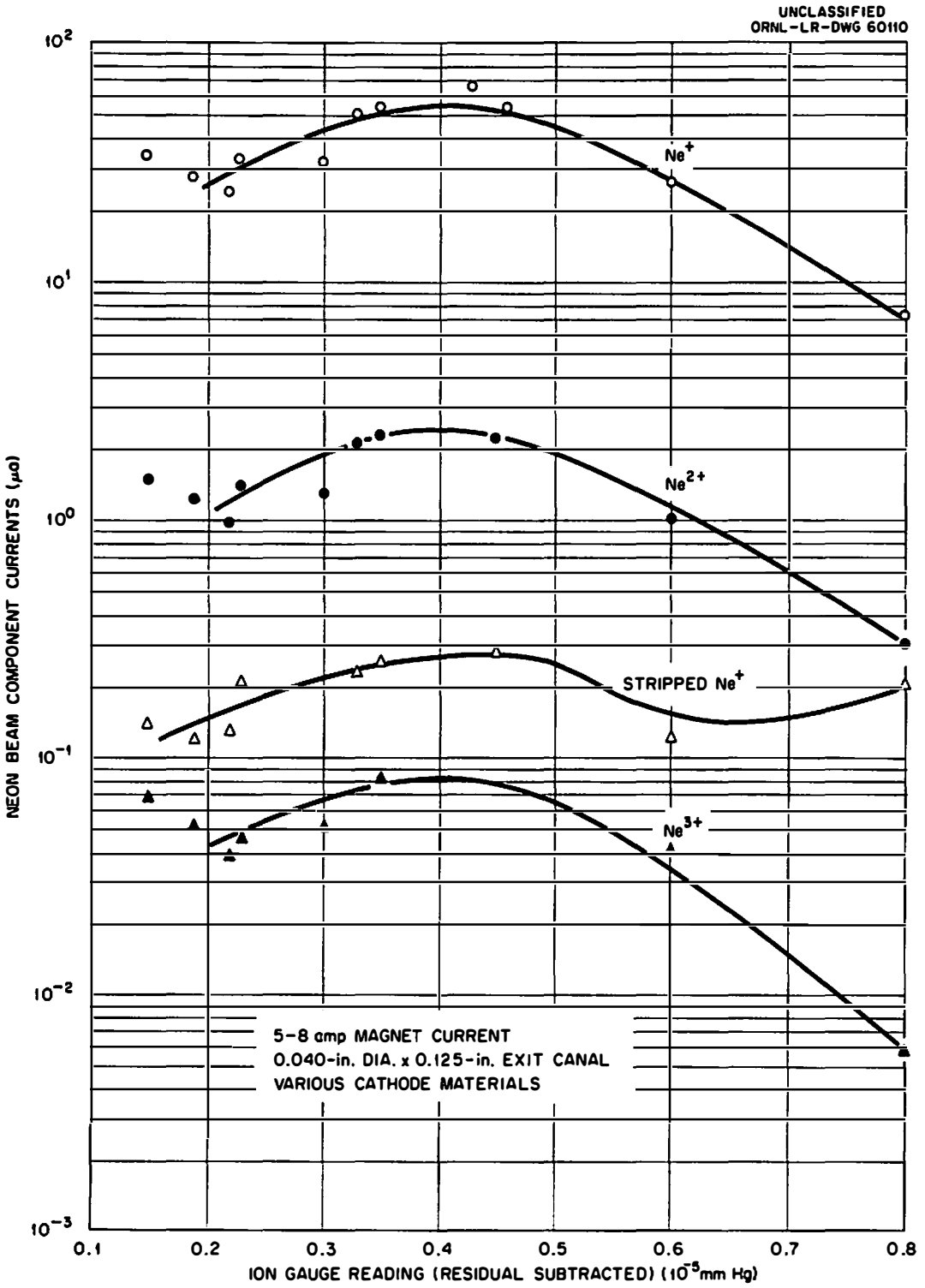

Fig. 16. Neon Output Components in the PIG Source.

Cockcroft-Walton analyzing system. An uncertain knowledge of the constituent gases in the beam path, and a geometrical complication, prevented more than the following qualitative corrections for the charge exchange.

Figure 16 contains some measurements of a beam component which was due to Ne^{+} being accelerated and then stripped to Ne^{2+} ahead of the magnet. From data in references 4 and 12, it can be estimated that the cross section σ_{21} (for a reduction in charge) of 200 kev Ne^{2+} ions, is about equal to the cross section σ_{12} (for stripping) of 100 kev Ne^{+} ions. This calculation assumes that the beam and stripping gas are both neon. At lower ion gauge readings this is not a valid assumption.

Thus the curve of stripped Ne^{+} is about comparable to the expected loss of the Ne^{2+} beam. The sharp departure in shape of this curve from the others at about 0.6×10^{-5} mm Hg would be consistent with a combination of increased charge exchange and increased neon concentration in the accelerator.

From a further use of the cross sections, the expected loss of Ne^{+} beam by neutralizing charge exchange would not be serious at the pressures used. Data are not available for σ_{32} at 300 kev, but this cross section is expected to be quite large. The loss of Ne^{3+} is likely to be serious in nearly all the data.

Similar calculations for argon indicated that equilibrium charge exchange may be occurring for all the components at ion gauge readings

of about 1 x 10^{-5} mm Hg or greater. However, the mixing of other gases in the beam path contributes an uncertainty to the estimates.

The shallower A^{3+} curve in Figure 15 for the most intense discharge suggests that charge exchange might not have been completely at equilibrium, and that the source characteristic was partly represented. Additional data were taken up to a discharge current of 300 ma., but above 60 ma. the rapid drifting of gas pressure and current precluded any trustworthy results. Water cooling did not help this runaway condition. In a general way qualitative observations of this performance confirmed the trend noticed below 60 ma., i.e., increased intensity appears to favor the multiple charge fractions.

The ion sources of references 2 and 3 had operated in an intense mode with relatively large (many milliamperes) total beams. But a weak beam had always been measured for the intense mode operation in the present work. From the first experiments in this mode it was not known whether the poor total beam in the present source were due to properties of the discharge or extraction, or to external conditions such as charge exchange.

A small pump was installed above the magnet. There was an appreciable decrease in the current of stripped Ne^{+} at low ion gauge readings, but not at high ones. It was not feasible to radically increase the pumping speed in the accelerator system.

Several possible "internal" conditions which could be studied were: (1) unfavorable conditions for an apparent competition between

improved extraction at a low flow and increased multiple charge formation at a higher flow, (2) excessive outgassing and a consequent detrimental effect by the contaminant ions, and (3) operation of the ion source at an intermediate intensity which was not great enough to supply rich multiple charge fractions.

Several changes were incorporated to test for the first effect. The lens was altered to give increased pumping right up to the canal. Different diameters and lengths were tested for the canal. The lens electrode shape was changed in such a way as to reduce the magnetic field divergence in the discharge region by a factor of four. Different cathode materials were tested in an attempt to increase the electron density in the gas.

Of these, only the cathode material had a significant effect on the maximum measured beams. Even so, only about a 20% improvement in the Ne^{3+} beam could be obtained with the best material, aluminum. This performance was, moreover, erratic. Presumably an oxide coating[18] increased the secondary emission, but it would not withstand continued operation.

A reduction in outgassing was attempted by substitution of several critical materials. Teflon, pyrex and boron nitride insulators each decreased the pumpdown time from that required by lavite insulators.

---

[18] J. D. Gow and J. S. Foster, Jr., University of California Radiation Laboratory report, UCRL-1698 (1952).

Also a stainless steel anode appeared to outgas less than the carbon one. However, none of these changes allowed a significant increase in the operating current.

IV. PULSED OPERATION OF THE PIG SOURCE

Ac power supply. An approach which could both reduce the outgassing and increase the intensity was to pulse the ion source. For the first attempts at this, advantage was taken of the natural rectifying characteristic of the PIG discharge by operating it from a 60 cps ac supply. A peak discharge current up to 0.9 amperes was reached, along with a duty cycle as low as 15 per cent. Such a reduced duty cycle can be achieved because the ion source does not "fire" until the applied voltage reaches a certain value in the cycle. Figure 17 shows some of the beam current pulses which were obtained with this type operation.

This method of operation appears not to have been reported in the literature, but the prospects were interesting enough to justify tests of some of the characteristics.

Only neon gas was used in these tests. Up to 2000 volts r.m.s. could be applied to the ion source by the use of a heavy duty transformer and a "Variac."

With the ac operation and a conventional exit canal (0.040 inch diameter by 1/8 inch long) the maximum total measured beam was 6.5 microamperes (dc average) and the maximum Ne^{3+} component was 0.085

UNCLASSIFIED
ORNL-LR-DWG 60111

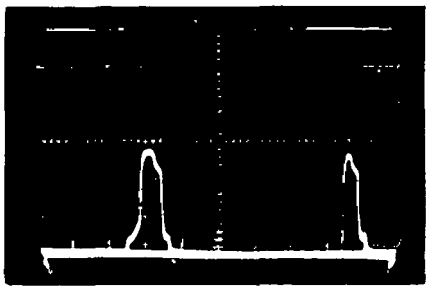

(*a*) TOTAL OUTPUT CURRENT PULSE; 1.6×10^{-6} mm Hg PRESSURE; AC VOLTAGE = 1700 rms

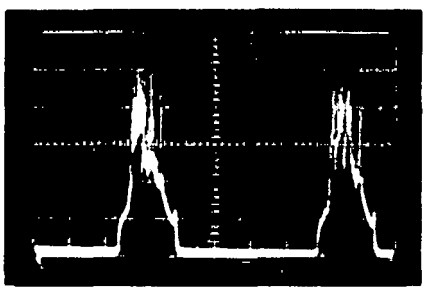

(*b*) TOTAL OUTPUT CURRENT PULSE; 4.3×10^{-6} mm Hg PRESSURE; AC VOLTAGE = 2000 rms

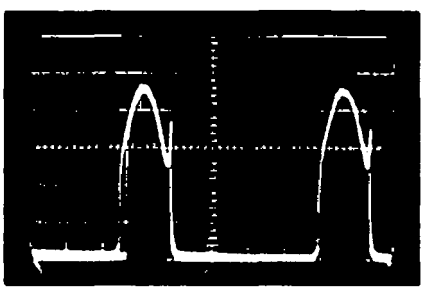

(*c*) SAME AS (*b*), BUT REDUCED AC VOLTAGE.

Fig. 17. Display of Output Pulses With A.C. Operation of the PIG Source.

microamperes. The operation was usually not stable below an ion gauge reading of about 0.7 to 0.8 x 10^{-5} mm Hg. Oscilloscope observations showed that at low pressure the ion source was failing to fire on random cycles.

Exit canals with about three times and ten times greater flow conductances were also tested. No significant change in output was noticed for the intermediate canal. The larger canal only increased the maximum measured beam currents to 10 microamperes total and 0.01 microamperes of Ne^{3+}.

A number of modified methods of operation were tested, but none produced a significant increase in the measured beam currents. A larger series resistor made possible lower pressure operation, but with reduced pulse intensities. A series rectifier was used, with a dc "keep-alive" voltage.[2] Also, a biasing dc voltage (for preventing polarity reversal) failed to improve the performance.

It was interesting that the lens could also be operated with an ac voltage, with only a slight reduction in the beam components.

Operation with a pulser. In order to have sharper and shorter pulses, a pulser was built. It was able to deliver one ampere pulses to a 2000 ohm load. The duty cycle was adjustable from 0.03 to greater than 0.10.

The source was tested with 0.040 inch diameter exit canals (and later with an 0.020 inch diameter canal). Neon gas was used. A 4000

volt dc supply was pulsed, and the pulses appearing across the source were about 1500 to 2000 volts. The internal impedance of the pulser was all the series resistance that was needed.

With the pressure below about 1.2×10^{-5} mm Hg the one ampere discharge current pulses would not fill out to the full (600 microsecond) length of the applied voltage pulse. Instead, they were sharp "spikes" about 4 microseconds long and one ampere high.

The measured Ne^{3+} current reached a maximum for a reading of 0.6×10^{-5} mm Hg on the ion gauge. The average dc value of the collected current at this pressure was 0.012 microamperes of Ne^{3+} and 17 microamperes of total beam. These currents are not impressive except when the small duty cycle is considered. The peak rate of the total beam appears to have approached that of the Anderson-Ehlers source.

As the gas flow was increased to an ion gauge reading of 1.2×10^{-5} mm Hg the pulses rather quickly filled out to the 600 microsecond length. This suddenness is not understood. In the full pulse operation the peak rates were reduced to values comparable with the maximum dc values except that the peak Ne^{3+} current collected was about twice as great as the dc maximum.

A way was not found to operate with full length pulses at an increased rate, or to lengthen the "high output" pulses. Table I lists some results which show the nature of the transition between the two types of operation. These results were obtained with an exit canal of 0.020 inches diameter and 1/8 inch long. Also, the duty cycle was increased to about 0.065.

TABLE I

PIG SOURCE CHARACTERISTICS, PULSED OPERATION

Ion Gauge Reading 10^{-5} mm Hg	I_D Average Current Milliamperes	Total Beam, Average Current Microamperes	Ne^+ Average Current Microamperes	Ne^{3+} Average Current Microamperes
0.48	< 1	13	4.0	0.006
0.55	< 1	-	4.0	0.010
0.69	< 1	-	4.0	0.011
0.78	~ 5	-	4.3	0.012
0.95	16	-	3.9	0.02
1.0	12	-	1.4	0.006
1.2	16	-	1.1	0.0035
1.5	25	-	0.45	0.0017
1.9	50	-	0.19	0.0011
2.7	52	4.3	0.08	0.00075
1.9	15	4.4	0.31	0.001
1.1	10	7.7	0.75	0.0027
0.86	10	7.5	0.65	0.0019
0.61	< 1	12.5	4.3	0.008

Alumimum cathodes were used in one test. They allowed operation at about half the pressure that was needed with titanium, and also the output current at high pressure was much increased. But the maximum measured total beam and multiply charged components were essentially the same as with titanium cathodes.

V. OPERATION ON THE VAN DE GRAAFF

Installation considerations. The low intensity mode of operation of the PIG source was used in the Van de Graaff. The low gas flow of this mode was particularly necessary in the Van de Graaff because of the ~ 25 liter per second pumping speed of the 12 foot long accelerator tube.

For simplicity of focussing the PIG source was designed so that its position relative to the accelerator tube was the same as that of the r.f. ion source. Still, a nearly doubled lens voltage was needed to focus the beam from the PIG source.

From considerations of the focussing properties of the accelerator system,[19] it was estimated that the entrance of the accelerator tube was acting like a single aperture lens which was too strong for the PIG source-lens combination. To weaken it, the top seven resistors of the Van de Graaff were paralleled with equal values. Following this, it was possible to focus with about 10 to 15 per cent less lens voltage. But 70 to 75 kv were still needed on the lens to focus the beam at

---

[19] M. M. Elkind, Rev. Sci. Instr. 24, 129 (1953).

about 5 Mv accelerator voltage. (The focussing lens voltage is about proportional to the accelerator voltage.) This was enough to cause "spitting" of the lens.

As one attempted remedy, the lens separation was increased from 3/8 inch to 7/16 inch. Also, the lens hole was decreased to strengthen the focussing lens slightly. The top lens plate of aluminum was replaced by stainless steel to reduce pitting from the sparks. A five liter per second PIG type pump was connected to the lens region to reduce the pressure there. Finally, a new ion source with reduced gas flow was fabricated. However, it had other difficulties and could not be used extensively.

Only a slight improvement resulted from these changes. Operation of the Van de Graaff was still limited to 5.1 or 5.2 Mv, because of beam instability introduced by lens breakdown.

The performance of an ion source on the Van de Graaff is intimately associated with the focussing properties of the accelerator tube. The r.f. ion source output usually measures more than 120 microamperes at the lens at the top of the accelerator, but usually no more than 50 microamperes is measured in a collector cup above the analyzing magnet.

Possibly the inherent focussing characteristics of the source and accelerator limit the accelerated beam. But also a pressure scattering effect has been suggested as a possible explanation of the loss of beam. In this effect either electrons or ions, because of ion-gas collisions, would collect along the electrodes of the accelerator tube.

(The inside of the accelerator tube is 3 inches in diameter at the center, and 5 inches in diameter at the ends.) This would be expected to distort the accelerating field, and result in an altered focussing characteristic of the accelerator tube.

The stripping required for heavy ions contributed another problem -- that of belt upcharge current. In spite of such precautions as a diaphragm and an auxiliary pump, the ion gauge reading in the Van de Graaff was as much as five to ten times higher than normal when the stripping gas was used. Electrons formed by the numerous ion-gas collisions travel up the accelerator and increase the belt charge required to maintain the terminal voltage. The belt upcharge limit for the accelerator was about 400 microamperes. This was often the limiting factor on the Ne^{3+} current that could be accelerated.

The new ion source mentioned above was designed to circumvent the gas leaks from the discharge region to the lens, by paths other than the exit canal. These had occurred mostly around the insulators. Even though tolerances of only several thousands of an inch were used, the relatively large circumference of the insulators resulted in a cross sectional area which was large compared to that of the exit canal. It was estimated that 5 to 30 times as much gas went through the leakage path as through the canal. The outer chamber of the ion source had to be pumped out to prevent a discharge in it.

In the revised source there were seals at all the insulator joints. After a little operation it was apparent that the leakage had

been beneficial. The reduced flow was very hard to control. Sometimes the ion source appeared to operate with 8 to 10 ma. discharge current about as it had on the Cockcroft-Walton with 200 ma. A larger exit canal diameter of 0.030 inches did little to relieve this. The rapid shorting from flaked cathode material was the critical factor. At the best, there were only a few hours of operation before a short occurred.

The 0.030 inch diameter canal which was used most of the time in the Van de Graaff was a compromise. The discharge region had to be swept adequately but the pressure at the lens needed to be minimized.

Performance in the Van de Graaff. Figure 18 shows the qualitative pressure characteristic of the PIG source in the Van de Graaff. This is not greatly different than it had been in the Cockcroft-Walton, even though the combined effect of the source, the accelerator, and stripping is included. The peak output characteristic is only estimated, as the belt upcharge limitation prevented operation in that region.

A total indicated beam of 110 microamperes was obtained above the magnet at one time, and routinely 70 to 80 microamperes were indicated. It is not known whether the reduced gas flow (about two to five times less than that of the r.f. ion source), different focussing characteristics, or some other factor allowed this increased accelerated beam.

The maximum Ne^{2+} and Ne^{3+} components could not be measured directly. They were collected as Ne^{5+} and Ne^{6+} components, respectively, after stripping and analysis in the magnet. The maximum measured quantities were 1.5 microamperes of Ne^{5+} and 0.04 microamperes of Ne^{6+}.

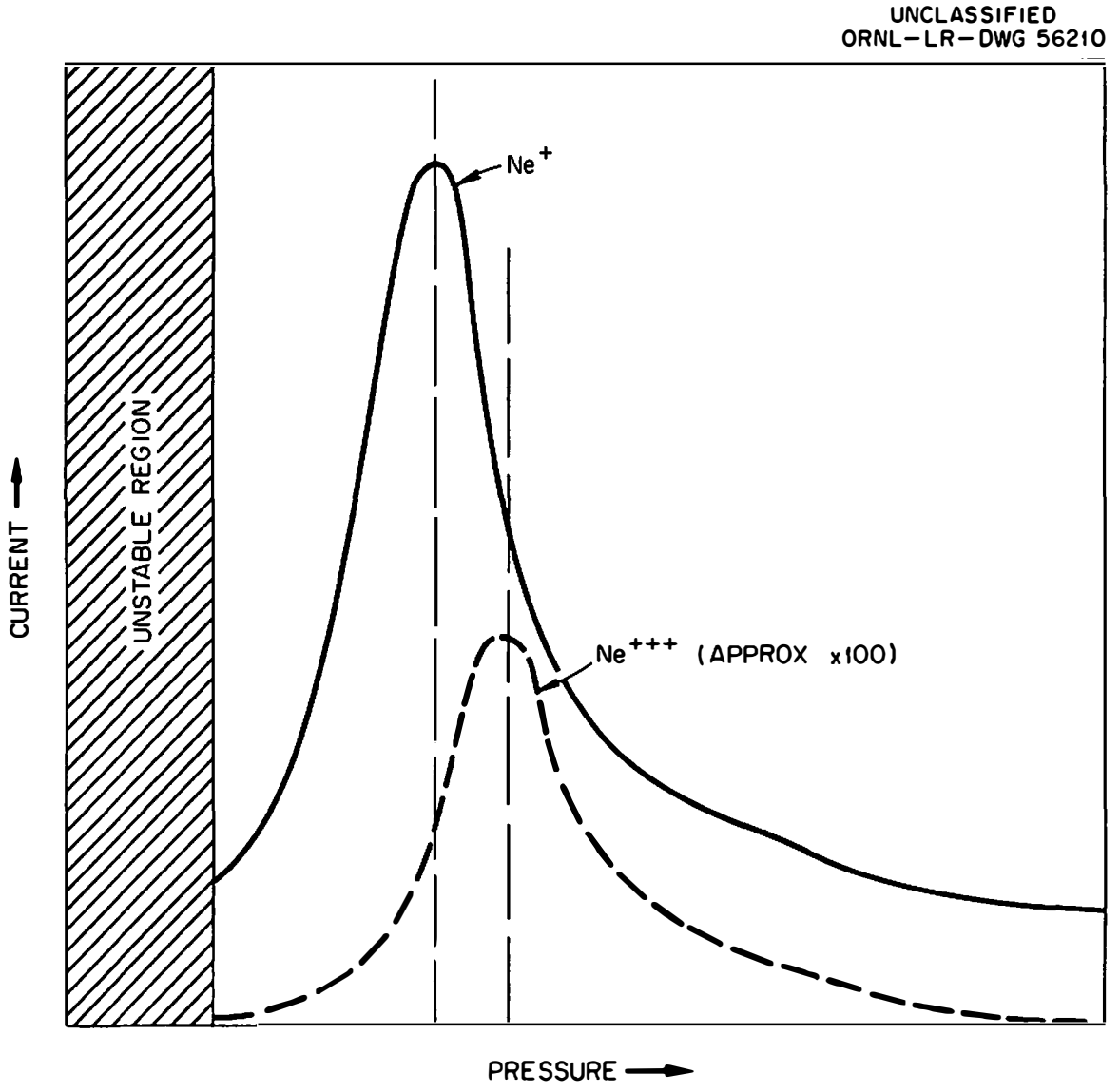

Fig. 18. Pressure Characteristic of the Heavy Ion PIG Source in the Van de Graaff.

At 10 Mev and 15 Mev ion energies, respectively, it can be estimated[20] that 23 per cent of the Ne^{2+} and 33 per cent of the Ne^{3+} ions were stripped and measured. Thus the corresponding estimated currents preceding the stripper are about 2.6 microamperes of Ne^{2+} and 0.06 microamperes of Ne^{3+}.

Nitrogen ion operation. Nitrogen gas was also used briefly in the PIG source on the Van de Graaff. The maximum measured beam components were more than an order of magnitude less than the corresponding ones for neon. No N^{3+} was found. The maximum measured singly charged component was about five microamperes. (Actually about ten microamperes of N_2^{2+} was collected.) There appeared to be several strong molecular nitrogen components.

VI. THE RADIO FREQUENCY ION SOURCE

The radio frequency ion source[21] which is routinely used on the ORNL 5.5 Mv Van de Graaff has a discharge in a pyrex bottle about one inch in diameter and seven inches long. A 70 megacycle rf oscillator delivers up to 25 watts to the gas and the gas bottle. The rf coupling to the discharge is usually by means of clips around the bottle (capacitive), but it can also be with the oscillator coil slipped over the bottle (inductive).

---

[20] R. L. Gluckstern, Phys. Rev. 98, 1817 (1955); E. L. Hubbard and E. J. Lauer, Phys. Rev. 98, 1814 (1955).

[21] C. D. Moak, H. Reese, and W. M. Good, Nucleonics 9, 18 (1951).

At the top of the bottle a metal "probe" is made positive by 0-5000 volts with respect to a tip at the bottom, which contains the exit canal. Thus the positive ions are driven to the canal. Focussing and further ionization occur at the top of the exit canal. A toroidal coil around the base supplies a magnetic field of up to a few hundred gauss. This is said to increase the discharge strength,[22] particularly at low gas pressure.

The normal variables of this ion source are the pressure, oscillator voltage, magnetic field strength and probe voltage. For this work the oscillator frequency, method of coupling, tip material and canal diameter were also varied. The testing was done with neon and argon gases on the Cockcroft-Walton accelerator.

At the outset there was an uncertainty introduced by a limitation on the maximum probe voltage. With the heavy ions, and at lower probe voltage than that for the peak output, there would occasionally be a bright "burning" at the tip which would usually ruin the bottle. For most of the data the probe voltage was set less than optimum to avoid this.

The pressure characteristic of the r.f. source appeared to be similar to that for the PIG source. However, the maximum multiple charge components measured in the Faraday cup were very weak while the ion source bottle was clean. With such operation, at a fairly low pressure, the ion source life appeared to be adequate.

---

[22] B. Koch and H. Neuert, Z. fur Naturf. 4a, 456 (1949).

At an increased pressure, or under some conditions at 30 megacycle operation, the pyrex bottle soon (in about 1/2 to 2 hours) became darkened with sputtered tip material. After this the multiply charged components would be increased, but the discharge would be unstable. Finally the discharge would fail and could not be started again.

As tip materials, aluminum, tantalum and nickel were all tested. There appeared to be no clear choice among them.

The standard canal diameter in this work was 0.066 inches. A 0.045 inch diameter canal and a 0.078 inch diameter canal were tested. The smaller canal did not seem to change the performance measurably. The large canal reduced the range of stable operating pressures, but it did not significantly alter the output.

A limited amount of testing was done by varying both the modes of coupling and the oscillator frequency (down to 20 megacycles). A mode of operation with increased multiple charge output was not found.

The maximum total output of the r.f. source was measured as 360 microamperes with neon. At such large beams less than 1/4 of the total beam measured above the magnet was bent and collected as components in the Faraday cup. The maximum Ne^{2+} and Ne^{3+} components were measured when a darkened bottle was used. They were 1.2 microamperes and 0.028 microamperes, respectively.

CHAPTER IV

THE COULOMB EXCITATION EXPERIMENTS

There are three parts to this chapter. They cover the experimental arrangement, the procedure, and a limited extraction of the experimental results. Primarily the experimental results given here are those that can be derived directly from the yields and angular distributions. The more detailed analyses are left for the next chapter, along with the interpretation.

I. THE EXPERIMENTAL ARRANGEMENT

Figure 19 shows, schematically, the main features of the accelerator and detection system. The ORNL 5.5 Mv Van de Graaff is the primary component. Except for the ion source and terminal, it is conventional. There are, however, some more or less unusual features in the auxiliary equipment.

The 90^{o} analyzing magnet, shown in Figure 20, could not bend the heavy ions sufficiently in the charge state at which they were accelerated. Therefore additional electrons were removed by an argon gas stripper. The gas was fed to the center of a tube about 18 inches long and 3/16 inch inside diameter, at about 20 microns pressure.

After stripping there are numerous beam components, each bent differently according to the charge before and after stripping. The

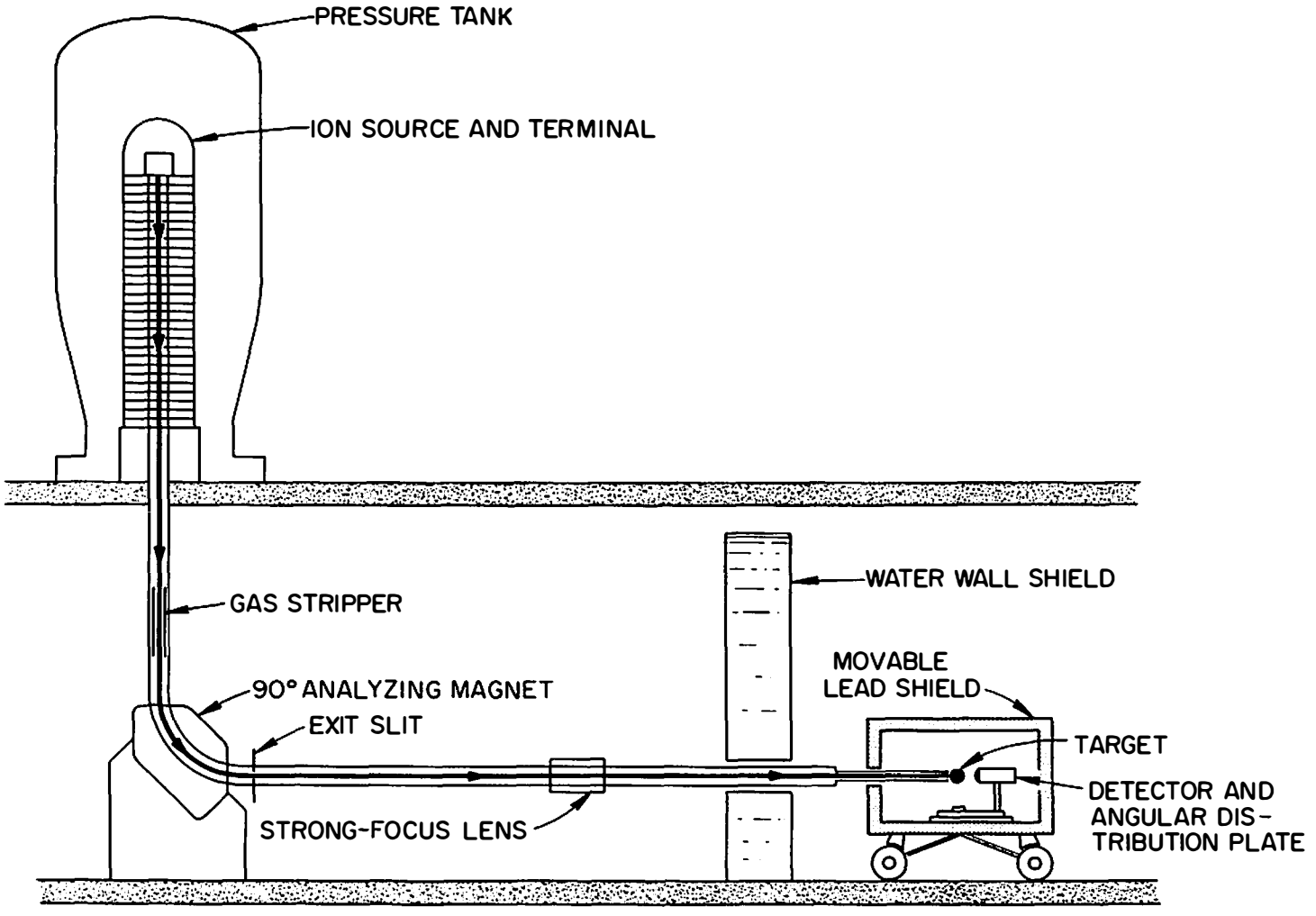

Fig. 19. Simplified Diagram of the Accelerator and Detector System.

UNCLASSIFIED
PHOTO 49734

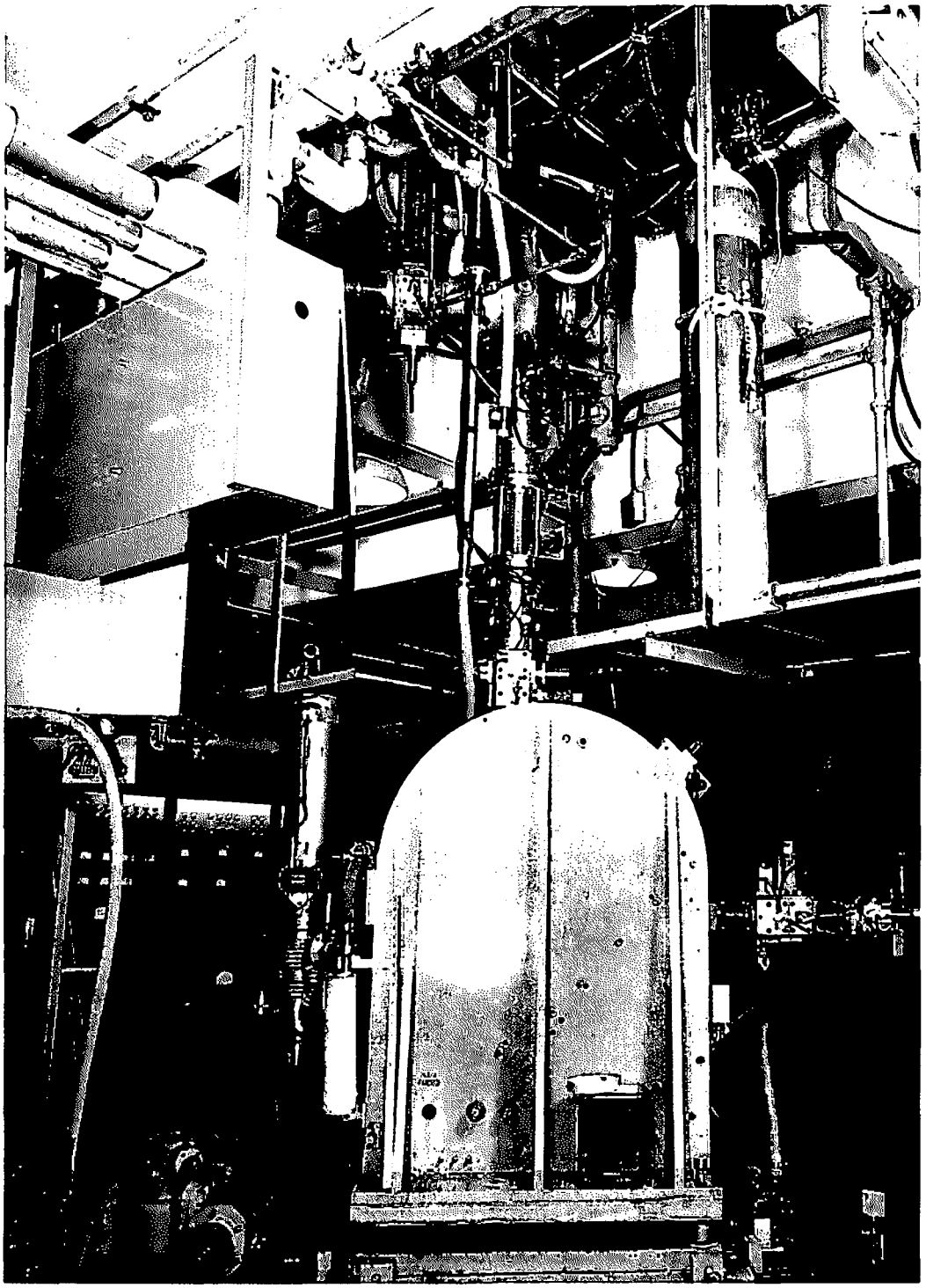

Fig. 20. Base and Analyzing Magnet of the ORNL 5.5 Mv Van de Graaff.

relative populations of neon components stripped by argon have been studied as a function of energy.[1]

There was about a 30-foot separation of the magnet and target. This necessitated additional pumping along the tube, and a strong-focussing lens.[2]

A large, movable lead shield housed the detector(s).[3] In the shield a graded copper and cadmium lining reduced the number of lead X-rays which reached the detector. In one measurement the shield reduced the low energy gamma ray background counting rate, with the Van de Graaff running, by a factor of about 1,000 from the rate in the room.

The detector(s) and angular distribution plate are accessible from the top by a sliding door. For all the work reported here, the detectors were 3 inch diameter by 3 inch long NaI(Tl) crystals mounted on DuMont type 6363 photomultiplier tubes. The angular distribution plate allowed placement of the detectors at any radii up to about 20 cm, and at accurately fixed 10° angular intervals. The plate could be adjusted to any location within about 1/4 mm.

Figure 21 schematically depicts the detector locations. The target was inclined 135° with respect to the beam direction. (Angles

---

[1] E. L. Hubbard and E. J. Lauer, Phys. Rev. 98, 1814 (1955); R. L. Gluckstern, Phys. Rev. 98, 1817 (1955).

[2] See C. H. Johnson, J. P. Judish and C. W. Snyder, Rev. Sci. Instr. 28, 942 (1957).

[3] P. H. Stelson and F. K. McGowan, Reactions Between Complex Nuclei, (John Wiley and Sons, Inc., New York, 1960), p. 47.

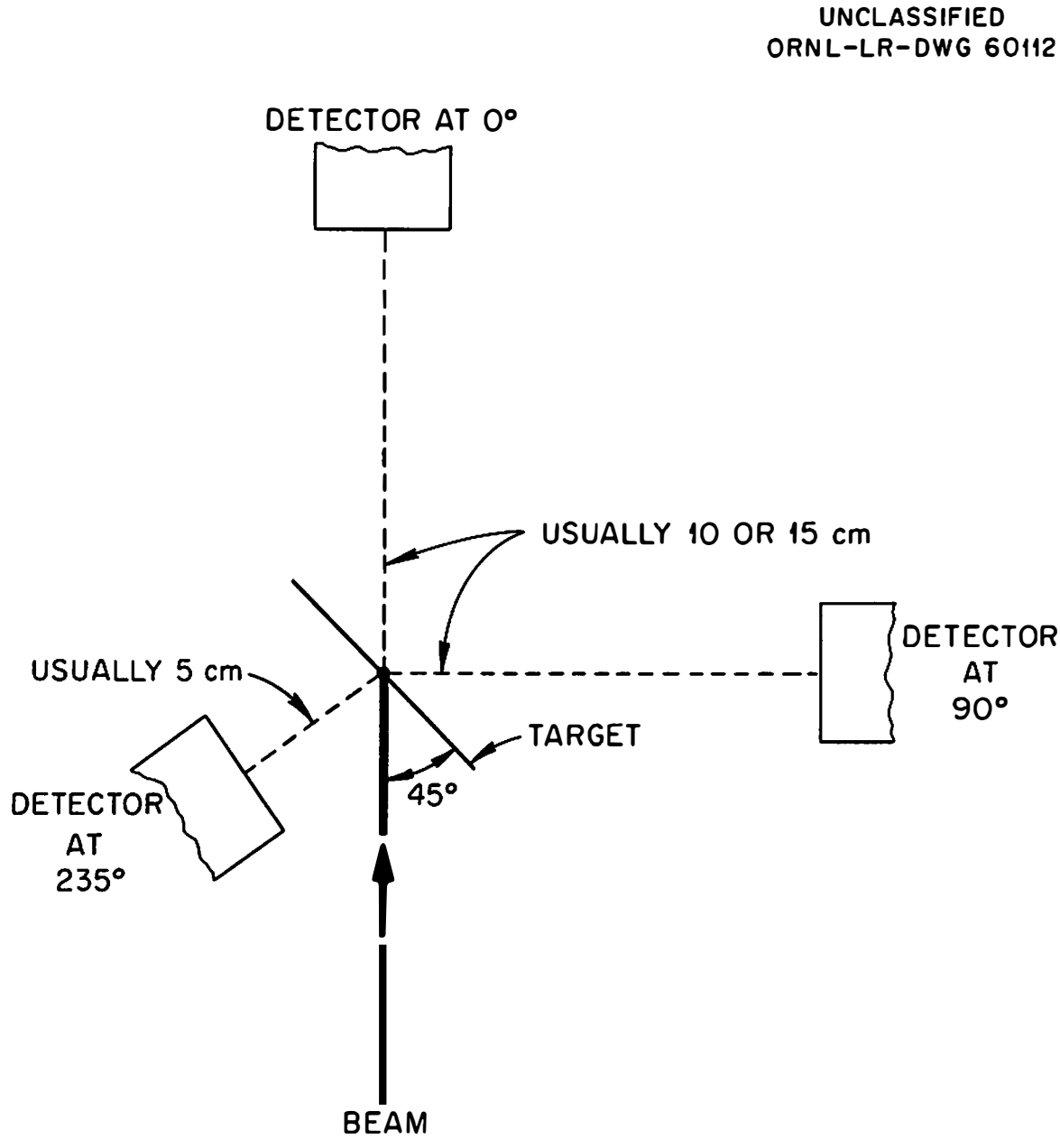

Fig. 21. γ-Ray Detectors, Top View.

are measured clockwise, from above, starting with the beam direction.) Anisotropy measurements could therefore be taken at 0° and 90° with similar geometries. Usually a 10- or 15-centimeter detector distance, h, was chosen for the anisotropy measurements as a compromise between a favorable counting rate and "poor geometry," (the "smearing" out of the distribution due to the finite detector size). Also, at greater distances the decentering error was reduced.

Yield measurements were normally made with the detector at 235° and 5 cm from the target. In this position $P_2(\cos \theta)$ is nearly zero and the yield measurement nearly represents an angle independent one.[4] Also, at this position the gamma rays need travel only through the 0.005 inch thick stainless steel tube extension to reach the detector. At frontal angles, they would have to travel through the thicker, variable targets. (Most of the gamma rays originate near the inside surface of the target.)

The electronic equipment for most of the experiments was conventional. A 256-channel pulse-height analyzer recorded and printed out the gamma ray spectra, both for yield and for angular anisotropy measurements. For the coincidence measurement of Fe^{57}, the "fast-slow" coincidence method was used.[5]

---

[4] P. H. Stelson and F. K. McGowan, Phys. Rev. 99, 112 (1955).

[5] See, e.g., P. R. Bell, Beta- and Gamma-Ray Spectroscopy, ed. Siegbahn, (North-Holland Publishing Co., Amsterdam, 1955), p. 133.

For each run, the total number of particles striking the target was measured with a current integrator. However, the possibility of charge exchange in the beam, in the interval between the magnet and the target, adds some uncertainty to the quantity. This is discussed in Section III of this Chapter.

The accelerator energy stability and the accuracy of the measurement of the energy are thought to be about as good as 0.2%. A servo system (in which the differential current to the magnet exit slits controls the terminal voltage by means of corona current) provides stability of the beam position to about one mm vertically. The horizontal movement (short term) is less than this. Known reaction thresholds provide the energy calibration of the magnet. A nuclear magnetic resonance probe monitors the magnetic field.

II. EXPERIMENTAL PROCEDURES

All of the Coulomb excitation experiments involved the selection of a suitable current for each target. Particularly for oxides and germanium metal, the heating of the target limited the current which could be used. In several cases the estimated limit was about 0.1 microampere. In each run, the bombardment was continued long enough to obtain a "statistically good" spectrum.

In the yield measurements, about six different bombarding energies from 8 to 15.4 Mev (on different days) were used with most of the targets of the eight medium-light nuclei. Less complete yield measurements (usually only at the maximum beam energy) were made on a number

of lighter and heavier elements. These were made to obtain a general survey of the neon ion Coulomb excitation character.

For the anisotropy measurements, spectra were taken at 0^{o} and 90^{o}. The anisotropy is defined as $A = \frac{W(0^{o})}{W(90^{o})} - 1$. The ratio $R = \frac{W(0^{o})}{W(90^{o})}$ was needed as accurately as possible. Two per cent estimated errors were typical. A rigorous procedure was used for positioning the beam, the detector plate, and the target mount. Individual values of R were normalized by comparing them with measurements of Mn^{55}, which was assumed to be isotropic.[3]

III. EXPERIMENTAL RESULTS

Compilation of basic results. In Table II the "best" present results for $\epsilon B(E2)$ and A_2 are listed. (A_2 is the angular distribution coefficient of Chapter II). The ϵ used here is defined as the ratio of the observed gamma ray yield to the total de-excitation of the state. It accounts for internal conversion and cascade gamma rays.

In Table II other reported values of $\epsilon B(E2)$ are given. The references, in many cases, were the latest known for a given work. For example, the review paper, reference b, contains a number of privately circulated revisions of original results. Other reported A_2 values are not listed, because very few have been given in the literature.

The assigned accuracy for all the $\epsilon B(E2)$ values listed in this Chapter, except for Mn^{55} and Zn^{67}, is $\pm$ 15 per cent. (See Appendix B.)

TABLE II

COMPILED YIELD AND ANGULAR DISTRIBUTION RESULTS

Nucleus	Level Kev.	Target Compound	Target Enrichment	$\epsilon B(E2)$ $e^2 \cdot 10^{-48} cm^4$	Other $\epsilon B(E2)$ Values	A_2
Li^7	478	Li_2Co_3	nat.	0.00076	0.00073[a]	-
F^{19}	197	CaF_2	nat.	0.005	0.005[a];0.003[b];0.002[b]	-
Na^{23}	438	NaCl	nat.	0.015	0.013[b];0.011[a];0.0095[c]	-0.015 ± 0.015*
Ti^{47}	160	TiO_2	0.856	0.028	0.040[b]	-0.035 ± 0.012
V^{51}	320	V_2O_5	nat.	0.013	0.013[c];0.012[d];0.0056[b]	$+0.239 \pm 0.015$
Cr^{53}	155	Metal	0.953	< 0.00005	0.015[b]; < 0.0001[e]	-
Mn^{55}	126	Metal	nat.	(0.031)**	0.087[b];0.075[b];0.057[f]	-
Fe^{57}	136	Fe_2O_3	0.838	0.037***	0.043[g];0.050[h];0.044[f]	-0.036 ± 0.025
Fe^{57}	364	Fe_2O_3	0.838	0.037	0.033[h]	$+0.132 \pm 0.018$
Ni^{61}	67	Metal	0.744	0.00064	0.00038[i]	-0.010 ± 0.021
Ni^{61}	282	Metal	0.744	0.0012	0.00090[i]	-
Zn^{67}	93	Metal	0.924	0.00011[f]	-	-

TABLE II (continued)

Nucleus	Level Kev.	Target Compound	Target Enrichment	$\epsilon B(E2)$ $e^2 \cdot 10^{-48} cm^4$	Other $\epsilon B(E2)$ Values	A_2
Zn^{67}	184	Metal	0.924	(0.018)**	0.032[i]	+0.227 ± 0.007
Ge^{73}	67	Metal	0.861	0.046	0.085[i]	+0.036 ± 0.015
As^{75}	199	As_2O_3	nat.	0.015	0.016[b];0.025[b]	-0.022 ± 0.017
As^{75}	280	As_2O_3	nat.	0.052	0.050[b];0.071[b]	-0.197 ± 0.026
Ru^{101}	127	Metal	0.911	0.028	0.061[b]	+0.114 ± 0.022
Pd^{110}	374	Metal	0.914	0.91	1.04[b];0.95[b];0.26[b]	//
Pr^{141}	145	Pr_6O_{11}	nat.	< 0.003	0.0036[j]	-
$Hf^{177,179}$	112	Metal	nat.	0.46***	0.59[b];0.39[k];0.84[l]	-
Ta^{181}	136	Metal	nat.	0.74	1.04[i];0.83[m];0.81[i];0.68[i]; 0.64[m];0.59[i];0.52[i]	-
Th^{232}	53	Metal	nat.	0.023	0.057[b];0.0096[b];0.02[n]	-

*The doppler effect was not included in the calculation.

**These values are suspect, because of possible surface layers.

TABLE II (continued)

***The measured γ-rays were unresolved ones from two transitions.

†Corrected for cascade γ-rays.

††Both A_2 and A_4 are significant. See the discussion.

[a]See reference 9.

[b]See the review article, reference 7.

[c]H. E. Gove and C. Broude, Reactions Between Complex Nuclei, (John Wiley and Sons, Inc., New York, 1960), p. 57.

[d]B. M. Adams, D. Eccleshall, and M. J. L. Yates, Reactions Between Complex Nuclei, (John Wiley and Sons, Inc., New York, 1960), p. 95.

[e]See reference 13.

[f]T. Huus, J. H. Bjerregard, and B. Elbek, Dan. Mat. fys. Medd. 30, No. 17 (1956). (The values here were calculated from those results, assuming $\alpha_T = 1.1\alpha_K$).

[g]See reference 14.

[h]G. F. Pieper and N. P. Heydenberg, Phys. Rev. 107, 1300 (1957).

[i]See reference 6.

[j]See reference 19.

[k]Data of Huus et al., as quoted in reference 6, was combined. See the discussion.

[l]Data of Heydenburg and Temmer, as quoted in reference 6, was combined. See the discussion.

[m]See reference 4.

[n]F. K. McGowan and P. H. Stelson, Phys. Rev. 120, 1803 (1960).

Except where stated otherwise, the gamma ray energies and energy level values are taken from the Nuclear Data Sheets.[6]

Method of extracting $\epsilon B(E2)$ and A_2 values. Only thick targets were used in this research. The projectile was completely stopped in the target. The calculated yield is obtained by integrating the cross section, as a function of projectile energy, over the range from incident energy to zero. The integrand must be weighted to account for the non-uniform energy loss throughout the projectile trajectory in the target. The weighting factor is the reciprocal of the stopping power, which is discussed in Appendix A.

The experimental yield, in gamma rays per incident particle, was obtained by using a standard analysis of the scintillation pulse-height spectrum.[4] Appendix C will give the detailed formulas for obtaining both the experimental and calculated yields. A comparison of these permits the evaluation of $\epsilon B(E2)$. For convenience in the present discussions, the formulas for the cross section and for calculating $\epsilon B(E2)$ are also given here. With a suitable insertion of constants, equation (16) from Chapter II becomes[7]

$$\sigma_{E2} = 4.819 \frac{A_1 K^2}{Z_2^2} E'B(E2) f_{E2}(\eta_i, \xi) \text{ barns} \qquad (28)$$

---

[6] Nuclear Data Sheets, (National Academy of Sciences, National Research Council, Washington, D. C.).

[7] See the review paper by K. Alder, A. Bohr, T. Huus, B. Mottelson, and A. Winther, Revs. Mod. Phys. 28, 432 (1956).

where A_1 is the projectile mass number, Z_2 is the target nuclear charge, $K = \frac{A_2}{A_1 + A_2}$ is a factor for center of mass corrections (A_2 is the target mass number) and $E' = E - \Delta E'$. E is the incident energy in Mev and $\Delta E' = \frac{\Delta E}{K}$, where ΔE is the excitation energy in Mev. B(E2) is the reduced transition matrix element in the conventional units, $e^2 \cdot 10^{-48}$ cm^4. The excitation function f_{E2} is, for the purposes here, the classical value in Figure 2, page 17.

The formula for the value of $\epsilon B(E2)$ is

$$\epsilon B(E2) = \frac{436.9\ A_2'\ Z_2^2}{A_1 n \eta\ K^2} \quad \frac{I'}{\int_0^E \frac{E' g(\xi) dE}{dE/d\rho x}} \tag{29}$$

Here n is the number of target nuclei per molecule, η is the isotopic fraction, and $g(\xi)$ is $1.2665\ f_{E2}(\xi)$. $dE/d\rho x$ is the stopping power, in kev - cm^2/mg. I' is the observed gamma-ray yield in gamma-rays per incident particle.

In this work the integral, in units of Mev - mg/cm^2, was determined numerically for each nuclear state of interest. The ORACLE computer at the ORNL was used. Figure 22 shows the "thick target integral" for three low-lying states in Fe^{57}, as a function of the incident energy E. The parameter ξ was obtained for each energy, at the same time. Because the yield is proportional to the thick target integral, curves such as Figure 22 are useful in considering bombarding conditions.

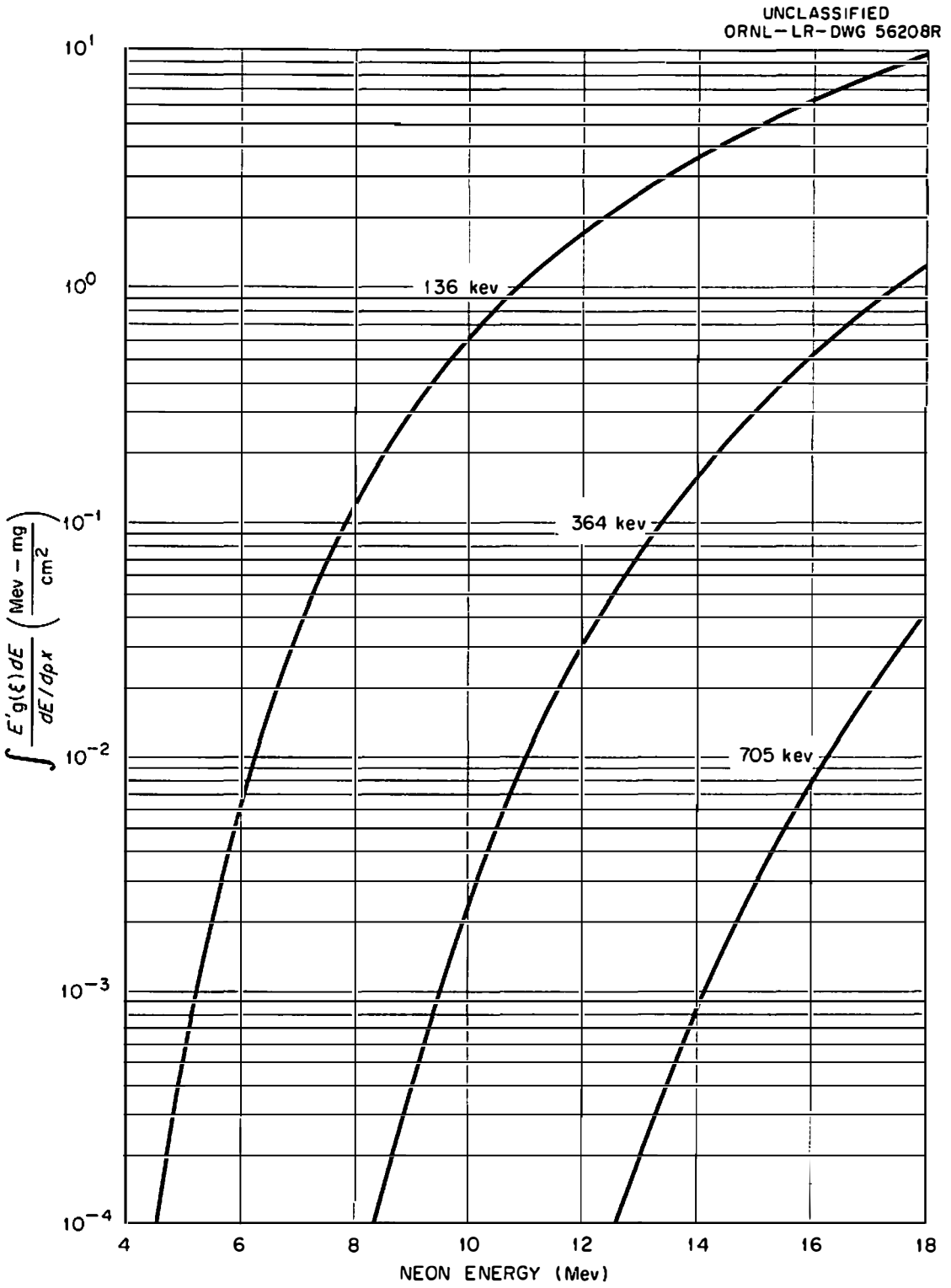

Fig. 22. Coulomb Excitation Thick Target Integrals, Neon Ions on an $Fe_2^{57}O_3$ Target.

A deviation from the predicted energy dependence of the yields appeared for some of the nuclei. It is seen, in Figure 23, as an energy dependence of the $\epsilon B(E2)$ values.

Among the possible reasons for the trend are: (1) a systematic error in the energy dependence of the $dE/d\rho x$ values used, (2) an unconsidered theoretical effect on the energy dependence, and (3) a systematic error in the recorded number of bombarding particles. The first two reasons appear unlikely. In particular, a number of experimenters use $dE/d\rho x$ as a constant in the region of interest, but the energy dependence used here would have a correction which was opposite to the observed trend. An error in the recorded number of particles might arise in several ways. Charge exchange in the beam, after the analyzing magnet, could cause the average ionic charge to be different from that assumed. It is estimated,[1] that this effect would cause less than five per cent variation in the $\epsilon B(E2)$. Another possibility is that charge exchange caused a small part of the beam to be deflected differently in the strong-focussing lens, so that it struck outside the 7/16 inch diameter target, but was still recorded as current. Estimates of the upper limit of this effect would correspond to a total $\epsilon B(E2)$ variation of about 7 per cent.

The angular distribution coefficient, A_2, was determined with the initial assumption that A_4 is zero. (Except for Pd^{110}, it is found that, coupled with a small particle parameter a_4, the small values of A_4 allow the term to be dropped. Then, if it is desired, a

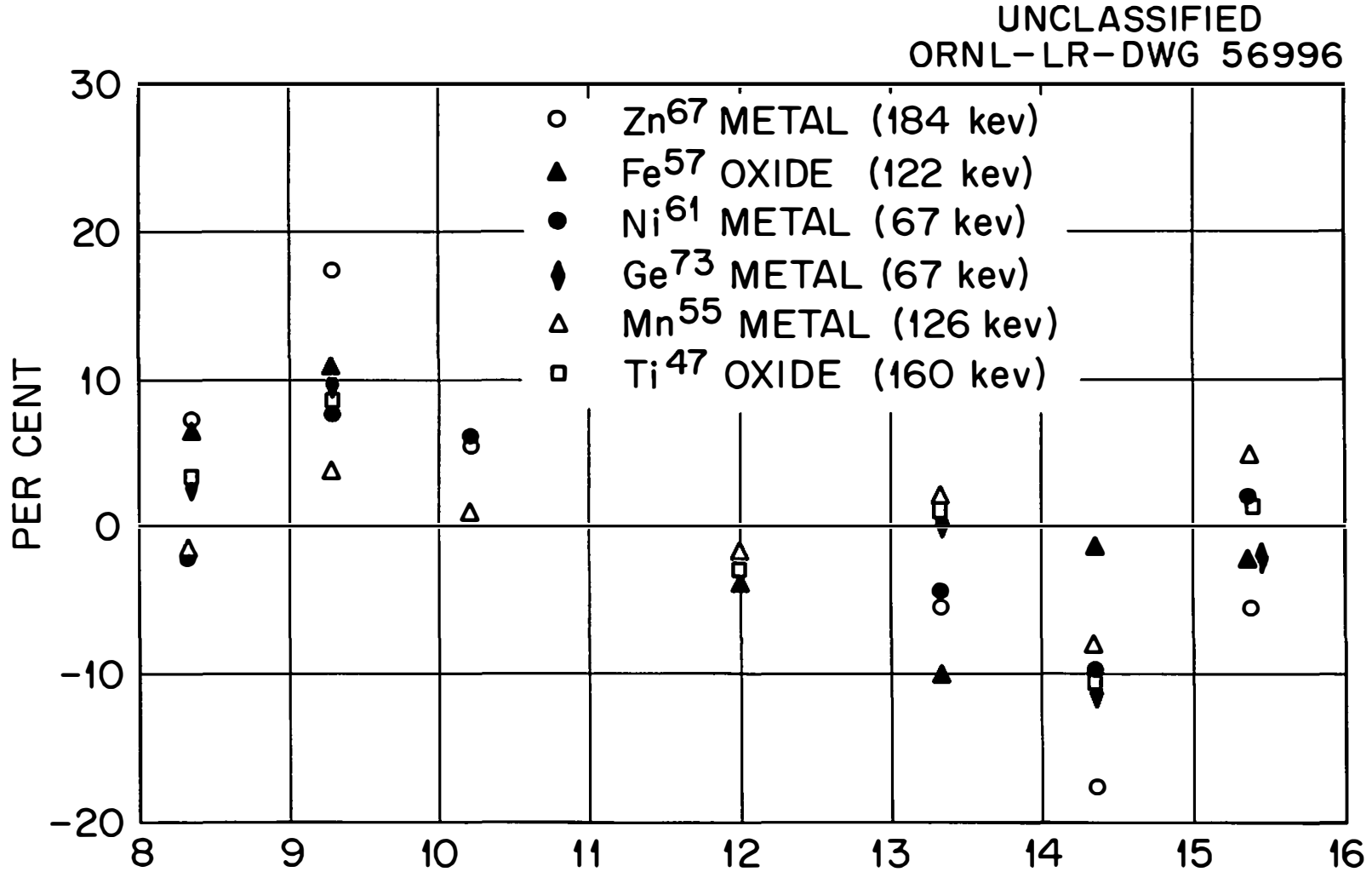

Fig. 23. Variation of Experimental $\epsilon B(E2)$ With Energy.

correction for the A_4 term can be estimated.) The ratio R is then written

$$R \equiv \frac{W(0^o)}{W(90^o)} = \frac{1 + a_2 A_2 g_2 \, P_2 \, (\cos 0^o)}{1 + a_2 A_2 g_2 \, P_2 \, (\cos 90^o)} \quad , \tag{30}$$

where g_2 is a factor which accounts for the finite detector solid angle.[8] From this the result is

$$A_2 = \frac{2}{a_2 g_2} \left(\frac{R - 1}{R + 2} \right) . \tag{31}$$

Li^7. The only measurement with this nucleus was the neon ion yield at 15.4 Mev. The observed value of 1.41×10^{-8} gamma rays per incident particle for the 478-kev gamma ray yield corresponds to an $\epsilon B(E2)$ value of 0.00076. This agrees with reference 9. That work, done at the same laboratory, was for neon ions up to 11 Mev. The present extension of the energy range, with similar results, is evidence for the Coulomb excitation character of the yield of the 478-kev state. This is in spite of the fact that the spectrum showed several peaks that were probably due to reactions.

Li^7 is the lightest nucleus bombarded in the present work. The symmetrized classical distance of closest approach,[10] 2a, was about

---

[8] M. E. Rose, Phys. Rev. 91, 610 (1953); H. I. West, Jr., University of California Radiation Laboratory report UCRL-5451, (1959).

[9] P. H. Stelson and F. K. McGowan, Nucl. Phys. 16, 92 (1960).

[10] The approximation used is that of reference 6, p. 457.

12 fermi (10^{-13} cm) for 15-Mev neon ions. This is the smallest value of 2a for any of the nuclei studied. Similarly the Coulomb barrier* for Li^7 was the lowest of all the nuclei considered. It was estimated to be 6.2 Mev in the center of mass system. (With 15 Mev neon ions bombarding Li^7, only 3.9 Mev is available in the center of mass system.)

F^{19}. The yield of the 197-kev state of F^{19} was measured to be 3.70×10^{-8} gamma rays per incident particle, with 11.9-Mev neon ions. From this the value of $\epsilon B(E2)$ was calculated to be 0.005, in agreement with reference 9. Because the de-excitation gamma rays are probably pure E2, three measured values for the mean lifetime of the state[6] can be used to directly estimate the B(E2) value, and thus obtain an additional comparison. They are very near to 1.25×10^{-8} sec, which corresponds to 0.0066 for the excitation B(E2). (The internal conversion coefficient should be very small.) Within the errors, this and the present result agree.

The 110-kev state was also excited. It is an E1 excitation, the only one known in the present work. The transition matrix element B(E1), was calculated. A yield of 3.34×10^{-9} gamma rays per incident particle was obtained with 11.9-Mev neon ions. From this, a value $B(E1) = 3.6\ e \cdot 10^{-30}\ cm^2$ was calculated. In reference 9, a value nearly twice as large, $6.3\ e \cdot 10^{-30}\ cm^2$, was reported. That result contained

---

*Defined as $E_B = \frac{Z_1 Z_2 e^2}{R}$, where $R = 1.5 \left(A_1^{1/3} + A_2^{1/3} \right)$ fermi.

an error of a factor of two.* The corrected value agrees with the present result.

A spectrum from 15.4-Mev neon ions was taken with a low amplifier gain. There were no measurable peaks above 197 kev in the spectrum, which extended to 2.8 Mev.

Na^{23}. Both the yield and the angular distribution were measured for the 438-kev state of this nucleus, using neon ions. The yield, 3.27×10^{-8} gamma rays per incident particle, corresponds to $\epsilon B(E2) = 0.015$, which is in reasonable agreement with the other reported values listed in Table II.

A single angular distribution measurement at 10 cm with 15.4-Mev neon ions gave $R = 0.984 \pm 0.016$ and $A_2 = -0.015 \pm 0.015$. This is not corrected for relativistic effects,[3] which would decrease the magnitude of A_2. The nearly isotropic result should be considered as slight evidence in favor of spin 3/2 for the excited state. (The ground state is spin 3/2.)

Reference 3 discusses the two possible spins of the excited state: 3/2 and 5/2. Spin 3/2 would theoretically predict R = 1.000. Spin 5/2 would, in conjunction with the measured lifetime, predict $R = 0.932 \pm 0.003$. The more complete experiments of reference 3 arrived at a value about intermediate between these. An earlier measurement[11] with 2.5 Mev helium ions gave $R = 0.922 \pm 0.040$, which favors spin 5/2.

---

*Privately communicated by P. H. Stelson.

[11] G. M. Temmer and N. P. Heydenburg, Phys. Rev. 104, 989 (1956).

Ti^{47}. The pulse-height spectrum of this nucleus when bombarded by 15.4-Mev neon ions, is given in Figure 24. The best value of $\epsilon B(E2)$ for the 160-kev state is not in essential disagreement with the other reported results. Table III lists the present results for different energies.

One set of angular distributions was made at 10.2 Mev, with the detector at 15 cm. The resulting value of R, 0.960 $\pm$ 0.013, corresponds to $A_2 = -0.035 \pm 0.012$.

TABLE III

NEON ION YIELDS FOR THE 160-KEV STATE OF Ti^{47}

AT VARIOUS BOMBARDING ENERGIES

Neon Energy Mev	Yield, I' γ-Rays/Inc. Part.	Integral* Mev-mg-cm^{-2}	$\epsilon B(E2)$ $e^2 \cdot 10^{-48}$ cm^4
8.34	1.70×10^{-9}	0.1210	0.0281
9.29	4.25×10^{-9}	0.2799	0.0305
12.01	19.0×10^{-9}	1.398	0.0272
13.38	34.2×10^{-9}	2.419	0.0283
14.36	41.8×10^{-9}	3.355	0.0250
15.38	63.9×10^{-9}	4.517	0.0284

*This is defined in Appendix C, and in Section II.

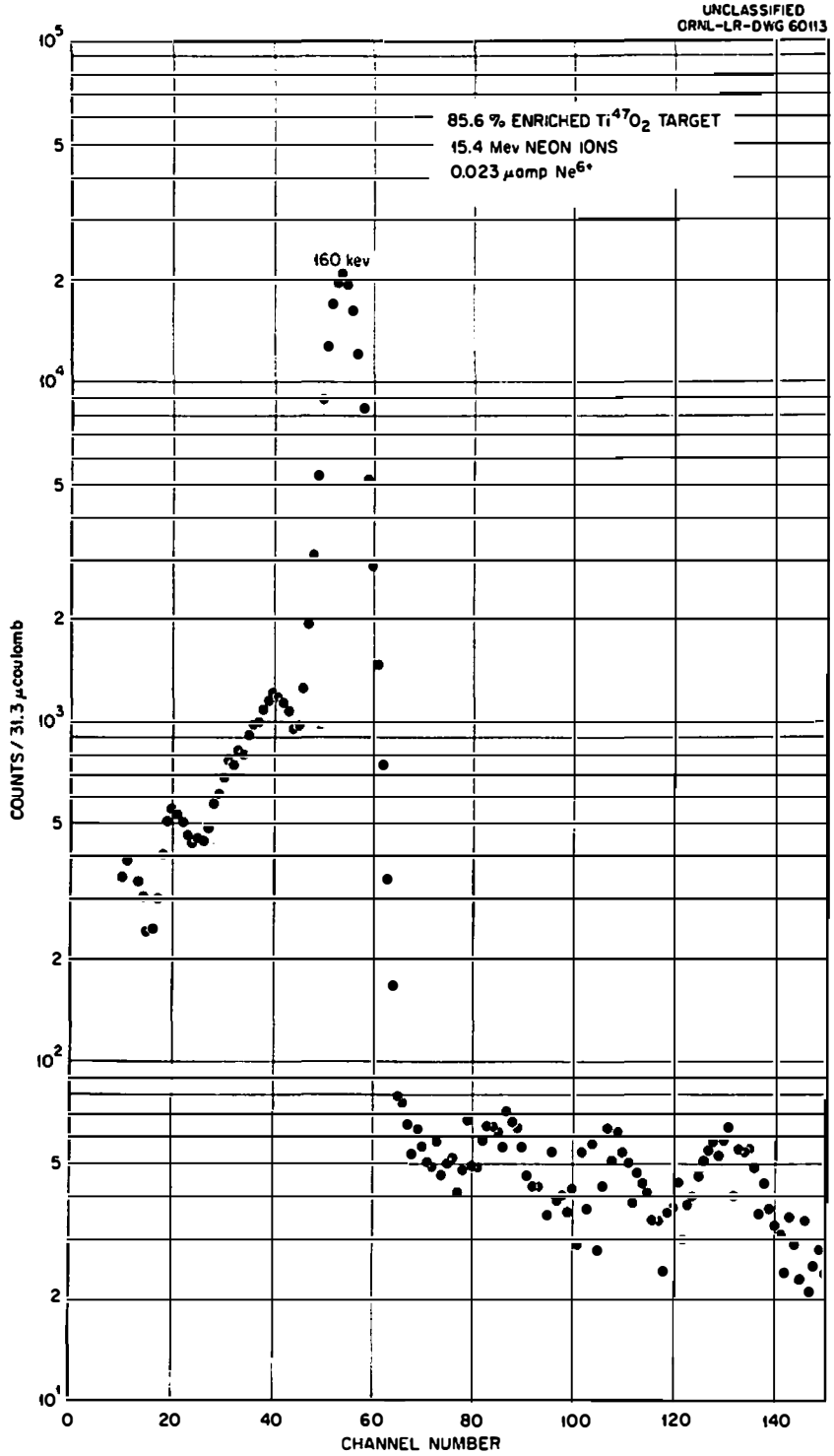

Fig. 24. Scintillation Pulse-Height Spectrum Produced by Bombardment of a $Ti^{47}O_2$ Target With Neon Ions.

V^{51}. Both neon and nitrogen ions were used in the yield measurements of the 320-kev state of V^{51}. The neon results are probably better because of uncertainties introduced by the weaker beam and molecular ions of nitrogen. Figure 25 shows the spectrum for 15.4-Mev neon ions.

Three sets of angular distribution measurements were taken. These are also listed in Table IV.

Cr^{53}. A 155-kev state has been reported for this nucleus.[12] However, its existence has been doubted by other workers.[13] During the present investigation, a search was made for this state, but the yield spectra showed no measurable peak at 155 kev. A yield of only 0.977×10^{-10} gamma rays per incident particle would have been quite noticeable at this position on the 13.4-Mev neon ion spectrum. This corresponds to an $\epsilon B(E2)$ of about 0.00005. It is concluded that: (1) the state doesn't exist, or (2) it has an $\epsilon B(E2)$ smaller than 0.00005, or (3) its spin and/or parity will not allow E2 Coulomb excitation. Spectra taken with 14.4-Mev neon ions did not show any significant peaks up to about one Mev.

Mn^{55}. The surface of this metallic target appears to form compounds very quickly in air. As a result the measured yields are probably the least trustworthy of any of the nuclei studied.

---

[12] Mark, McClelland, and Goodman, quoted in reference 7.

[13] D. G. Alkhazov, et al., Soviet Physics, JETP, 37, 1086 (1960).

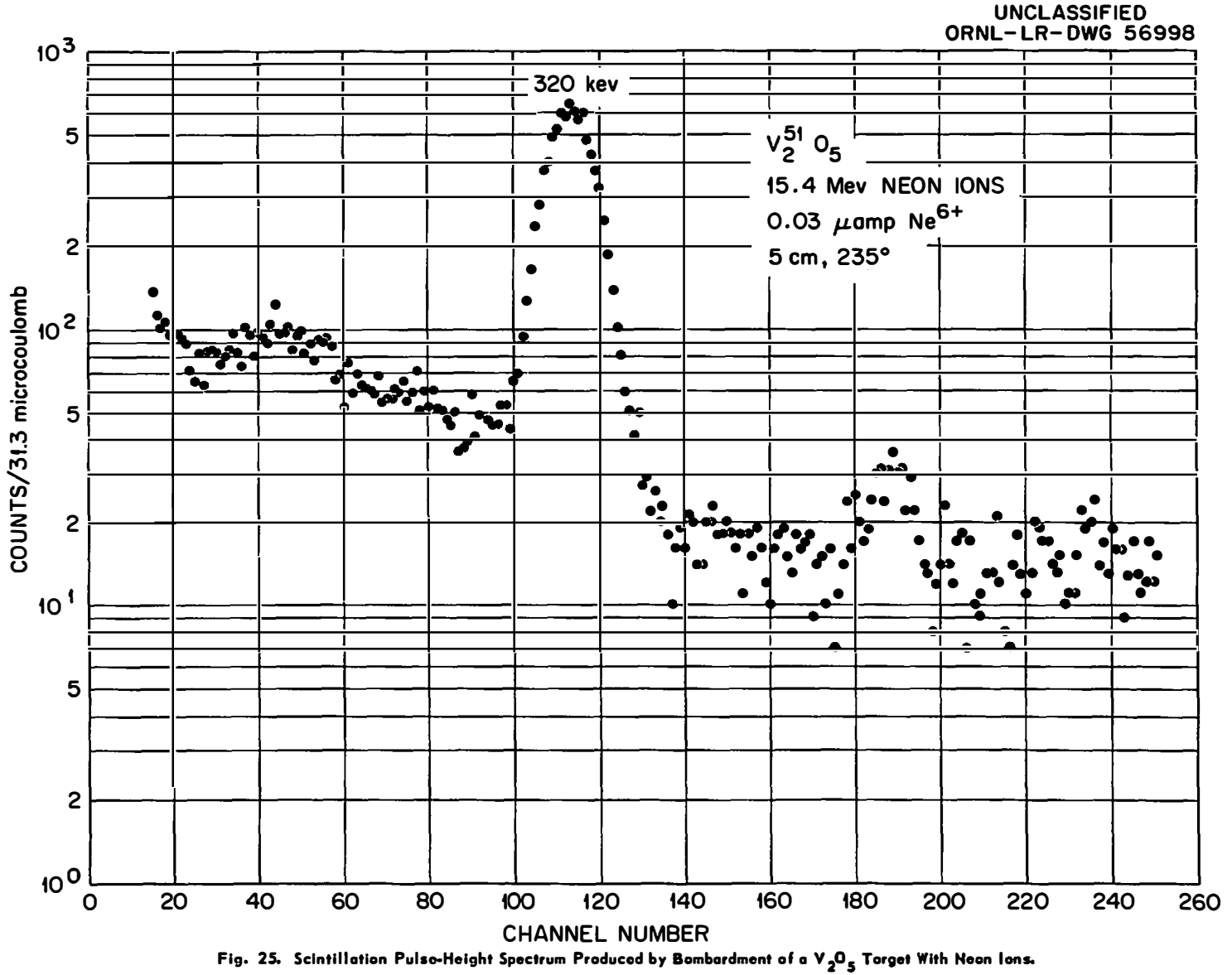

Fig. 25. Scintillation Pulse-Height Spectrum Produced by Bombardment of a V_2O_5 Target With Neon Ions.

TABLE IV

YIELD AND ANGULAR DISTRIBUTION MEASUREMENTS FOR THE 320-KEV STATE OF V^{51}

Ion	Energy Mev.	Yield, I' $\frac{\gamma\text{-Rays}}{\text{Inc. Part.}}$	Integral Mev-mg-cm^{-2}	$\epsilon B(E2)$ $e^2 \cdot 10^{-48}$ cm^4	R	h cm	$\bar{a}_2$
Neon	15.38	4.87×10^{-9}	0.784	0.0127	-	-	-
Neon	15.38	-	-	-	1.282 ± 0.028	10	0.826
Neon	15.38	-	-	-	1.376 ± 0.028	10	0.826
Neon	15.38	-	-	-	1.266 ± 0.028	10	0.826
Nitrogen	9.65	2.10×10^{-9}	0.3374	0.0152	-	-	-

Nevertheless, they are listed in Table V. The angular distribution was measured only several times absolutely, and the results were isotropic, within the fairly large absolute errors of about ± 2 per cent; this confirms the more extensive measurements of reference 3. Therefore, the distribution was used as a normalization for the angular distribution measurements of the other nuclei. Figure 26 shows the spectrum obtained with 15.4-Mev neon ions.

TABLE V

YIELD MEASUREMENTS FOR THE 126-KEV STATE OF Mn^{55}

Ion	Energy Mev	Yield, I' γ-rays/Inc. Part.	Integral Mev-mg-cm^{-2}	$\epsilon B(E2)$ $e^2 \cdot 10^{-48}$ cm^4
Neon	8.34	6.84×10^{-9}	0.3087	0.0309
Neon	9.29	15.0×10^{-9}	0.6407	0.0326
Neon	10.21	25.7×10^{-9}	1.129	0.0317
Neon	12.01	58.4×10^{-9}	2.633	0.0309
Neon	13.38	98.6×10^{-9}	4.296	0.0320
Neon	14.36	119×10^{-9}	5.767	0.0289
Neon	15.38	178×10^{-9}	7.543	0.0329
Nitrogen	8.05	33.3×10^{-9}	1.896	0.0296

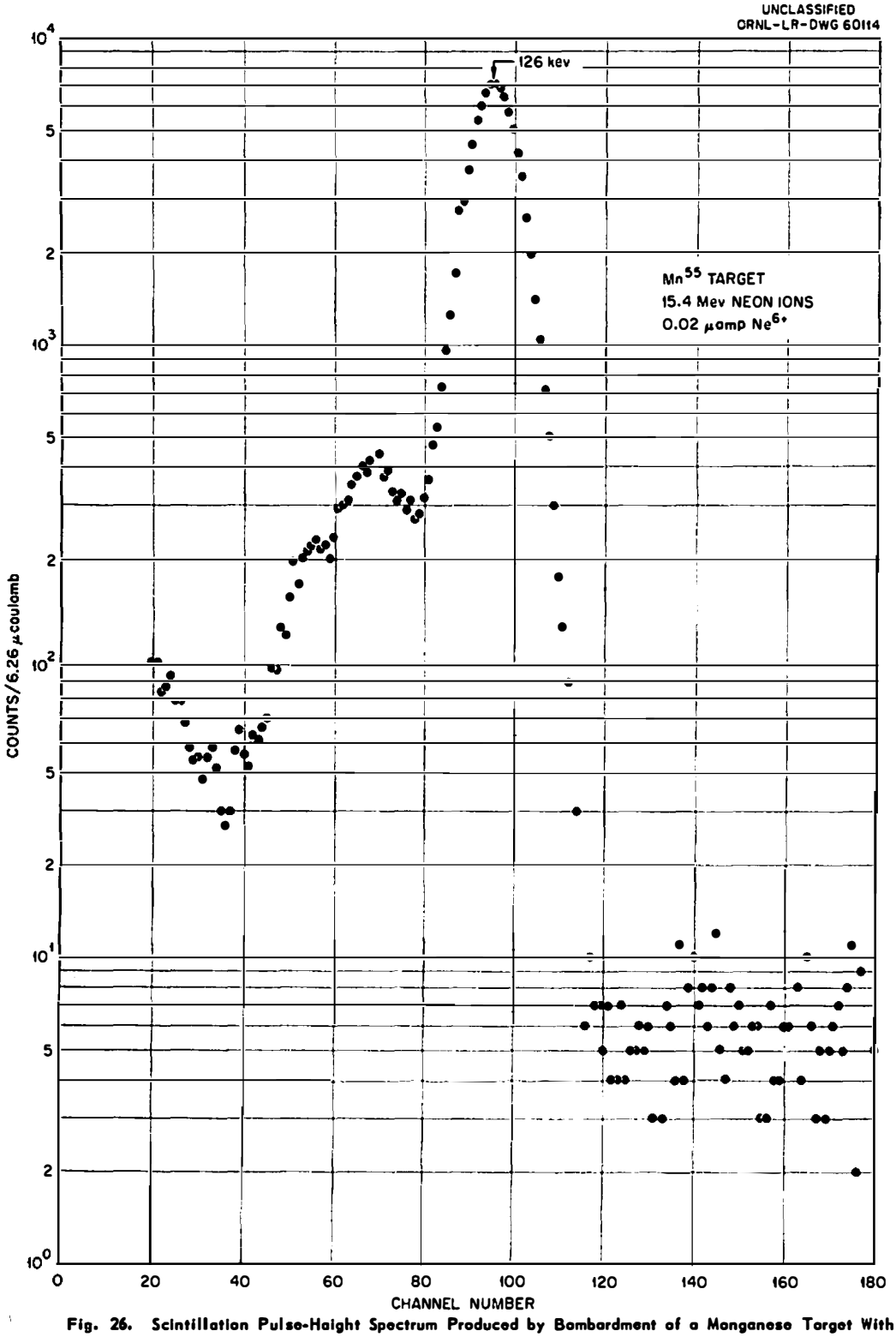

Fig. 26. Scintillation Pulse-Height Spectrum Produced by Bombardment of a Manganese Target With Neon Ions.

Fe^{57}. This is the first case discussed in this chapter, in which the de-excitation is not back to the ground state. Rather, it is primarily to the 14-kev excited state. The combined 136-kev and 122-kev gamma ray yields are included in the $\epsilon B(E2)$. This cascade-to-crossover ratio was measured roughly from the "hump" on the side of the 122-kev gamma ray. (See Figure 27). The value deduced was about 9. A more accurate measurement of 8.6 ± 0.2 has been reported.[14]

At the two highest bombarding energies the 364-kev state was excited sufficiently for quantitative measurements. This state also decays mostly to the 14-kev state. A cascade-to-crossover value could not be estimated, and apparently none has been reported.

The 364-kev state also cascades through the 136-kev state. The yield of the 228-kev crossover gamma ray was measured directly and in coincidence with the 122-kev gamma ray. The best value for this cascade-to-crossover ratio is 0.075 ± 0.011.

With Hg^{203} and Be^{7} radioisotopes for the energy calibrations the two principle gamma rays were measured to be 355 ± 4 kev and 126 ± 4 kev. The accepted values of reference 6 were obtained by more accurate means (a bent crystal spectrometer) and are expected to be better.

Tables VI and VII contain the results for Fe^{57}.

---

[14] A. T. G. Ferguson, M. A. Grace, and J. O. Newton, Nucl. Phys. 17, 9 (1960).

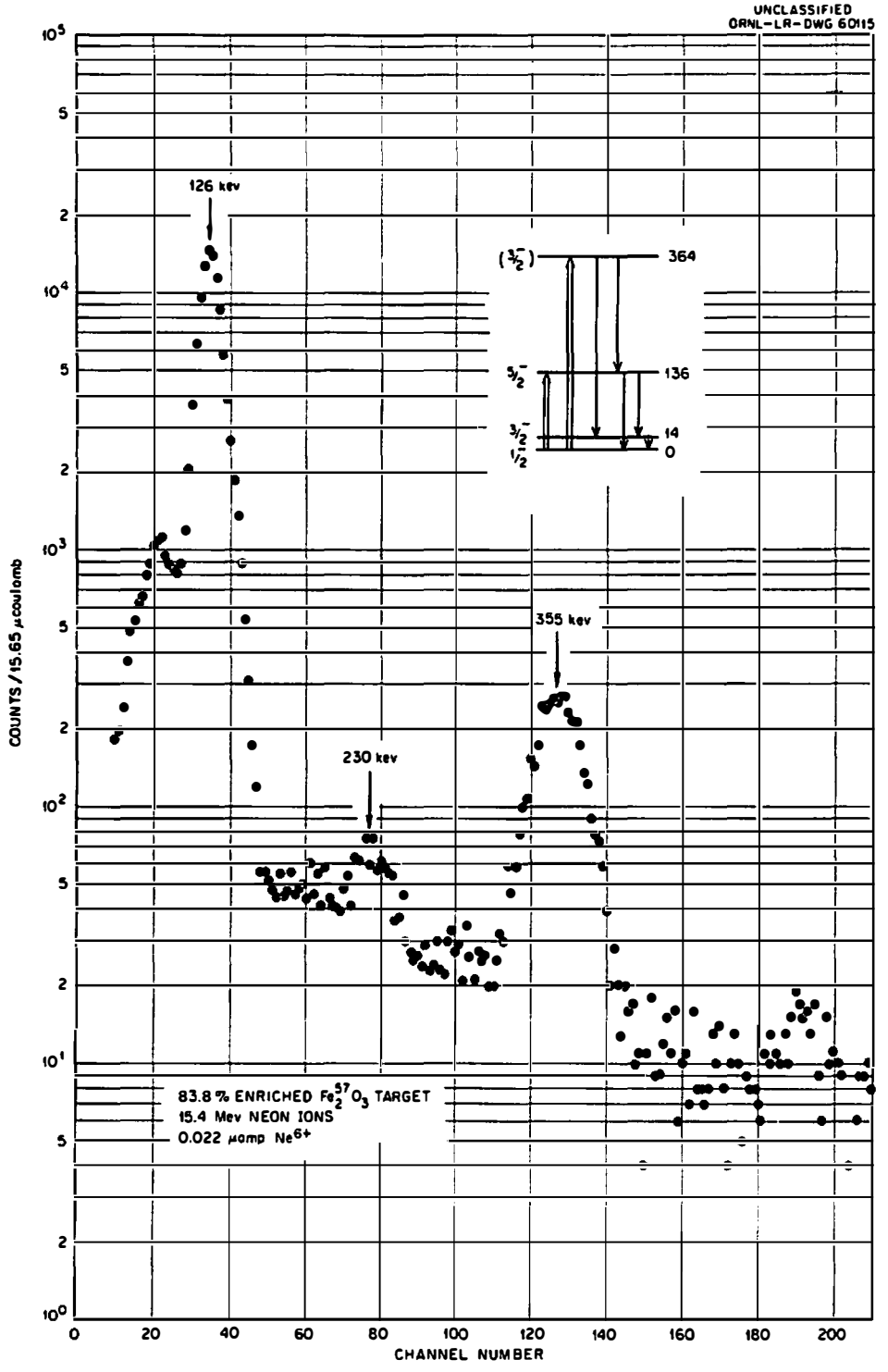

Fig. 27. Scintillation Pulse-Height Spectrum Produced by Bombardment of an $Fe_2^{57}O_3$ Target With Neon Ions.

TABLE VI

YIELD MEASUREMENTS FOR Fe^{57}

Neon Energy Mev.	γ-Ray Energy Kev.	Yield $\frac{\gamma\text{-Rays}}{\text{Inc. Part.}}$	Integral Mev-mg-cm^{-2}	$\epsilon B(E2)$ $e^2 \cdot 10^{-48}$ cm^4
8.34	122 + 136	2.56×10^{-9}	0.1641	0.0401
9.29	122 + 136	5.96×10^{-9}	0.3674	0.0417
12.01	122 + 136	24.5×10^{-9}	1.736	0.0362
13.38	122 + 136	38.8×10^{-9}	2.952	0.0340
14.36	122 + 136 *	58.7×10^{-9}	4.055	0.0372
	350 *	2.96×10^{-9}	0.1974	0.0386
15.38	122 + 136 *	73.8×10^{-9}	5.414	0.0350
	228 *	3.82×10^{-10}	-	-
	350 *	4.89×10^{-9}	0.3670	0.0342
15.38	228**	8.44×10^{-11}	-	-

*Simultaneous Measurements.

**In coincidence with the 122-kev gamma ray. The total efficiency of the 122-kev counter was 0.241. This corresponds (considering the internal conversion coefficient) to a singles yield of 3.6×10^{-10} γ-rays/inc. part. for the 228-kev gamma ray.

TABLE VII

ANGULAR DISTRIBUTION MEASUREMENTS FOR Fe^{57}

Neon Energy Mev	γ-Ray Energy kev		R	h* cm	$\bar{a}_2$
10.21	122 + 136		0.952 ± 0.025	15	0.747
15.38	122 + 136	**	0.946 ± 0.029	10	0.593
	350		1.188 ± 0.031	10	0.882
15.38	122 + 136	**	0.958 ± 0.029	10	0.593
	350		1.113 ± 0.031	10	0.882
15.38	122 + 136	**	0.949 ± 0.029	10	0.593
	350		1.140 ± 0.031	10	0.882
15.38	122 + 136	**	0.999 ± 0.029	10	0.593
	350		1.143 ± 0.031	10	0.882

*h is the distance from the target to the front face of the crystal.

**Simultaneous measurements.

Ni^{61}. Figure 28 shows the relatively weak excitation of the 67-kev and 282-kev levels in Ni^{61}. Although the 215-kev cascade gamma ray is not apparent, the evidence against its existence is not strong.

Nitrogen ions were also used for yield measurements, which are listed in Table VIII. The difference between the present $\epsilon B(E2)$ values and the earlier ones listed in Table II is not outside the experimental errors.

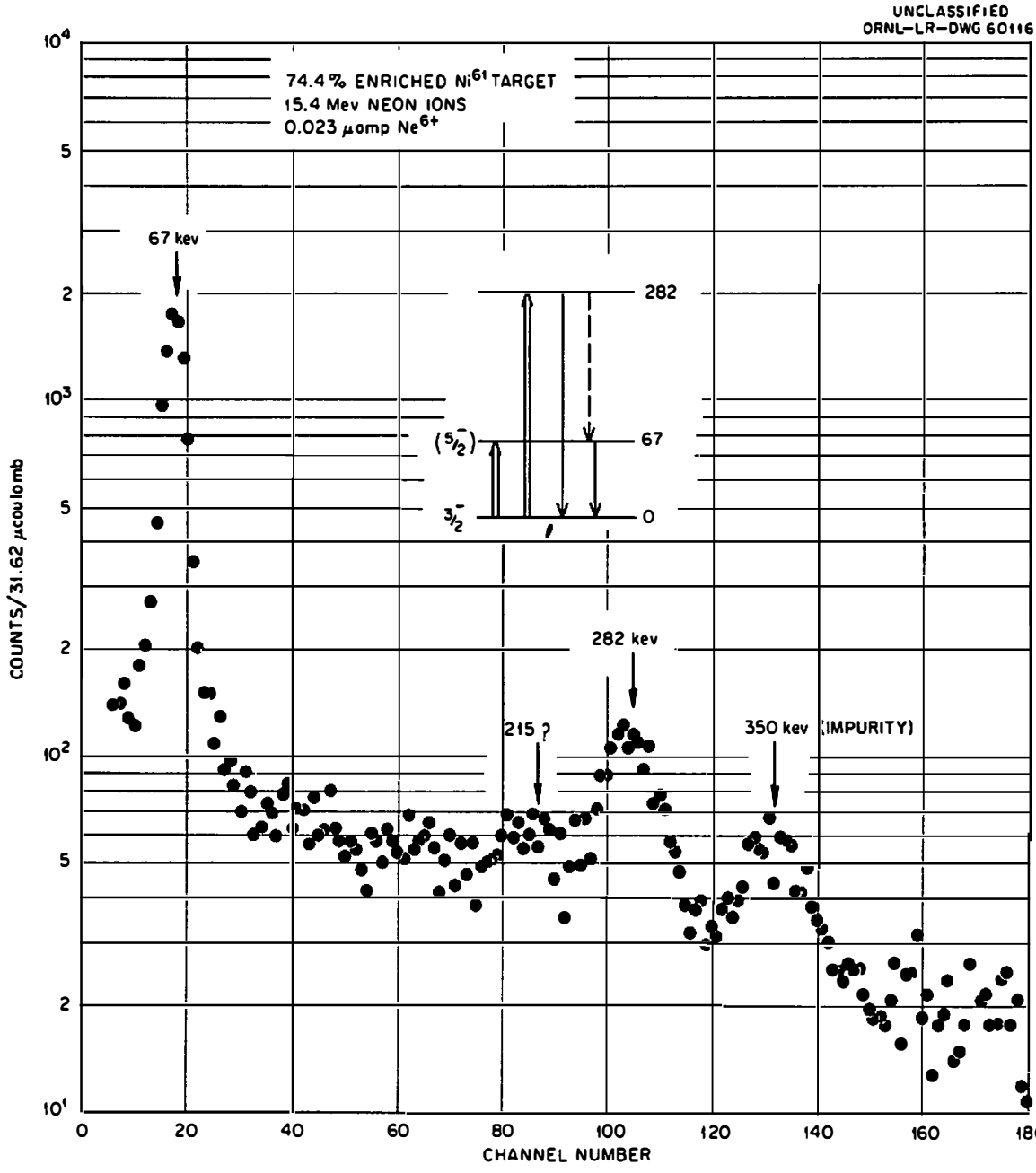

Fig. 28. Scintillation Pulse-Height Spectrum Produced by Bombardment of a Ni^{61} Target With Neon Ions.

TABLE VIII

YIELD AND ANGULAR DISTRIBUTION MEASUREMENTS FOR Ni^{61}

Ion	Ion Energy Mev	State Kev	Yield $\frac{\gamma\text{-Rays}}{\text{Inc. Part.}}$	Integral Mev-mg-cm^{-2}	$\epsilon B(E2)$ $e^2 \cdot 10^{-48}$ cm^4	R*	$\bar{a}_2$
Ne	8.34	67	3.90×10^{-10}	1.490	0.000623	-	-
Ne	9.29	67	6.89×10^{-10}	2.393	0.000686	-	-
Ne	10.21	67	9.89×10^{-10}	3.486	0.000676	-	-
Ne	13.38	67	22.1×10^{-10}	8.655	0.000609	-	-
Ne	14.36	67	26.0×10^{-10}	10.81	0.000574	-	-
Ne	15.38	67	36.0×10^{-10}	13.16	0.000651	-	-
Ne	15.38	282	5.26×10^{-10}	1.022	0.00122	-	-
N	9.06	67	1.43×10^{-9}	6.334	0.000660	-	-
N	9.65	67	1.75×10^{-9}	7.659	0.000668	-	-
N	9.65	282	1.71×10^{-9}	0.4325	0.00116	-	-
Ne	10.21	67	-	-	-	0.990 ± 0.018	0.592
Ne	10.21	67	-	-	-	0.992 ± 0.018	0.592

*Measured with h = 10 cm.

Angular distribution measurements were made, but the weak excitation prevented any significant analysis of the 282-kev state. The results for the 67-kev state are contained in Table VIII.

Zn^{67}. Only the 93-kev and 184-kev states were evident on the spectrum, Figure 29, of Zn^{67}. The 184-kev state was the most strongly excited, and its 91-kev cascade gamma rays were not resolvable from the 93-kev gamma rays. The numerous 93-kev lower cascade gamma rays nearly obscured the direct excitation of the 93-kev state. But, contrary to a previous report,[15] the present results showed a direct excitation of the lower state. Figure 30 shows the deviation of the combined 91-kev and 93-kev gamma ray yield curve from both the experimental and theoretical 184-kev curves. If the 91-kev and 93-kev gamma ray yields were from cascade only, their dependence on bombarding energy should be the same as the 184-kev gamma rays. In Chapter V, the analysis for obtaining separately the 91-kev and 93-kev gamma ray properties, is discussed. Table IX lists the yield measurements for Zn^{67}.

The angular distributions for the 184-kev gamma rays and for the combined 91-kev and 93-kev gamma rays were measured. They are listed in Table X.

---

[15] G. M. Temmer and N. P. Heydenberg, Phys. Rev. 96, 426 (1954).

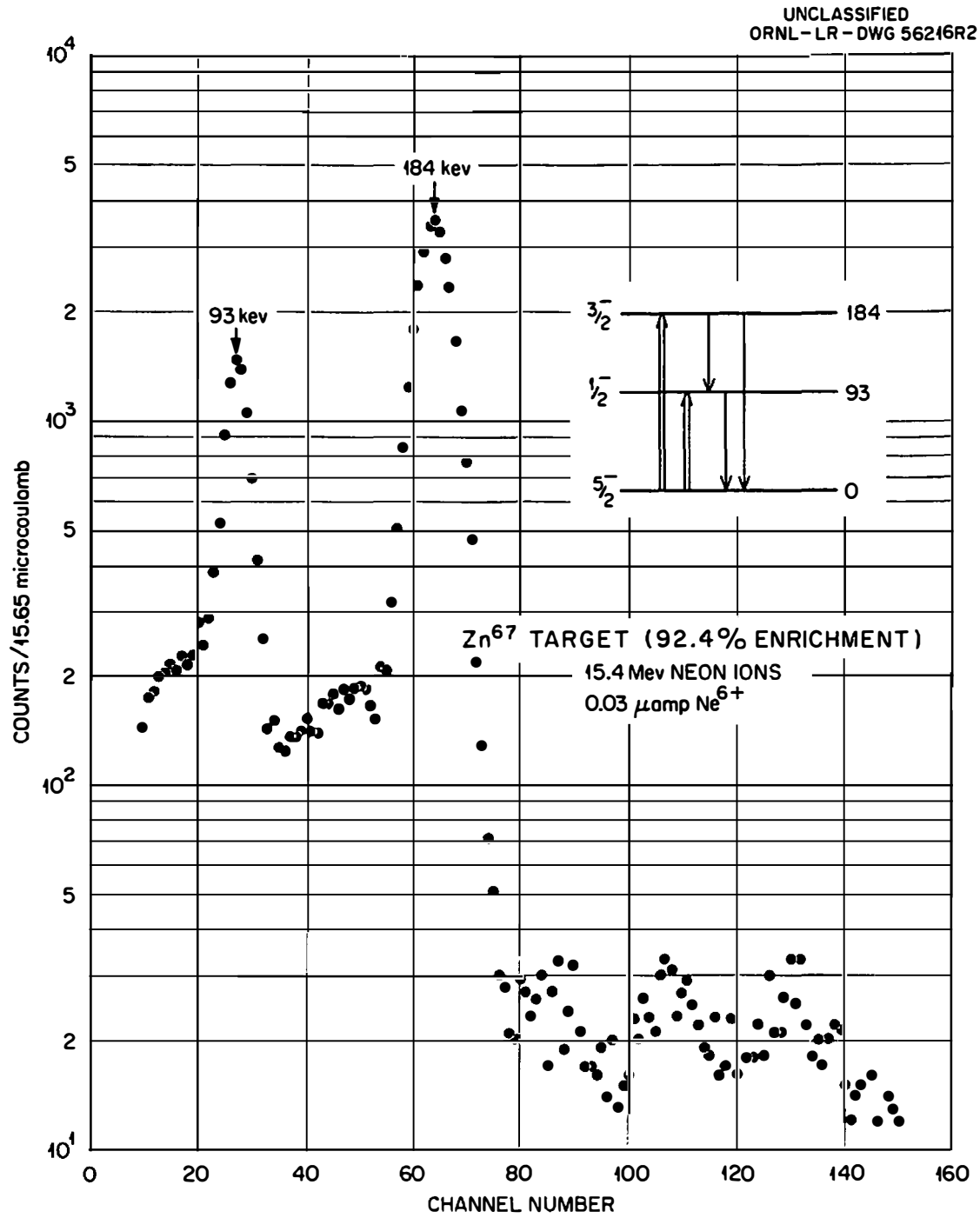

Fig. 29. Scintillation Pulse-Height Spectrum Produced by Bombardment of Zn^{67} With 15.4 Mev Ne^{20} Ions.

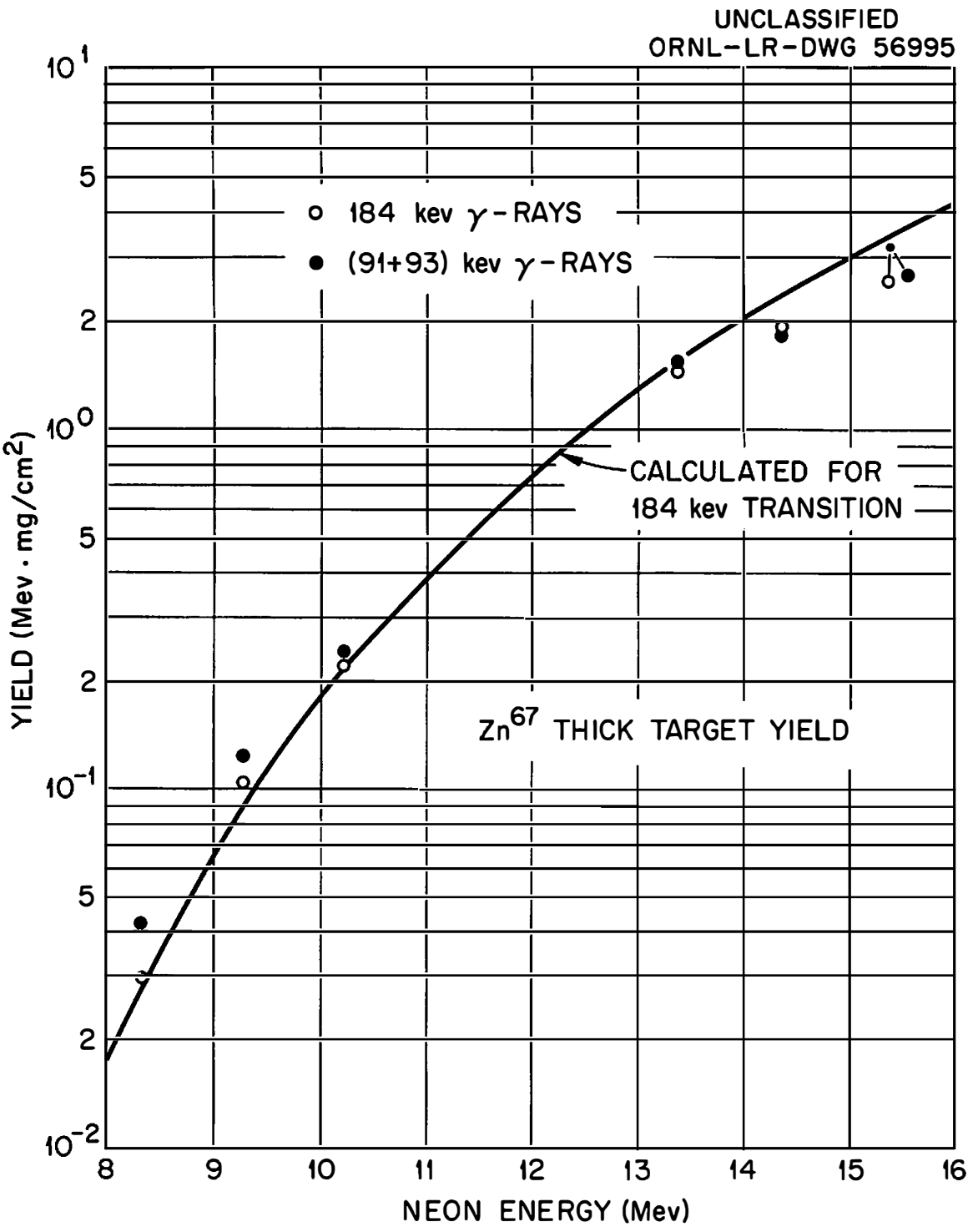

Fig. 30. Energy Dependence of 184-kev and (93-kev + 91-kev) γ-Ray Yields of Zn^{67}.

TABLE IX

YIELD MEASUREMENTS FOR Zn^{67}

Ion	Ion Energy Mev	γ-Ray Energy Kev	Yield γ-Rays/Inc. Part.	Integral Mev-mg-cm^2	$\epsilon B(E2)$ $e^2 \cdot 10^{-48}$ cm^4
Ne	8.34	184	2.17×10^{-10}	0.02789	0.0180
Ne	8.34	93 + 91	8.21×10^{-11}	-	-
Ne	9.29	184	7.51×10^{-10}	0.08728	0.0199
Ne	9.29	93 + 91	23.0×10^{-11}	-	-
Ne	10.21	184	17.0×10^{-10}	0.2085	0.0189
Ne	10.21	93 + 91	45.8×10^{-11}	-	-
Ne	13.38	184	106×10^{-10}	1.524	0.0161
Ne	13.38	93 + 91	292×10^{-11}	-	-
Ne	14.36	184	149×10^{-10}	2.325	0.0148
Ne	14.36	93 + 91	350×10^{-11}	-	-
Ne	15.38	184	250×10^{-10}	3.395	0.0170
Ne	15.38	93 + 91	611×10^{-11}	-	-
N	9.65	184	1.03×10^{-8}	1.623	0.0184
N	9.65	93 + 91	2.76×10^{-9}	-	-

TABLE X

ANGULAR DISTRIBUTIONS MEASURED IN Zn^{67}

Neon Energy Mev	γ-Ray Energy Kev		R	h cm	$\bar{a}_2$
10.21	184	*	1.314 ± 0.015	10	0.891
10.21	93 + 91	*	1.107 ± 0.031	10	0.891
10.21	184	*	1.309 ± 0.015	10	0.891
10.21	93 + 91	*	1.144 ± 0.031	10	0.891
15.38	184	*	1.238 ± 0.015	15	0.722
15.38	93 + 91	*	1.100 ± 0.034	15	0.722

*Simultaneous measurements.

The average value of $\epsilon B(E2)$ is lower than the previously reported value,[16] in which helium ions were used, by more than the probable errors. One possible explanation is that a heavy layer of compound formed on the metallic target surface, similar to that mentioned for Mn^{55}. The surface appearance was good, but it does not rule this out. Equation (29) would predict, both from an increased dE/dox and an increased A_2', that such a layer would decrease the yield. This effect would be more pronounced with heavy ions whose penetrability is less. The existence of a significant layer on Zn, however, has not been confirmed.

[16] G. M. Temmer and N. P. Heydenburg, quoted in reference 6.

Ge^{73}. Of the low-lying states in Ge^{73}, only the excitation of the 67-kev state appeared on the spectrum, which is shown in Figure 31. The existence of a cascade gamma ray to the 13.5-kev state could not be determined from this spectrum. The analysis is not sensitive to this, however, as the backscatter peak from 67 kev falls at about the same energy as the 53-kev cascade gamma ray would. Table XI contains the yield and angular distribution results.

The best value for $\epsilon B(E2)$, 0.046, is considerably lower than a value quoted from helium ion work.[16] However, as errors were not quoted for the other result, it is not known whether there is a significant disagreement.

As^{75}. Only 15.4-Mev neon ions were used to excite As^{75}. The excitation of the 199-kev and 280-kev levels is shown in Figure 32. The reported[6] weak 81-kev cascade gamma ray is not discernible on this spectrum. To test for possible excitation of the 265-kev state,[6] an energy calibration was made, based on Hg^{203}, and the shape and width of the peak in As^{75} was carefully studied. It is estimated that if there were 265-kev gamma rays in the spectrum, their yield was less than ten per cent of the 280-kev gamma ray yield. The results for the 199-kev and 280-kev gamma rays are listed in Table XII.

Ru^{101}. The results for excitation of the 127-kev state in Ru^{101} are given in Table XIII. No explanation has been found for the large (18 per cent) difference in the $\epsilon B(E2)$ values at the two bombarding

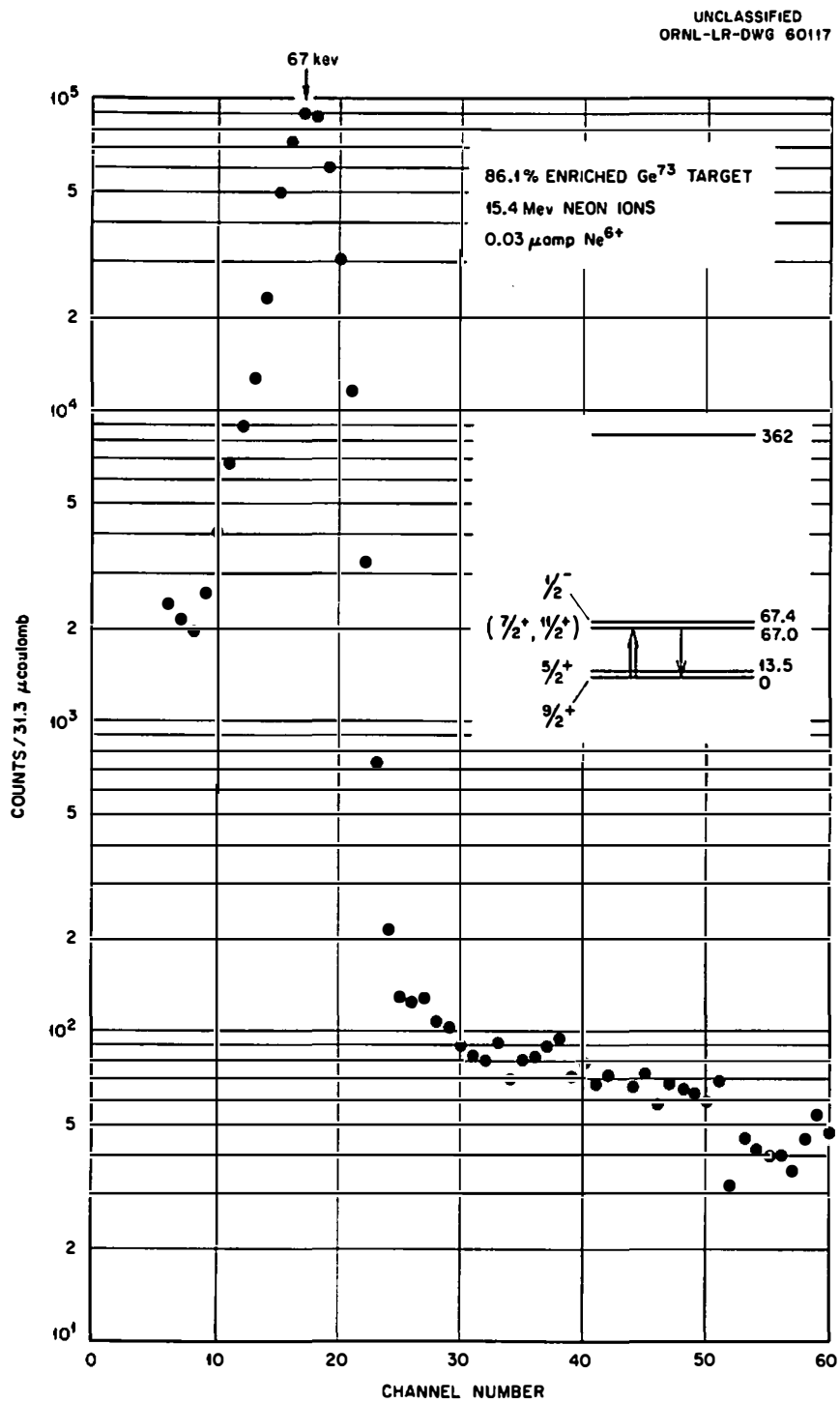

Fig. 31. Scintillation Pulse-Height Spectrum Resulting From Bombardment of Ge^{73} With Neon Ions.

TABLE XI

YIELD AND ANGULAR DISTRIBUTION MEASUREMENTS ON Ge^{73}

Neon Ion Energy	Yield γ-rays/Inc. Part.	Integral Mev-mg-cm^{-2}	$\epsilon B(E2)$ $e^2 \cdot 10^{-48}$ cm^4	R	h cm	$\bar{a}_2$
8.34	1.97×10^{-8}	1.324	0.0473	-	-	-
9.29	3.53×10^{-8}	2.212	0.0508	-	-	-
13.38	13.0×10^{-8}	8.963	0.0461	-	-	-
14.36	14.5×10^{-8}	11.24	0.0410	-	-	-
15.38	19.5×10^{-8}	13.85	0.0449	-	-	-
8.34	-	-	-	1.041 ± 0.011	10	0.730
10.21	-	-	-	1.029 ± 0.011	15	0.616

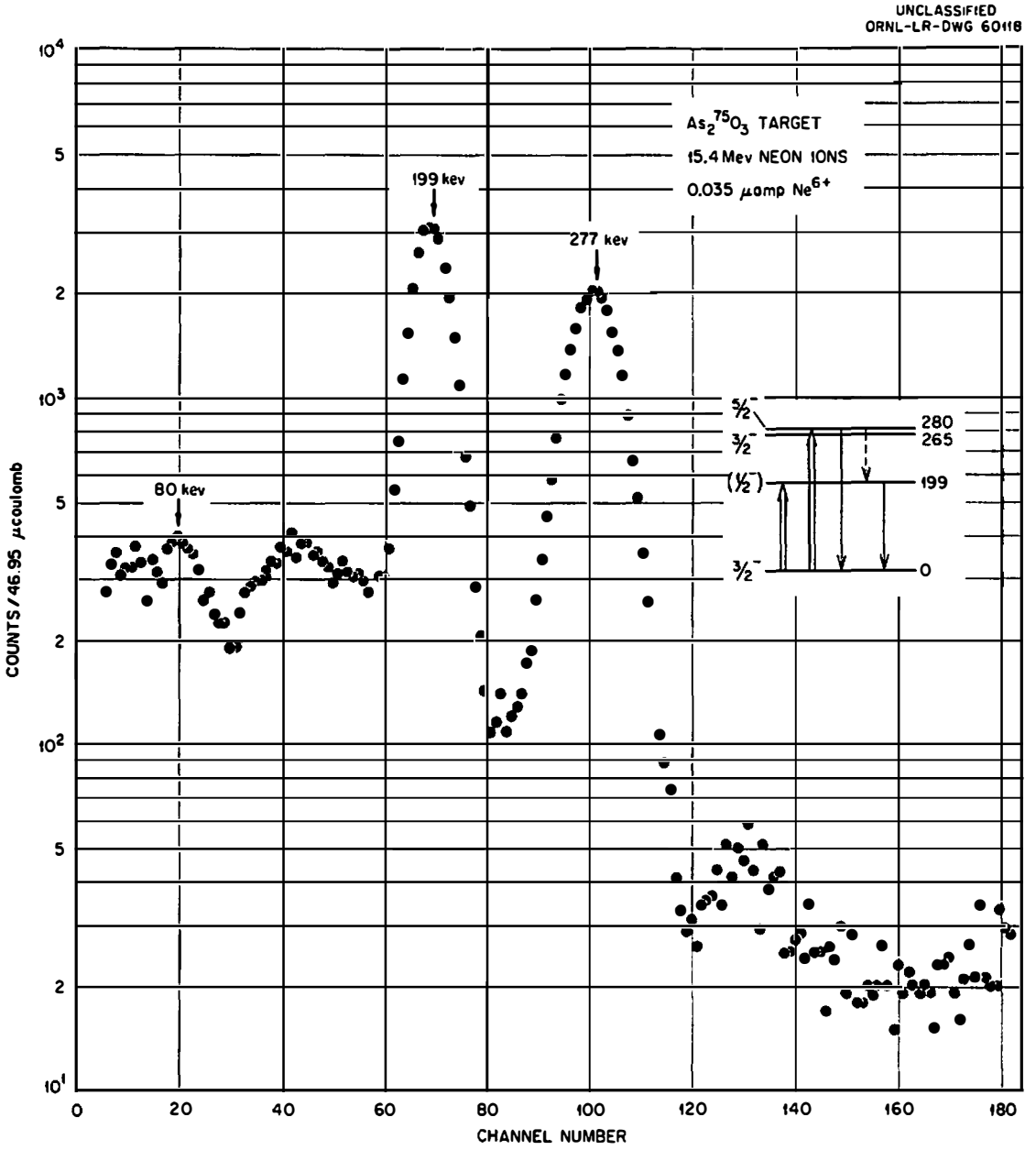

Fig. 32. Scintillation Pulse-Height Spectrum Produced by Bombardment of an As_2O_3 Target With Neon Ions.

TABLE XII

YIELD AND ANGULAR DISTRIBUTION MEASUREMENTS OF As^{75}

γ-Ray Energy Kev.	Target	Yield γ-Rays/Inc. Part.	Integral Mev-mg-cm^{-2}	$\epsilon B(E2)$ $e^2 \cdot 10^{-48}$ cm^4	R	h cm	$\bar{a}_2$
199 } *	Oxide	8.29×10^{-10}	2.056	0.0152	-	-	-
280 } *	Oxide	8.80×10^{-10}	0.6468	0.0515	-	-	-
199 } *	Oxide	-	-	-	1.009 ± 0.029	10	0.762
280 } *	Oxide	-	-	-	0.828 ± 0.038	10	0.858
199 } *	Oxide	-	-	-	0.979 ± 0.029	10	0.762
280 } *	Oxide	-	-	-	0.735 ± 0.038	10	0.858
199 } *	Metal	-	-	-	0.973 ± 0.029	10	-
280 } *	Metal	-	-	-	0.785 ± 0.038	10	-

*Simultaneous Measurements.

TABLE XIII

YIELD AND ANGULAR DISTRIBUTION MEASUREMENTS FOR Ru^{101}

Neon Energy Mev	Yield γ-Rays/Inc. Part.	Integral Mev-mg-cm^{-2}	$\epsilon B(E2)$ $e^2 \cdot 10^{-48}$ cm^4	R	h cm	$\bar{a}_2$
14.36	1.36×10^{-8}	3.599	0.0254	-	-	-
15.38	2.37×10^{-8}	5.152	0.0310	-	-	-
10.21	-	-	-	1.141 ± 0.037	15	0.887
10.21	-	-	-	1.141 ± 0.037	15	0.887
10.21	-	-	-	1.126 ± 0.037	15	0.887
15.38	-	-	-	1.060 ± 0.037	10	0.698
15.38	-	-	-	1.128 ± 0.037	10	0.698
15.38	-	-	-	1.208 ± 0.037	15	0.698

energies, or for the disagreement with the other value listed in Table II.

Pd^{110}. The 374-kev state in this nucleus was used for a test of the heavy ion angular distribution. There is an apparently unattenuated strong anisotropy[17] associated with the 0-2-0 spin sequence. With measurements at only two angles, it was not possible to uniquely determine experimental values for both A_2 and A_4, because of the strong dependence on A_4.

The large measured value of R, however, is consistent within 1.4 standard deviations, with the predicted theoretical value. Table XIV contains the results for Pd^{110}.

Pr^{141}. A 145-kev state has been reported for Pr^{141}, but it was not measurably excited in this work. It has also been reported that this level was not excited with 6 Mev helium ions.[18] By a method similar to that for Cr^{53}, the present work would predict an upper limit of 1.9×10^{-10} gamma rays incident particle for the yield of such a transition when 14.4-Mev neon ions were used. This corresponds to an $\epsilon B(E2)$ value of 0.003.

The present work would predict that if the level is E2 Coulomb excited, as the spins and parity[6] indicate is possible, the $\epsilon B(E2)$

---

[17] F. K. McGowan and P. H. Stelson, Phys. Rev. 106, 522 (1957).

[18] N. P. Heydenburg and G. M. Temmer quoted in reference 7.

TABLE XIV

YIELD AND ANGULAR DISTRIBUTION MEASUREMENTS FOR Pd^{110}

Neon Energy Mev	Yield γ-Rays/Inc. Part.	Integral Mev-mg-cm^{-2}	$\epsilon B(E2)$ $e^2 \cdot 10^{-48}$ cm^4	R	$\bar{a}_2$	$\bar{a}_4$
13.38	0.774×10^{-9}	0.006337	0.921	-	-	-
14.36	2.17×10^{-9}	0.01822	0.897	-	-	-
15.38	5.50×10^{-9}	0.04599	0.900	-	-	-
15.38	-	-	-	1.585 ± 0.035*	0.987	-0.1125

*Taken at h = 10 cm.

value would be less than 0.003. Another quoted value[19] is 0.0036 $\pm$ 0.00072. A value of $\epsilon B(E2)$ can also be calculated from the lifetime and multipole mixture, both of which have been measured.[6] Using a value of 0.5 for the internal conversion coefficient, 0.08 $\pm$ 0.02 for the multipole mixture, and $(2.7 \pm 0.2) \times 10^{-9}$ seconds for the mean lifetime, one obtains $\epsilon B(E2) = 0.002 \pm$ (a factor of two).

Hf. A natural Hf target was used to test the neon ion Coulomb excitation in the region $A \approx 180$. One measurement was made, with 15.4-Mev ions. The 112-kev state in Hf^{177} and the 122-kev state in Hf^{179} were not resolved. The combined yield, 2.22×10^{-8} gamma rays per incident particle, was used to find an effective value of $\epsilon B(E2) = 0.46$. The result agrees with that of reference 4, which was obtained similarly from proton excitation of a natural Hf target. To allow comparison with results for separated isotopes, they were combined according to the natural isotopic abundances. Ignoring the mass and gamma ray energy difference, the formula for combining the Hf^{177} and Hf^{179} results is

$$\epsilon B(E2)^{177+179} = 0.43\ \epsilon B(E2)^{179} + 0.57\ \epsilon B(E2)^{177} \qquad (32)$$

For this the natural isotopic abundances $\eta^{177} = 0.185$ and $\eta^{179} = 0.138$ were used. The two combined $\epsilon B(E2)$ values obtained this way, and given in Table II, bracket the present result.

---

[19] I. Kh. Lemberg, Reactions Between Complex Nuclei, (John Wiley and Sons, Inc., New York, 1960), p. 112.

Ta^{181}. A number of values for $\epsilon B(E2)$ have been reported[6] for the 136-kev state in Ta^{181}, all for proton or helium ion bombardment. The present value, 0.74, was obtained from 11.8-Mev neon ion bombardment which gave a yield of 4.82×10^{-9} gamma rays per incident particle. It falls about centrally among the other quoted values.

Th^{232}. One yield measurement with 15.4-Mev neon ions was made for the 53-kev state of Th^{232}. The results were 5.09×10^{-9} gamma rays per incident particle, for which $\epsilon B(E2) = 0.0232$. This agrees, within about 15%, with a recent result obtained with 4-Mev helium ions.[20] It is between the other two values listed in Table II.

---

[20] F. K. McGowan and P. H. Stelson, Phys. Rev. 120, 1803 (1960).

CHAPTER V

DISCUSSION OF THE ANALYSES AND RESULTS

The nuclei considered in this chapter are Ti^{47}, V^{51}, Mn^{55}, Fe^{57}, Ni^{61}, Zn^{67}, Ge^{73}, and As^{75}. For each of these the results of Chapter IV are extended and combined with other types of nuclear data. In Section I the transitions and level properties which can be treated collectively are taken up. Section II contains details of individual analyses and several applications of current nuclear models.

I. PROPERTIES TREATED COLLECTIVELY

An estimate of the collective motion associated with the low energy states of nuclei can be obtained from the enhancement in strength of their E2 transitions. This was discussed briefly in Chapter II in connection with equation (27) for the single-particle estimates for B(E2).

The $\epsilon B(E2)$ values of Table II are used for determining the enhancement factors F. ϵ as used in the present work was defined in Chapter IV. It is calculated for a given transition from a knowledge of the cascade gamma ray branching ratio and the internal conversion coefficients.

The total internal conversion coefficients (α_T) used in the analyses were taken from experimental results or from the theoretical

values which are listed in the tables of Rose[1] or Sliv.[2]

Values of ϵ resulting from each of the two processes can be calculated separately and multiplied together. The factor which accounts for internal conversion of the observed gamma rays is

$$\epsilon_\alpha = \frac{1}{1 + \alpha_T} \quad . \tag{33}$$

The partial contribution to ϵ from the cascade process as used here is

$$\epsilon_R = \frac{1}{1 + R'} \tag{34}$$

where R' is the cascade-to-crossover ratio for decay by gamma ray emission and internal conversion electron emission.

The excitation B(E2) which results from the division of $\epsilon B(E2)$ by ϵ must be converted to a decay B(E2) for comparison with the $B(E2)_{s.p.}$ used in this thesis. (In equation (7) the state f is now the ground state.) The relation between excitation and decay transitions is

$$\frac{B(E2)_{dec.}}{B(E2)_{exc.}} = \frac{(2j_g + 1)}{(2j_e + 1)} \quad , \tag{35}$$

where j_e is the spin of the excited state and j_g is the spin of the ground state.

Explicitly the B(E2) enhancement factor F is defined as

$$F = \frac{B(E2)_{dec.}}{B(E2)_{s.p.}} \quad . \tag{36}$$

For the various transitions, F is listed in Table XV, along with pertinent quantities leading to its determination.

---

[1] M. E. Rose, Internal Conversion Coefficients, (North-Holland Publishing Company, Amsterdam, 1958).

[2] L. A. Sliv and I. M. Band, issued in the U. S. A. as Report 57 ICC K1, Physics Department, University of Illinois.

TABLE XV

E2 TRANSITION ENHANCEMENT FACTORS

Nucleus	Transition (kev)	j_g	j_e	ϵ	$B(E2)_{dec.}$ ($e^2 \cdot 10^{-48}$ cm^4)	$B(E2)_{s.p.}$ ($e^2 \cdot 10^{-48}$ cm^4)	F
Ti^{47}	160	$5/2^-$	$(7/2^-)$	0.99	0.021	0.0013	16
V^{51}	320	$7/2^-$	$5/2^-$	1.0	0.017	0.0019	9
Mn^{55}	126	$5/2^-$	$(7/2^-,3/2^-)$	0.99	(0.023)	0.0016	(14)
Fe^{57}	136	$1/2^-$	$5/2^-$	0.98	0.013	0.0013	10
Fe^{57}	364	$1/2^-$	$(3/2^-)$	0.92	0.020	0.0013	15
Fe^{57}	122*	$3/2^{-*}$	$5/2^-$	-	0.0072**	0.0016	5
Ni^{61}	67	$3/2^-$	$(5/2^-,1/2^-)$	0.89	0.00048	0.0017	0. 3
Ni^{61}	282	$3/2^-$	-	0.99	0.0012***	0.0014***	0. 8
Zn^{67}	93	$5/2^-$	$1/2^-$	0.65	0.00053**	0.0048	0. 1
Zn^{67}	184	$5/2^-$	$3/2^-$	0.88	(0.031)	0.0029	(11)
Zn^{67}	91*	$1/2^{-*}$	$3/2^-$	-	$\leq$ 0.0010**	0.0016	$\leq$ 0. 7
Ge^{73}	67	$9/2^+$	$(7/2^+)$	0.80	0.072	0.0030	24
As^{75}	199	$3/2^-$	$(1/2^-)$	0.98	0.031	0.0038	8
As^{75}	280	$3/2^-$	$5/2^-$	0.97	0.036	0.0023	16

*Upper cascade gamma rays.

**These values are obtained indirectly. See the discussions.

***The statistical factor is omitted, as j_e is not known.

Due to the uncertainty of some of the spins (in parentheses) and the approximate nature of the $B(E2)_{s.p.}$, the results of Table XV have not been assigned errors. Moreover, the values have been rounded.

Each transition, unless forbidden by the spin selection rule, was found to have an appreciable M1 decay component. A B(M1) matrix element characterizes the magnetic dipole transition in a manner which is analogous to the B(E2) case. The B(M1) also have single-particle estimates[3] for the decay from an initial (excited) state i to the final (usually ground) state f. In case $|j_f - j_i| = 1$, this is

$$B(M1)_{s.p.} = \frac{1}{4\pi} (g_s - g_l)^2 \, C(j_>, j_<) \, \frac{2j_f + 1}{2j_< + 1} \quad . \tag{37}$$

$B(M1)_{s.p.}$ is in the units $\left(\frac{e\hbar}{2Mc}\right)^2$, and the parameters g_s and g_l depend on the odd nucleon in the nucleus. The factors g_s and g_l are not known. The free nucleon values were used. For a proton, $g_s = 5.585$ and $g_l = 1$; for a neutron $g_s = -3.826$ and $g_l = 0$. The remaining quantities are the same as those in equation (27) for the $B(E2)_{s.p.}$.

As there was no appreciable M1 excitation, the M1 transition properties must be obtained from the decay gamma ray and level characteristics. Where the gamma ray multipole mixture δ is known, the B(M1) are obtained from the B(E2). The formulas giving the relationship are[4]

---

[3] See, e.g., A. Bohr and B. Mottelson, Dan. Mat. fys. Medd. 27, No. 16 (1953).

[4] See, e.g., J. M. Blatt and V. F. Weisskopf, Theoretical Nuclear Physics, (John Wiley and Sons, Inc., New York, 1952), p. 595.

$$T(M1) = 1.744 \times 10^{13}\, \Delta E^3\, B(M1)\,, \tag{38}$$

$$T(E2) = 1.226 \times 10^{13}\, \Delta E^5\, B(E2)\,, \tag{39}$$

and

$$T(E2) = \delta^2\, T(M1)\,. \tag{40}$$

The latter formula is implied in the definition of δ. Here T(M1) and T(E2) are the M1 and E2 gamma ray transition probabilities in the units $(\text{seconds})^{-1}$. ΔE is the gamma ray energy in Mev, and B(M1) and B(E2) are in the conventional units $\left(\frac{e\hbar}{2Mc}\right)^2$ and $e^2 \cdot 10^{-48}$ cm^4, respectively.

δ was obtained from A_2, the measured anisotropy coefficient, in all of the cases where the spins in question were known, and where the method was more sensitive than that using the excited state lifetime. For the Coulomb excitation sequence $j_1(E2)j_2(E2 + M1)j_3$, curves of δ versus A_2 were plotted for all of the common spin possibilities. The data for the curves were taken from the standard γ-γ angular correlation theory.[5] Figure 33 is one such graph, which was used with Zn^{67} and Ru^{101}.

Sometimes solid-state effects set up electric or magnetic fields at the nucleus which attenuate the measured angular distribution.[6] The intermediate (excited) state is perturbed by an amount dependent upon the fields, the nuclear lifetime, and the nuclear moments which

---

[5] See, e.g., L. C. Biedenharn and M. E. Rose, Revs. Mod. Phys. 25, 729 (1953); also L. C. Biedenharn, Nuclear Spectroscopy, B, (Academic Press, New York, London, 1960), p. 732.

[6] A. Abragam and R. V. Pound, Phys. Rev. 92, 943 (1953).

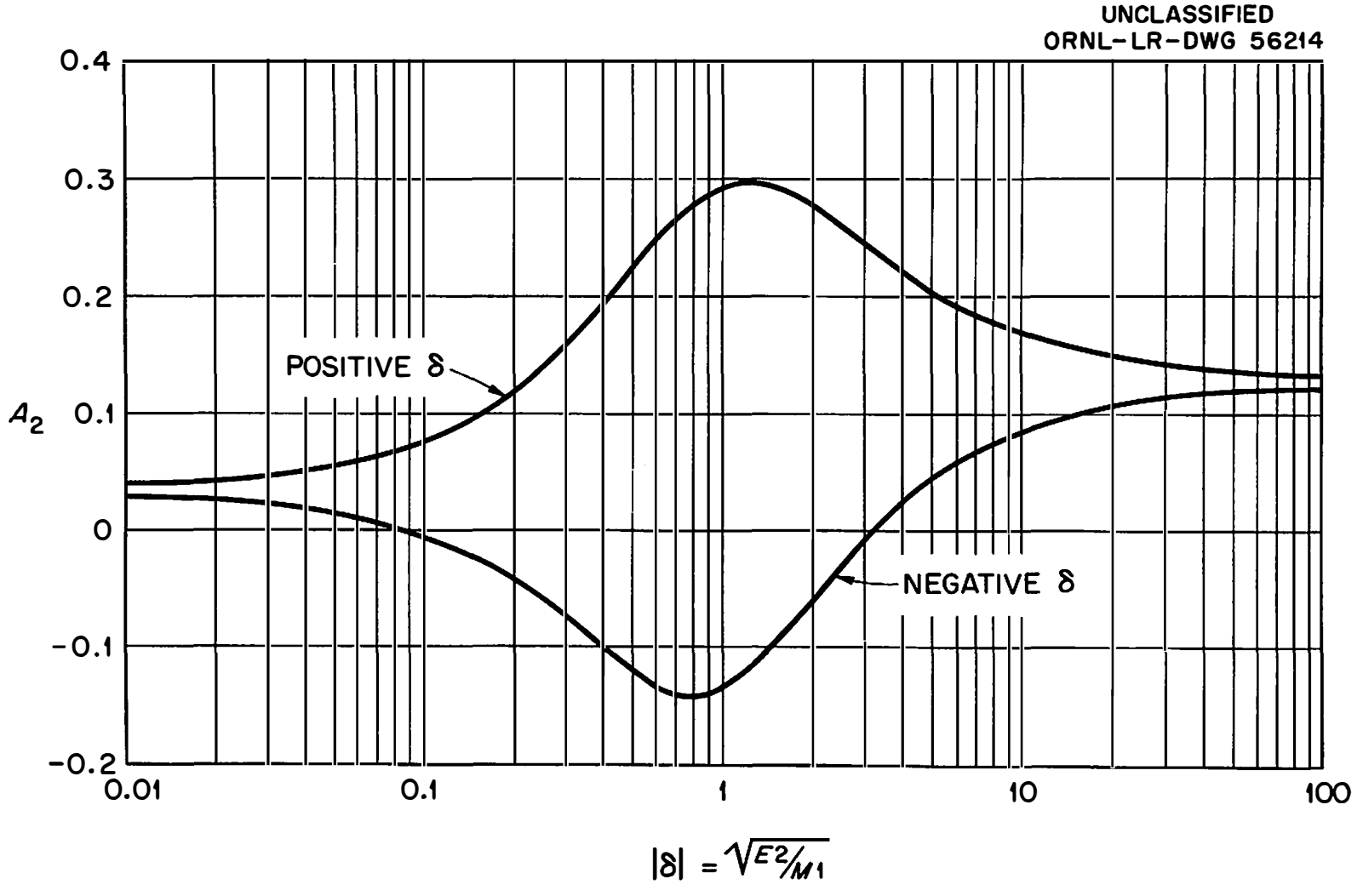

Fig. 33. E2-M1 Mixture (δ) as a Function of A_2 for the 5/2 (E2) 3/2 (E2 + M1) 5/2 Sequence.

couple to the fields. The partial (or total) loss of nuclear orientation information by the intermediate state produces the attenuation.

The measured lifetime of a state, in conjunction with the B(E2), will also yield a value for the magnitude of δ (but not for the sign). Even when the angular distribution information does yield an accurate result for δ for a given gamma ray transition, it is advisable to test its consistency with the value obtained from the mean lifetime τ, if it is known. The determination from τ requires the relation

$$\frac{1}{\tau} \equiv T = [T(E2) + T(M1)] \, (1 + \alpha_T) \, , \tag{41}$$

where T is the total transition probability for the excited state.

A factor F' is defined for the B(M1) case in analogy with the enhancement factor for B(E2) values

$$F' = \frac{B(M1)}{B(M1)_{s.p.}} \, . \tag{42}$$

F' is usually less than unity and it will therefore be called an "inhibition factor." It is often written as a fraction, to exhibit this feature. Table XVI lists the values obtained in the present work.

Turning now to a different character of the nuclei, it is useful to classify the various nuclei of interest according to a certain aspect of their collective motion. These nuclei are in, or near, a vibrational region. Adjacent even-even nuclei exhibit the characteristic enhanced 2^+ vibrational level, and a more-or-less harmonic relationship of the first two levels.

One description of these odd-A nuclei consists of an odd nucleon coupled to the collective oscillations. A parameter, q, has been

TABLE XVI

M1 TRANSITION INHIBITION FACTORS

Nucleus	Transition (kev)	τ (10^{-9} sec.)	δ^2	B(M1) $\left(\frac{e\hbar}{2Mc}\right)^2$	$B(M1)_{s.p.}$ $\left(\frac{e\hbar}{2Mc}\right)^2$	F'
Ti^{47}	160	0.32 ± 0.10[a]	0.0086 ± 0.003	0.0438	1.48	1/34
V^{51}	320	0.31 ± 0.08[b]	0.269 ± 0.09	0.0045	2.86	1/640
Mn^{55}	126	0.34 ± 0.10[a]	0.0084[a]	(0.0305)	2.15	(1/70)
Fe^{57}	136	12.7 ± 0.5[a]	*	*	*	*
Fe^{57}	364	-	(0.0071 or 34.7)**	-	1.16	-
Fe^{57}	122	-	0.036 ± 0.008[c]	0.00209	1.38	1/670
Ni^{61}	67	7.5 ± 0.5[d]	0.000067 ± 0.000015***	0.0227***	1.38	1/60***
Ni^{61}	282	-	-	-	-	-
Zn^{67}	93	13700 ± 1400[e]	*	*	*	*
Zn^{67}	184	1.45 ± 0.15[a]	0.26 ± 0.04	0.00342	1.67	1/490
Zn^{67}	91	-	≤ 0.0010	0.00685	1.16	1/170

TABLE XVI (continued)

Nucleus	Transition (kev)	τ (10^{-9} sec.)	δ^2	B(M1) $\left(\frac{e\hbar}{2Mc}\right)^2$	$B(M1)_{s.p.}$ $\left(\frac{e\hbar}{2Mc}\right)^2$	F'
Ge^{73}	67	2.33 ± 0.20[a]	≤ 0.0036	0.0632	1.92	1/30
As^{75}	199	1.30 ± 0.15[f]	0.189 ± 0.08	0.00462	3.34	1/720
As^{75}	280	0.4 ± 0.2[f]	~ 0.27	~ 0.0085	2.00	$\sim 1/240$

*Pure E2 decay.

**Assumes an excited state spin of $3/2^-$.

***Assumes an excited state spin of $5/2^-$.

[a]See reference 11.

[b]N. N. Delyagen and M. Preisa, Soviet Physics, JETP 9, 1127 (1959).

[c]G. R. Bishop, et al., Phil. Mag. 46, 951 (1955).

[d]R. E. Holland, F. J. Lynch and E. N. Shipley, Bull. Am. Phys. Soc. II, 5, 424 (1960).

[e]W. E. Meyerhof, L. G. Mann and H. I. West, Jr., Phys. Rev. 92, 758 (1953).

[f]E. N. Shipley, F. J. Lynch and R. E. Holland, Bull. Am. Phys. Soc. II, 4, 404 (1959).

given,[7] which characterizes the strength of the coupling of the odd nucleon to the vibrations. It is calculated in terms of the properties of the adjacent even-even nuclei as

$$q = \left(\frac{5}{16\pi}\right)^{1/2} \frac{k}{(\hbar\omega_2 \cdot C)^{1/2}} , \tag{43}$$

where k is a coupling parameter and is usually taken to be about 40 Mev. Also, $\hbar\omega_2$ is the energy of the first 2^+ excited state in Mev for an adjacent even-even, and C is the (quadrupole vibration) surface tension parameter in Mev for that nucleus. C is calculated from the phonon model,[7] as

$$C = 5/2 \frac{\hbar\omega_2}{\beta^2} , \tag{44}$$

where β^2 is obtained from equation (26). (The B(E2) in equation (26) is for the upward transition; it is five times larger than the decay B(E2).)

The interpretation suggested for q is that values less than unity denote weak coupling, values from one to three denote intermediate coupling, and values above three suggest an approach to strong coupling. Aside from specifying the need for different calculational approaches in the theory, these classes in a broad way specify the extent of the development of collective motion in the nucleus. For calculational

---

[7] See the parameter $x = qj^{-1/2}$ in reference 3. See also Alder et al, Revs. Mod. Phys. 28, 432 (1956), and D. C. Choudhury, Dan. Mat. fys. Medd. 28, No. 4 (1954).

purposes q can also be written

$$q = \left(\frac{\overline{\beta^2}}{8\pi}\right)^{1/2} \frac{k}{\hbar\omega_2} \tag{45}$$

and

$$q = \left(\frac{F}{10Z^2}\right)^{1/2} \frac{k}{\hbar\omega_2}\,, \tag{46}$$

where F is the B(E2) enhancement of the transition between the ground state and the state at $\hbar\omega_2$, and Z is the nuclear charge. (Both of these are for the adjacent even-even nucleus.)

Table XVII lists the calculated values of C and q. They were obtained from equations (44) and (45). For certain of the even-even nuclei the vibrational parameters appear to change rapidly. Therefore in Table XVII $\beta_{r.m.s.}$[8] and $\hbar\omega_2$[9] are, where possible, the average of those for two adjacent even-even nuclei which bracket the one of interest. The particular choices of adjacent nuclei were determined by the available data.

The effects of single closed shells at V^{51} and Ni^{61} are evident in the low values for q. Conversely, the higher values of q for Ge^{73} and As^{75} show the effects of the addition of a number of nucleons beyond the closed shells.

---

[8] P. H. Stelson, Proceedings of the International Conference on Nuclear Structure, Kingston, Canada, (University of Toronto Press, Toronto, 1960), p. 791.

[9] Nuclear Data Sheets, (National Academy of Sciences, National Research Council, Washington, D. C.)

TABLE XVII

VIBRATIONAL COUPLING PARAMETERS

Nucleus	Adjacent Nuclei	$\overline{\beta_{r.m.s.}}$	$\overline{\hbar\omega_2}$ (Mev)	$\bar{C}$ (Mev)	q
$_{22}Ti^{47}_{25}$	$_{22}Ti^{46}_{24}$, $_{22}Ti^{48}_{26}$	0.265	0.94	34	2.2
$_{23}V^{51}_{28}$	$_{24}Cr^{52}_{28}$	0.255	1.43	55	1.4
$_{25}Mn^{55}_{30}$	$_{26}Fe^{56}_{30}$	0.255	0.84	33	2.4
$_{26}Fe^{57}_{31}$	$_{26}Fe^{56}_{30}$	0.255	0.84	33	2.4
$_{28}Ni^{61}_{33}$	$_{28}Ni^{60}_{32}$, $_{28}Ni^{62}_{34}$	0.19	1.39	96	1.1
$_{30}Zn^{67}_{37}$	$_{30}Zn^{66}_{36}$, $_{30}Zn^{68}_{38}$	0.22	1.06	55	1.7
$_{32}Ge^{73}_{41}$	$_{32}Ge^{72}_{40}$, $_{32}Ge^{74}_{42}$	0.275	0.72	24	3.0
$_{33}As^{75}_{42}$	$_{32}Ge^{74}_{42}$, $_{34}Se^{76}_{42}$	0.31	0.58	15	4.3

II. DISCUSSION OF INDIVIDUAL NUCLEI

$_{22}Ti^{47}_{25}$. A value[10] of $\alpha_T = 0.0036 \pm 0.0009$ was used in the analysis of the 160-kev state of Ti^{47}. The quantity for δ^2 in Table XVI was determined from the B(E2) and τ. The measured value of A_2 for this transition (-0.035 ± 0.017) is consistent with the tabulated value of δ^2 (0.0086 ± 0.003) for an excited state spin of either $3/2^-$ or $(7/2^-)$.[9] The possibility of correlation attenuation would in addition allow a spin assignment of $5/2^-$. Holland and Lynch,[11] using the measured lifetime, a theoretical value for α_T, and $\epsilon B(E2) = 0.040$, have calculated δ^2 to be 0.013. They assumed a spin of 7/2 for the excited state.

The E2 character of the excitation has been confirmed by Bromley et al[12] with He^3- and He^4-induced Coulomb excitation.

The $5/2^-$ spin of the ground state was measured,[9] but the $(7/2^-)$ assignment of the excited state appears to be based on plausibility arguments.[13] The β^- decay of Sc^{47} (with an assumed ground state spin of $7/2^-$) to both the ground and first excited states of Ti^{47}, and the β^+ decay of V^{47} (with an assumed ground state spin of $3/2^-$) to only the

---

[10] L. S. Cheng and M. L. Pool, Phys. Rev. 90, 886 (1953).

[11] R. E. Holland and F. J. Lynch, Phys. Rev. 121, 1464 (1961).

[12] D. A. Bromley, J. A. Kuehner, and E. Almqvist, Phys. Rev. 115, 586 (1959).

[13] L. J. Lidofsky and V. K. Fischer, Phys. Rev. 104, 759 (1956).

ground state of Ti^{47}, were considered evidence for the higher choice of spin for the 160-kev state in Ti^{47}. (The partial M1 character of the 160-kev gamma ray ruled out spin $9/2^-$.) These ground state spin assignments for Sc^{47} and V^{47} were assumed from the shell model. The ground state spin of V^{47} has since been listed[9] as $(5/2^-)$.

In another work,[14] the results of $Ti^{46}(d,p)Ti^{47}$ reactions indicated that three units of orbital angular momentum are transferred to Ti^{47} in the 160-kev state by the captured neutron ($l_n = 3$). This would reject $3/2^-$ as the spin, but would allow $5/2^-$ or $7/2^-$.

Using shell model wave functions and an upper limit on the measured $l_n = 3$ mode for possible ground state neutron capture, Rietjens et al[14] have concluded that there is less than a 3% (in intensity) admixture of $f_{5/2}$ in a ground state with a nearly pure $(f_{7/2})^7$ wave function. (Both the two protons and the five neutrons outside closed shells were considered as $f_{7/2}$ particles, with the two protons coupling to $J = 0$.)

On the other hand, the B(E2) enhancement factor of 16 (in Table XV) indicates the presence of collective effects. Ti^{46} and Ti^{48} have spectra suggesting possible vibrations. The calculated parameters in Table XVII suggest further that Ti^{47} is likely to have a fair degree of collective motion.

---

[14] L. H. Th. Rietjens, O. M. Bilaniuk, and M. H. MacFarlane, Phys. Rev. 120, 527 (1960).

$_{23}V^{51}_{28}$. The large anisotropy ($A_2 = 0.239 \pm 0.015$) of the measured angular distribution of V^{51} allowed a unique spin assignment of $5/2^-$ for the 320-kev excited state. This relatively clear cut case has a margin of error of about ten standard deviations from the nearest reasonable alternative assignment. From the measured value of A_2, δ was determined to be $+ 0.52 \pm 0.07$. This is consistent with the measured lifetime and the $\epsilon B(E2)$ value.

Several shell model calculations have been made recently for V^{51}. With only three particles outside closed shells this nucleus provides an interesting case. It appears that the introduction of enough configuration mixing[15] into the ground state to explain the observed magnetic moment, would be inconsistent with the observed high inhibition of the B(M1) (about 1/640 in Table XVI). This question is still unresolved. An M1 transition would be seniority forbidden[16] from an excited stated $(f_{7/2})^3_{5/2}$ with seniority three to a ground state $(f_{7/2})^3_{7/2}$ with seniority one if both states are quite pure. Another description which would predict a forbidden M1 transition is that of a single proton coupled to a core which changes its spin by two in the transition.[17]

---

[15] See, e.g., T. Komoda, Proceedings of the International Conference on Nuclear Structure, Kingston, Canada, (University of Toronto Press, Toronto, 1960), p. 498.

[16] G. Racah, Proceedings of the Rehovoth Conference on Nuclear Structure, (North-Holland Publishing Company, Amsterdam, 1958), p. 155.

[17] A. deShalit, Phys. Rev. 122, 1530 (1961).

The E2 enhancement of about 9 suggests the presence of some collective motion. Other experimenters (referenced in Table II, Chapter IV) have obtained similar values for $\epsilon B(E2)$. They have also excited a state at 930 kev. The enhancement of that state, from the average of their $\epsilon B(E2)$ values and a value obtained by Lemberg,[18] is about five if a spin of $3/2^-$ is assumed for the state.

These results suggest that a collective treatment might be useful in conjunction with the Kisslinger-Sorensen theory.[19] Unfortunately, the low effective degeneracy of the shell from 20 to 28 nucleons leads to poor solutions of the pairing correlation theory. Two different calculations were used for V^{51} in reference 19. In one approach an exact diagonalization was performed of the pairing force and a P_2 force under the assumption of a degenerate $f_{7/2}$ level. Three combinations of strengths of the pairing and P_2 forces were used. In the other approach, the $d_{3/2}$ subshell below and the $p_{3/2}$ and $f_{5/2}$ subshells above were included in the single-particle levels used in the calculations. The possible existence[20] of a positive parity state at 645 kev suggested the breaking of the 20-proton shell.

Neither of the above approaches resulted in a very satisfactory simultaneous fit of the 320-kev and 930-kev levels. It is possible that

---

[18] I. Kh. Lemberg, Reactions Between Complex Nuclei, (John Wiley and Sons, Inc., New York, 1960), p. 112.

[19] L. S. Kisslinger and R. A. Sorensen, Dan. Mat. fys. Medd. 32, No. 9 (1960).

[20] S. Ofer and R. Wiener, Phys. Rev. 107, 1639 (1957).

the expected errors in the pairing correlation approximation (of the order of the effective pair degeneracy) may have been too large for good fits to be expected. Also, the authors pointed out the inadequacy of their perturbation treatment of the long range residual force.

In that work[19] a relation was given, but not evaluated, for the energy shift predicted for a one quasi-particle state as a result of coupling to a vibrating core. Such calculations were completed for the present work, because of the implied collective effects mentioned above. However the results for this case were unreasonably sensitive to the choice of the long range force parameter X.

$\underline{25Mn30}$. The present research did not add much information about Mn^{55}. The $\epsilon B(E2)$ is suspect, and the angular distribution was nearly isotropic.

To give some continuity to the present discussions of the group of nuclei it is of interest to compare several aspects of Mn^{55} with those of Ti^{47} and Fe^{57}. The low energy spectra of Mn^{55} and Ti^{47} are similar, but that for Fe^{57} is quite different. The calculated coupling characteristic is not greatly different* for the three nuclei. However, the odd nucleon for Fe^{57} is (on the shell model basis) a $p_{3/2}$ neutron while for Mn^{55} it is an $f_{7/2}$ proton. Ti^{47} has an odd $f_{7/2}$ neutron.

Each of these nuclei has three particles outside one closed shell and two particles outside the other closed shell. The shell

---

*A different coupling parameter,[3] $x = qj^{-1/2}$, would be about 1.5 times greater for Fe^{57} than the other two nuclei. It is doubtful that this is significant.

model would anticipate some differences for levels of a $p_{3/2}$ particle and an $f_{7/2}$ one, but the quantitative differences of these three nuclei have not been explained by any simple consideration.

$_{26}Fe^{57}_{31}$. The analysis of the experimental data for Fe^{57} was more complex than for the previous nuclei. Figure 34 shows the level scheme[9] up to about one Mev, with the excitations and gamma rays observed in this research. The 14-kev gamma rays could not be detected in the equipment which was employed.

The internal conversion coefficients[21] used in the analysis were $\alpha_T(122) = 0.016 \pm 0.008$ and $\alpha_T(136) = 0.11 \pm 0.003$. A combination of the 350-kev yield, the 122-kev plus 136-kev yield, the two cascade-to-crossover ratios, and the coincidence gated detector efficiency, were used to determine the solution for the experimental quantities in the tables. The results are consistent with the measured lifetime for the 136-kev state.

The measured value of A_2, 0.132 ± 0.015, for the 350-kev gamma ray is consistent with a spin of $3/2^-$ or $5/2^-$ for the 364-kev state. The value $3/2^-$ was reported recently,[22] and therefore it was used for

---

[21] These were combined from results of D. E. Alburger and M. A. Grace, Proc. Phys. Soc. 67A, 280 (1954), and T. Huus et al, Dan. Mat. fys. Medd. 30, No. 17 (1956).

[22] V. F. Vervier and G. A. Bartholomew, Proceedings of the International Conference on Nuclear Structure, Kingston, Canada, (University of Toronto Press, Toronto, 1960), p. 650.

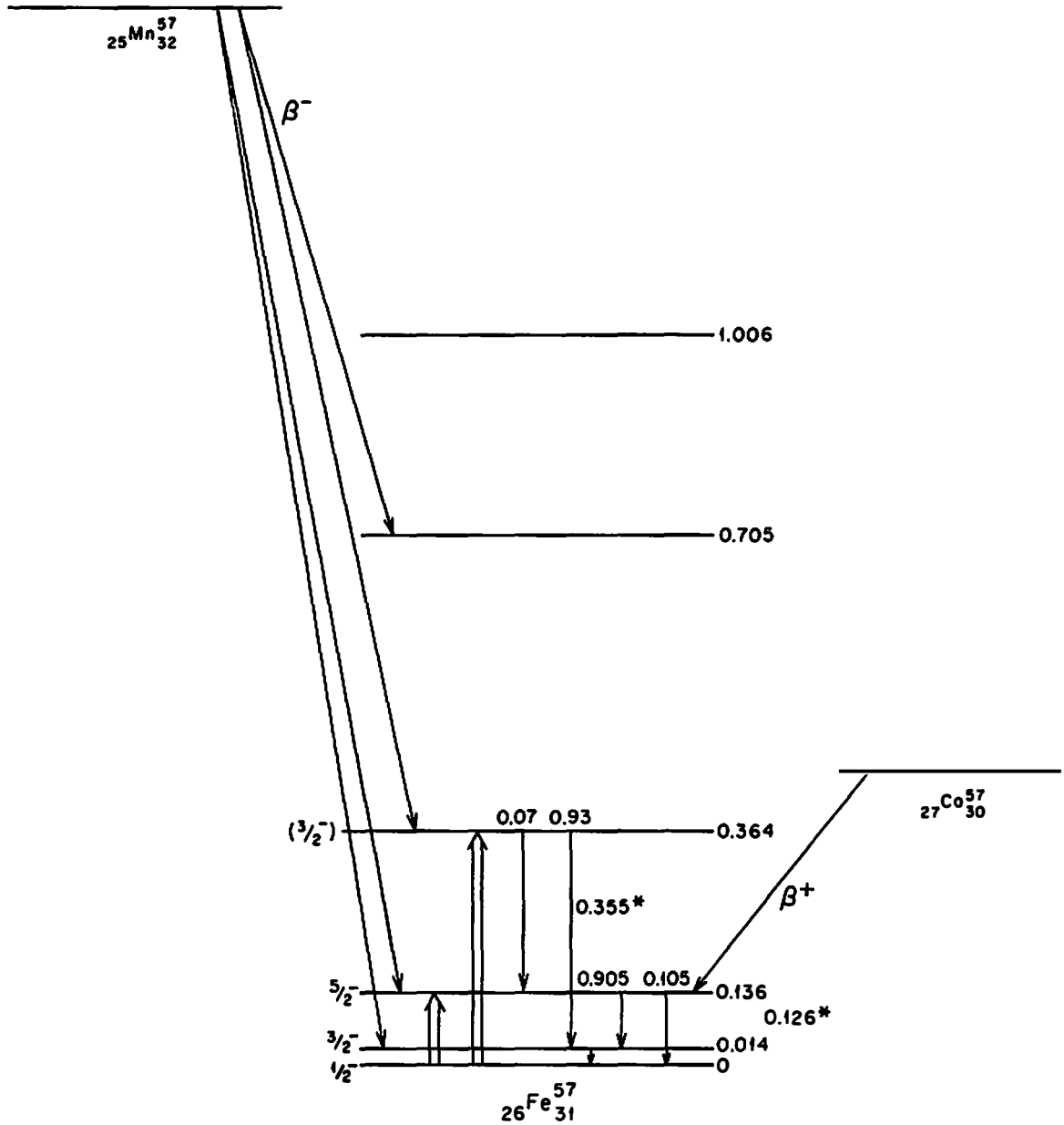

*VALUES MEASURED IN THIS RESEARCH

Fig. 34. Level Scheme for Fe^{57}.

determining the two values of δ^2 listed in Table XVI. The lifetime of this state has not been measured. Consequently, one of these values could not be eliminated. The smaller value for δ^2 results in F' = 2.8, which would be the largest in Table XVI. The larger value for δ^2 results in F' = 1/1750, which would be the smallest in the table. Lifetimes of $(2.8 \pm 1.6) \times 10^{-12}$ seconds and $(3.8 \pm 1.0) \times 10^{-10}$ seconds, respectively, would be predicted from these and the B(E2). However, the possibility of correlation attenuation makes these predictions uncertain.

In Table XVII the value of q is 2.4, which implies an intermediate coupling situation. Several authors[22,23] have attempted calculations with the assumption of a permanent deformation for Fe^{57}. Their Nilsson model calculations have predicted deformations of opposite sign.

If one interprets Fe^{57} as vibrational, there is a sum rule[7] which is used in the case of intermediate coupling. It states that the sum of all the $B(E2)_{exc.}$ values for the odd-A nucleus should be roughly equal to the $B(E2)_{exc.}$ of the first excited state (at the energy $\hbar\omega_2$) of the even-even nucleus adjacent to it. The sum should include all of the levels in the odd-A nucleus up to several times $\hbar\omega_2$. In Fe^{57} the sum for the 136-kev and 364-kev excitations is 0.078. The $B(E2)_{exc.}$ for the 845-kev state in Fe^{56} is about 0.10. The sum rule would predict that there are not likely to be many additional strongly enhanced

---

[23] R. D. Lawson and M. H. MacFarlane, Bull. Am. Phys. Soc. II, 6, 77 (1960).

low energy E2 transitions in Fe^{57}. If the sum rule is found in the future to be greatly exceeded, it would be evidence[24] that the coupling is approaching that of a deformed nucleus.

$_{28}Ni^{61}_{33}$. In the analysis of the 67-kev and 282-kev levels of Ni^{61} the internal conversion coefficients used were $\alpha_T(67) = 0.12$ and $\alpha_T(282) = 0$. δ^2 was obtained for the 67-kev state from the B(E2) and the measured lifetime. The lifetime of the 282-kev state is not known, and the weak excitation prevented an extraction of an A_2 coefficient for this state.

The less-than-single-particle values for the B(E2) matrix elements and the relatively low values of β and q all are evidence that Ni^{61} has less collective motion than most of the nuclei studied. However, Coulomb excitation with helium ions[25] has given evidence for a state at 659 kev, in which the enhancement is of the order of 10 (depending on the spin, which is not known).

The pairing correlation model of Kisslinger and Sorensen has made predictions for Ni^{61}. Figure 35 shows some of the original results and some obtained in the present work. The possible existence of the collective effects suggested that a calculation would be of interest for the energy shift due to coupling of the odd nucleon to the oscillation.

---

[24] F. K. McGowan and P. H. Stelson, Phys. Rev. 109, 901 (1958).

[25] L. W. Fagg, E. H. Geer, and E. A. Wolicki, Phys. Rev. 104, 1073 (1956).

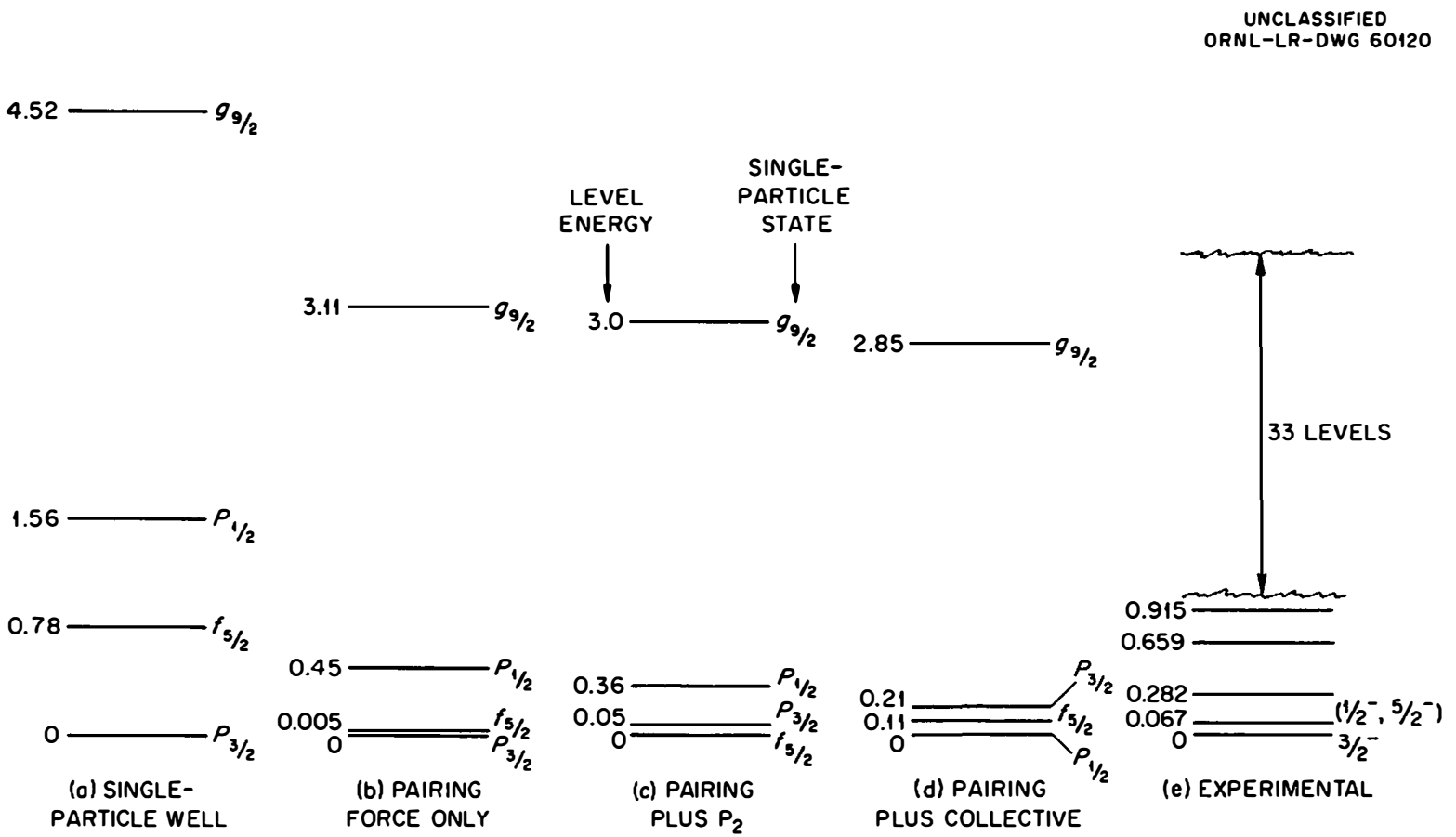

Fig. 35. Calculated Effect of Pairing and Long Range Residual Forces on Single-Particle Levels in Ni^{61}.

This was carried out in the same way as it had been done for V^{51}. The result of this calculation is in Figure 35d. It is not clear that the collective result is an improvement. The approximations in the solutions of the energies ($\Omega^{-1} \approx 1/3$) may obscure the relative usefulness of the various approaches.

It was necessary for Kisslinger and Sorensen to use a theoretical single-particle well for the nickel isotopes, as the levels of Ni^{57} are not known. It was not feasible in the present manual calculations to test the sensitivity of the results to the assumed well. It was possible, however, to vary the strength of the long range force, X, in the collective calculations. The levels showed a fairly sensitive dependence to small changes in X, although not nearly so much so as for V^{51}.

Reference 19 pointed out that quasi-particle levels near the Fermi surface ($E = \lambda$) are less strongly coupled to the oscillation than those far from the Fermi surface. From this the low B(E2) values measured for the 67-kev and 282-kev states, and the enhanced value for the 659-kev level, might imply that λ should be fairly low. The value they found was 0.38 Mev. It would be of interest to know whether changes could be made to the single-particle well, which would simultaneously lower λ and also improve the arrangement of the predicted individual levels.

From Figure 35 it is clear that accurate experimental spin assignments would be an aid in judging the various approaches and in guiding new ones. Coulomb excitation with lighter ions or more energetic heavy ions may be able to provide some of these spins, by the

fortunate circumstance that the ground state spin of Ni^{61} is 3/2. Thus both 3/2 and 1/2 excited states would result in isotropic angular distributions for E2 excitation. Only spins of 5/2 and 7/2 would be allowed for any distribution which was not isotropic. Furthermore, the 7/2 spin would require pure E2 de-excitation.

$_{30}Zn^{67}_{37}$. Figure 36 shows the level scheme of Zn^{67} up to one Mev. Gamma rays from above the 184-kev state have been omitted for clarity. The present results call for a revision of the spins from the accepted values[9] of $3/2^-$ for the 93-kev state and $5/2^-$ for the 184-kev state.

In the analysis $\alpha_T(184) = 0.014$, $\alpha_T(91) = 0.063$, and $\alpha_T(93) = 0.54$ were used. From the deviation of the 91-kev plus 93-kev yield from the 184-kev yield, as a function of energy, the small amount of direct excitation of the 93-kev state was calculated. The result agrees with the measured lifetime of the 93-kev state within 10 per cent if the de-excitation is pure E2 in character and if the spin of the state is $1/2^-$. Also, a cascade-to-crossover ratio for gamma rays, $R = 0.13 \pm 0.015$, was calculated as an intrinsic part of this analysis. This falls among other published values.

The large measured value, $A_2 = +0.227 \pm 0.007$, for the anisotropy coefficient of the 184-kev gamma rays, allowed a unique spin assignment of $3/2^-$ for the 184-kev state. The nearest other assignment would require an A_2 value which was lower than the measured one by about 15 times the assigned error. Of the two possible values of δ predicted from the measured value of A_2, only the smaller one (0.51 ± 0.04) is

UNCLASSIFIED
ORNL-LR-DWG 60121

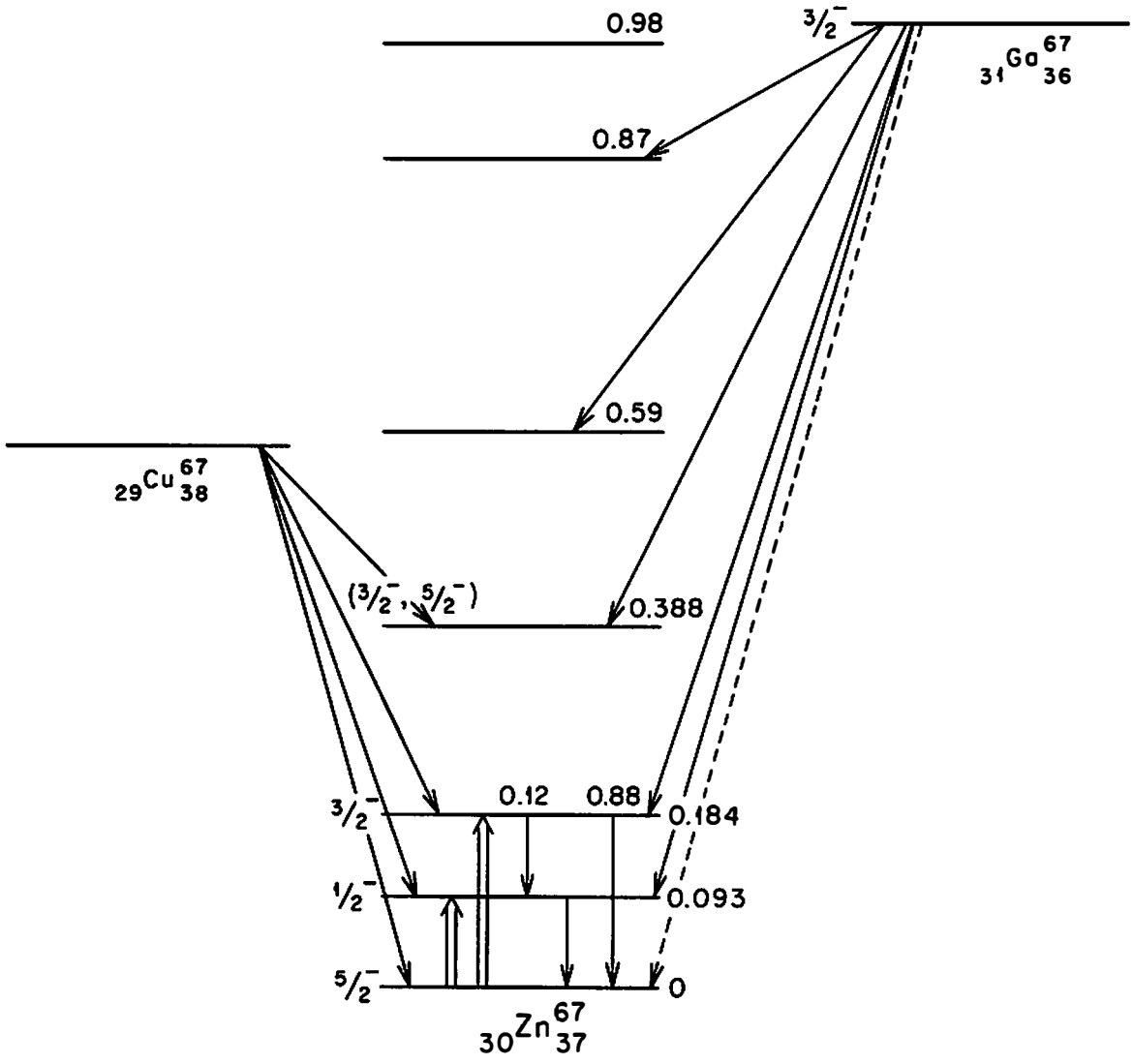

Fig. 36. Level Scheme for Zn^{67}.

consistent with the measured lifetime listed in Table XVI and a reasonable $\epsilon B(E2)$. The value of $\epsilon B(E2)$ predicted by δ and the lifetime is 0.032 ± 0.0074.

The 1.37×10^{-5} second measured lifetime of the 93-kev state is so long that the 93-kev gamma rays are probably isotropic. With this assumption the cascade-to-crossover ratio for the decay of the 184-kev state can be used to subtract them from the 91-kev plus 93-kev angular distribution. The result, $A_2 = 0.197 \pm 0.032$, would permit only $1/2^-$, $3/2^-$ or $5/2^-$ for the spin of the 93-kev state. The minimum value of δ for $3/2^-$ or $5/2^-$ would require a B(M1) inhibition of about 1/36,000, which seems unrealistic. There would also be poor agreement with the measured values of $\alpha_T(91)$ for either of these spins. If the state had positive parity, the measured lifetime of the 93-kev state would correspond to an E1 transition 10^4 times slower than is observed from the direct Coulomb excitation of the 93-kev state.

The spins listed in reference 9 for Zn^{67}, were all based[26] ultimately on the pure M1 character of the 184-kev gamma ray. This purity was assumed (incorrectly) from measured internal conversion coefficients. The present, more sensitive determination of δ would not permit the E2 component to be near zero.

This evidence, coupled with the above agreement of the lifetime with the estimated pure E2 transition, strongly favors a spin assignment of $1/2^-$ for the 93-kev state.

---

[26] L. H. Th. Rietjens and H. J. Van den Bold, Physica 21, 701 (1955).

From γ-γ angular correlations,[26] reinterpreted, it is possible to predict the spin of the 388-kev state as $3/2^-$ or $5/2^-$. The strong anisotropies for the (870-388-92) and (388-184-0) γ-γ angular correlations would not permit a spin assignment of $7/2^-$ or $1/2^-$ for the 388-kev state.

The ground state and first two excited states of Zn^{67} have a spin sequence which would be consistent with single-particle shell model assignments for $f_{5/2}$, $p_{1/2}$ and $p_{3/2}$, respectively. The inhibition of the B(M1) for the 184-kev transition could be understood on this basis as 1-forbiddenness. The 91-kev B(M1) inhibition could not be interpreted this way. The closeness of the level spacing would require a deviation from the pure single-particle shell theory.

A description of the intermediate coupling of a single neutron to a one phonon oscillating core could possibly predict both the observed spin sequence and the narrow spacing. Examples of such spectra have been calculated.[27]

The enhancement factor of 0.1 for the 93-kev E2 transition is one of the few cases known from Coulomb excitation measurements with such a small value. This, the weak B(E2) for the 91-kev transition, and the rather low values of $\beta_{r.m.s.}$ and q are all a bit surprising, in view of the 9 nucleons outside closed shells. (A possible closed shell at 40 nucleons[28] would explain this, however.)

---

[27] See, e.g., C. D. Choudhury, Dan. Mat. fys. Medd. 28, No. 4 (1954); and N. K. Glendenning, Phys. Rev. 119, 213 (1960).

[28] See, e.g., S. G. Nilsson, Dan. Mat. fys. Medd. 29, No. 16 (1955).

$_{32}Ge^{73}_{41}$. The 67.0-kev state was studied in Ge^{73}. From the angular distribution, a coefficient $A_2 = + 0.036 \pm 0.015$ was obtained, which does not give a sensitive determination of δ. Therefore the lifetime and B(E2) value were used. A theoretical value for the internal conversion coefficient ($\alpha_T = 0.229$) was also inferred from this calculation. No β decay to this state has been reported, presumably because of the different parity and spins of the ground states of the nuclei which decay to Ge^{73}.

The B(E2) enhancement of this transition is the largest of Table XV. Also $\beta_{r.m.s.}$ and q indicate the development of collective effects. Two protons and four neutrons have been added to Zn^{67}. It appears that one must attach more importance to the two protons that Ge^{73} has in excess of Zn^{67} than to the four added neutrons. There have been other examples[29] of the increased importance of added pairs of nucleons near single closed shells.

$_{33}As^{75}_{42}$. The 199-kev and 280-kev states in As^{75} were excited and their characteristics were studied. Values of $\alpha_T(199) = 0.02$ and $\alpha_T(280) = 0.008$ were used in the analysis. Also a 1.3 per cent cross-over[9] was included in the calculations.

For the 280-kev state, the measured A_2 value predicts a spin assignment of $5/2^-$. (The nearest alternative assignment would require an A_2 value six standard deviations lower.) This confirms the accepted

---

[29]See, e.g., B. L. Cohen and R. E. Price, Phys. Rev. 121, 1441 (1961).

value[9] which was based on the comparative gamma ray lifetime from a $9/2^+$ state above. Two possible values, - 0.52 or - 1.03, are predicted for δ from the present measurement of A_2. But A_2 is near the peak of the curve, and its assigned experimental errors would allow any value for δ from - 0.34 up to - 1.40. Two other measurements of δ are known. They are - 0.42 $\pm$ 0.05[30] and - 0.75.[31]

Therefore the present lower value, - 0.52, was used in the analysis. This value of δ would predict a mean lifetime of 3.0×10^{-10} seconds, in agreement with the measured value listed in Table XVI. Metzger and Todd predicted a value of 2.4×10^{-10} for the mean lifetime from their data, using the same method.

For the 199-kev state, the measured A_2 value, - 0.022 $\pm$ 0.017, was small, and could not be used to determine δ accurately. From the lifetime and the B(E2), a value of δ was calculated which is consistent with the measured value of A_2, and a spin of $1/2^-$, $3/2^-$, or $5/2^-$ for the 199-kev state. (The latter value would be less likely.) For the analysis, the listed[9] probable spin, $(1/2^-)$, was used.

---

[30] F. R. Metzger and W. B. Todd, Nucl. Phys. 10, 220 (1959).

[31] H. J. Van den Bold, J. Van de Geijn, and P. M. Endt, Physica 24, 23 (1958).

CHAPTER VI

SUMMARY AND CONCLUSIONS

The work for this thesis began with a study, on the ORNL 200-kev Cockcroft-Walton, of the possible use of the radio frequency ion source for multiply charged heavy ion production. When the results of this seemed unfavorable for the intended research, a PIG type ion source was designed and tested. It was capable of supplying usable quantities of Ne^{3+} ions, and was installed and used in the ORNL 5.5 Mv Van de Graaff accelerator.

Multiply-charged components from the PIG source were not as copious as those from several larger PIG sources that had been reported as having been used in entirely different environments. In attempting to increase these components in the present design, a number of difficulties were mapped out. Ac and pulsed operation were briefly studied, and it appears that additional work in this area would be of interest.

Anode extraction of the ion source was not attempted but this might provide increased multiple charge components. The difficulties of such extraction in a conventional Van de Graaff were pointed out. However, the usefulness of a much increased Ne^{3+} beam or a usable Ne^{4+} beam would be considerable, and might warrant a study of this.

The Ne^{2+} and Ne^{3+} beams in this work were used for Coulomb exciting low lying levels in eighteen nuclei from Li^{7} to Th^{232}. The $\epsilon B(E2)$ were extracted from these yields and compared with published

data. There were specific deviations, but generally there was agreement with the large body of Coulomb excitation data which has been obtained mostly with lighter ions.

Heavy ions are able to provide Coulomb excitation yields and angular distributions which are generally freer of complexities than those obtained with protons and helium ions. This is particularly the case for lighter nuclei. In the present research, the character of transitions from Coulomb excitation of eight odd-A nuclei from Ti^{47} to As^{75} were studied in detail.

The angular distribution measurements provided strong evidence for unique spin assignments for four of the levels which were excited. Two of these assignments (in Zn^{67}) conflict with accepted values, and two of them confirm accepted values. The E2 matrix elements were determined for 14 transitions in the eight nuclei, and M1 matrix elements were determined for 10 transitions.

Existing applications of the pairing correlation theory to V^{51} and Ni^{61} were considered further. The enhanced transitions suggest that a collective approach in the framework of this theory might be useful for these nuclei. Specific observations were made on the bearing of the present data on shell model and collective aspects of the low energy structure of some of the nuclei. It is concluded that additional Coulomb excitation with lighter ions or more energetic heavy ions would be particularly useful for these nuclei. This should provide an informative adjunct to the present results, which yield

relatively uncomplicated data about the lowest levels. Furthermore, some of the questionable aspects of the present data might be checked.

BIBLIOGRAPHY

BIBLIOGRAPHY

Abragam, A. and R. V. Pound, Phys. Rev. 92, 943 (1953).

Adams, B. M., D. Eccleshall, and M. J. L. Yates. Reactions Between Complex Nuclei, ed. A. Zucker. New York: John Wiley and Sons, Inc., 1960. p. 95.

Alburger, D. E. and M. A. Grace, Proc. Phys. Soc. 67A, 280 (1954).

Alder, K., A. Bohr, T. Huus, B. Mottelson, and A. Winther, Revs. Mod. Phys. 28, 432 (1956).

Alder, K. and A. Winther, Dan. Mat. fys. Medd. 29, No. 19 (1955).

Alder, K. and A. Winther, Dan. Mat. fys. Medd. 32, No. 8 (1960).

Alfven, H. Cosmical Electrodynamics. London: Oxford University Press, 1950. p. 49.

Alkhazov, D. G., D. S. Andreyev, A. P. Greenberg, and I. Kh. Lemberg, Nucl. Phys. 2, 65 (1956).

Alkhazov, D. G., A. P. Greenberg, G. M. Gusinskii, K. I. Erokhina, and I. Kh. Lemberg, Soviet Physics, JETP 37, 1086 (1960).

Anderson, C. E. Reactions Between Complex Nuclei, ed. A. Zucker. New York: John Wiley and Sons, Inc., 1960. p. 67.

Anderson, C. E. and K. W. Ehlers, Rev. Sci. Instr. 27, 809 (1956).

Backus, J. The Characteristics of Electrical Discharges in Magnetic Fields, ed. A. Guthrie and R. K. Wakerling. New York: McGraw-Hill Book Company, Inc., 1949. p. 345.

Bang, J., Dan. Mat. fys. Medd. 32, No. 5 (1960).

Bardeen, J., L. N. Cooper, and J. K. Schrieffer, Phys. Rev. 108, 1175 (1957).

Bell, P. R. Beta- and Gamma-Ray Spectroscopy, ed. K. Siegbahn. Amsterdam: North-Holland Publishing Company, 1955. p. 133.

Belyaev, S. T., Dan. Mat. fys. Medd. 31, No. 11 (1959).

Biedenharn, L. C. Nuclear Spectroscopy, B, ed. F. Ajzenberg-Selove. New York: Academic Press, 1960. p. 732.

Biedenharn, L. C., J. L. McHale, and R. M. Thaler, Phys. Rev. 100, 376 (1955).

Biedenharn, L. C. and M. E. Rose, Revs. Mod. Phys. 25, 729 (1953).

Biedenharn, L. C. and M. E. Rose, Oak Ridge National Laboratory Report ORNL 1789 (1954).

Blatt, J. M. and V. F. Weisskopf. Theoretical Nuclear Physics. New York: John Wiley and Sons, Inc., 1952.

Bleakney, W., Phys. Rev. 36, 1303 (1930).

Bogolyubov, N. N., JETP, USSR 34, 58 and 73 (1958).

Bogolyubov, N. N., Nuovo Cimento 7, 794 (1958).

Bohr, A., Dan. Mat. fys. Medd. 26, No. 14 (1952).

Bohr, A. Comptes Rendus du Congres International de Physique Nucleaire, ed. P. Gugenberger. Paris: Dunod, 1959. p. 203.

Bohr, A. and B. Mottelson, Dan. Mat. fys. Medd. 27, No. 16 (1953).

Bohr, A. and B. Mottelson, Dan. Mat. fys. Medd. 30, No. 1 (1955).

Bohr, A., B. Mottelson, and D. Pines, Phys. Rev. 110, 936 (1958).

Breit, G., M. E. Ebel, and J. E. Russell, Phys. Rev. 101, 1504 (1956).

Brink, D. M. Progress in Nuclear Physics, 8, ed. Frisch. New York: Pergammon Press, 1960. p. 97.

Bromley, D. A. Proceedings of the Rehovoth Conference on Nuclear Structure, ed. H. J. Lipkin. Amsterdam: North-Holland Publishing Company, 1958. p. 108.

Bromley, D. A., J. A. Kuehner, and E. Almqvist, Phys. Rev. 115, 586 (1959).

Brown, S. C. Basic Data of Plasma Physics. The Technology Press of The Massachusetts Institute of Technology, and New York: John Wiley and Sons, Inc., 1959.

Cheng, L. S. and M. L. Pool, Phys. Rev. 90, 886 (1953).

Choudhury, D. C., Dan. Mat. fys. Medd. 28, No. 4 (1954).

Cohen, B. L. and R. E. Price, Phys. Rev. 121, 1441 (1961).

Davydov, A. S. and G. F. Filippov, Nucl. Phys. 8, 237 (1958).

Dushman, S. Vacuum Technique. New York: John Wiley and Sons, Inc., 1955. p. 350.

Elbek, B. and C. K. Bockelman, Phys. Rev. 105, 657 (1957).

Elbek, B., G. Igo, F. S. Stephens, Jr., and R. M. Diamond. Reactions Between Complex Nuclei, ed. A. Zucker. New York: John Wiley and Sons, Inc., 1960. p. 102.

Elkind, M. M., Rev. Sci. Instr. 24, 129 (1953).

Elliot, J. P. and A. M. Lane. Encyclopedia of Physics, XXXIX, ed. S. Flugge. Berlin, Gottingen, Heidelberg: Springer-Verlag, 1957. p. 241.

Fagg, L. W., E. H. Geer, and E. A. Wolicki, Phys. Rev. 104, 1073 (1956).

Ferguson, A. T. G., M. A. Grace, and J. O. Newton, Nucl. Phys. 17, 9 (1960).

Glendenning, N. K., Phys. Rev. 119, 213 (1960).

Gluckstern, R. L., Phys. Rev. 98, 1817 (1955).

Gluckstern, R. L. and G. Breit. Reactions Between Complex Nuclei, ed. A. Zucker. New York: John Wiley and Sons, Inc., 1960. p. 77.

Gove, H. E. and C. Broude. Reactions Between Complex Nuclei, ed. A. Zucker. New York: John Wiley and Sons, Inc., 1960. p. 57.

Gow, J. D. and J. S. Foster, Jr., University of California Radiation Laboratory Report UCRL 1698 (1952).

Hall, H. D., Rev. Sci. Instr. 29, 367 (1958).

Hall, T. A., Phys. Rev. 79, 509 (1950).

Heckman, H. H., B. L. Perkins, W. G. Simon, F. M. Smith and W. H. Barkas, Phys. Rev. 117, 544 (1960).

Holland, R. E. and F. J. Lynch, Phys. Rev. 121, 1464 (1961).

Hubbard, E. L. and E. J. Lauer, Phys. Rev. 98, 1814 (1955).

Huus, T., J. H. Bjerregard, and B. Elbek, Dan. Mat. fys. Medd. 30, No. 17 (1956).

Huus, T. and C. Zupancic, Dan. Mat. fys. Medd. 28, No. 1 (1953).

Johnson, C. H., J. P. Judish, and C. W. Snyder, Rev. Sci. Instr. 28, 942 (1957).

Jones, P. R., F. P. Ziemba, H. A. Moses, and E. Everhart, Phys. Rev. 113, 182 (1959).

Jones, R. J. and A. Zucker, Rev. Sci. Instr. 25, 562 (1954).

Kamke, D. Encyclopedia of Physics, XXXIII, ed. S. Flugge. Berlin, Gottingen, Heidelberg: Springer-Verlag, 1956. p. 82.

Koch, B. and H. Neuert, Z. fur Naturf. 4a, 456 (1949).

Komoda, T. Proceedings of the International Conference on Nuclear Structure, Kingston, Canada, ed. D. A. Bromley and E. W. Vogt. Toronto: University of Toronto Press, 1960. p. 498.

Kisslinger, L. S. and R. A. Sorensen, Dan. Mat. fys. Medd. 32, No. 9 (1960).

Kistemaker, J., Nucl. Instr. and Meth. 11, 179 (1961).

Landau, L., Physik Z. Sowjetunion 1, 88 (1932).

Lawson, R. D. and M. H. MacFarlane, Bull. Am. Phys. Soc. II, 6, 77 (1960).

Lemberg, I. Kh. Reactions Between Complex Nuclei, ed. A. Zucker. New York: John Wiley and Sons, Inc., 1960. p. 112.

Lidofsky, L. J. and V. K. Fischer, Phys. Rev. 104, 759 (1956).

Little, P. F. Encyclopedia of Physics, XXI, ed. S. Flugge. Berlin, Gottingen, Heidelberg: Springer-Verlag, 1956. p. 638.

Lorrain, P., Can. J. Research, A25, 338 (1947).

Marion, J. B. Nuclear Data Tables, Part 3, National Academy of Sciences, National Research Council, Washington, D. C., 1960.

Massey, H. S. W. and E. H. S. Burhop. Electronic and Ionic Impact Phenomena. London: Oxford University Press, 1952. p. 38.

Maxwell, L. R., Rev. Sci. Instr. 2, 129 (1931).

Mayer, M. G. and J. H. Jensen. Elementary Theory of Nuclear Shell Structure. New York: John Wiley and Sons, Inc., 1955.

McClelland, C. L. and C. Goodman, Phys. Rev. 91, 760 (1953).

McGowan, F. K. and P. H. Stelson, Phys. Rev. 99, 127 (1955).

McGowan, F. K. and P. H. Stelson, Phys. Rev. 106, 522 (1957).

McGowan, F. K. and P. H. Stelson, Phys. Rev. 109, 901 (1958).

McGowan, F. K. and P. H. Stelson, Phys. Rev. 120, 1803 (1960).

McGowan, F. K. and P. H. Stelson, Phys. Rev. 122, 1274 (1961).

Metzger, F. R. and W. B. Todd, Nucl. Phys. 10, 220 (1959).

Migdal, A. B., JETP, USSR 37, 249 (1959).

Migdal, A. B., Nucl. Phys. 13, 655 (1959).

Moak, C. D., H. Reese and W. M. Good, Nucleonics 9, 18 (1951).

Mottelson, B. The Many Body Problem, ed. C. Dewitt. New York: John Wiley and Sons, Inc., 1959. p. 283.

Mottelson, B. Proceedings of the International Conference on Nuclear Structure, Kingston, Canada, ed. D. A. Bromley and E. W. Vogt. Toronto: University of Toronto Press, 1960. p. 525.

Mottelson, B. and S. G. Nilsson, Dan. Mat. fys. Skrifter, 1, No. 8 (1959).

Moszkowski, S. A., Phys. Rev. 89, 474 (1953).

Moszkowski, S. A. Beta- and Gamma-Ray Spectroscopy, ed. K. Siegbahn. Amsterdam: North-Holland Publishing Co., 1955. p. 373.

Moszkowski, S. A. Encyclopedia of Physics, XXXIX, ed. S. Flugge. Berlin, Gottingen, Heidelberg: Springer-Verlag, 1957. p. 411.

Mullin, C. J. and E. Guth, Phys. Rev. 82, 141 (1951).

Nilsson, S. G., Dan. Mat. fys. Medd., 29, No. 16 (1955).

Nuclear Data Sheets, National Academy of Sciences, National Research Council, Washington, D. C., 1960.

Ofer, S. and R. Wiener, Phys. Rev. 107, 1639 (1957).

Papineau, M. A., Comptes Rendus 242, 2933 (1956).

Penning, F. M., Physica 4, 71 (1937).

Penning, F. M. and J. H. A. Mobius, Physica 4, 1190 (1937).

Racah, G. Proceedings of the Rehovoth Conference on Nuclear Structure, ed. H. J. Lipkin. Amsterdam: North-Holland Publishing Company, 1958. p. 155.

Rietjens, L. H. Th., O. M. Bilaniuk, and M. H. MacFarlane, Phys. Rev. 120, 527 (1960).

Rietjens, L. H. Th. and H. J. Van den Bold, Physica 21, 701 (1955).

Rose, M. E., Phys. Rev. 91, 610 (1953).

Rose, M. E. Elementary Theory of Angular Momentum. New York: John Wiley and Sons, Inc., 1957.

Rose, M. E. Internal Conversion Coefficients. Amsterdam: North-Holland Publishing Company, 1958.

Rutherford, E. R., J. Chadwick, and C. D. Ellis. Radiations from Radioactive Substances. Cambridge: Cambridge University Press, 1930. p. 247.

Salz, F., R. G. Meyerand, Jr., E. C. Lary, and A. P. Walch, Phys. Rev. Letters 6, 523 (1961).

Scharff-Goldhaber, G., and J. Weneser, Phys. Rev. 98, 212 (1955).

Sliv, L. A. and I. M. Band, Physics Department, University of Illinois Report 57 ICC KI.

Stelson, P. H. Proceedings of the International Conference on Nuclear Structure, Kingston, Canada, ed. D. A. Bromley and E. W. Vogt. Toronto: University of Toronto Press, 1960. p. 787.

Stelson, P. H. and F. K. McGowan, Phys. Rev. 99, 112 (1955).

Stelson, P. H. and F. K. McGowan, Phys. Rev. 110, 489 (1958).

Stelson, P. H. and F. K. McGowan. Reactions Between Complex Nuclei, ed. A. Zucker. New York: John Wiley and Sons, Inc., 1960. p. 47.

Stelson, P. H. and F. K. McGowan, Nucl. Phys. 16, 92 (1960).

Stelson, P. H. and F. K. McGowan, Phys. Rev. 121, 209 (1961).

Stier, P. M., C. F. Barnett, and G. E. Evans, Phys. Rev. 96, 973 (1954).

Stromberg, H. D., University of California Radiation Laboratory Report UCRL 5119 (1959).

Temmer, G. M. and N. P. Heydenberg, Phys. Rev. 96, 426 (1954).

Temmer, G. M. and N. P. Heydenberg, Phys. Rev. 104, 967 (1956).

Ter-Martirosyan, JETP, USSR 22, 284 (1952).

Valatin, J. G., Nuovo Cimento 7, 843 (1958).

Van den Bold, H. J., J. Van de Geijn, and P. M. Endt, Physica 24, 23 (1958).

Vervier, J. F. and G. A. Bartholomew. Proceedings of the International Conference on Nuclear Structure, Kingston, Canada, ed. D. A. Bromley and E. W. Vogt. Toronto: University of Toronto Press, 1960. p. 650.

Weisskopf, V. F., Phys. Rev. 53, 1018 (1938).

Weisskopf, V. F., Phys. Rev. 83, 1073 (1951).

West, H. I., Jr., University of California Radiation Laboratory Report UCRL 5451 (1959).

Whaling, W. Encyclopedia of Physics, XXXIV, ed. S. Flugge. Berlin, Gottingen, Heidelberg: Springer-Verlag, 1956. p. 194.

Wilets, L. and M. Jean, Phys. Rev. 102, 788 (1956).

Wilkinson, D. H. Nuclear Spectroscopy, B, ed. F. Ajzenberg-Selove. New York: Academic Press, 1960. p. 861.

Worthing, A. G. and J. Geffner. Treatment of Experimental Data. New York: John Wiley and Sons, Inc., 1943.

APPENDICES

APPENDIX A

THE STOPPING POWER FOR HEAVY IONS

To obtain the calculated thick target yield from Coulomb excitation, which is used in extracting the $\epsilon B(E2)$, the stopping power for projectiles in the target must be considered. (See Appendix C.) For protons and helium ions there is experimental data on the stopping power of many target materials.[1] But for heavy ions there is little published information of this type.

For the present work a method of conversion of the light ion data, attributed to Papineau,[2] was used for determining the stopping power of the target materials for neon and nitrogen ions. In this method, a universal curve of the effective ionization (as a fraction of the total nuclear charge) versus a characteristic velocity ($v/Z^{2/3}$) is assumed to hold. Such a curve is shown in Figure 37. The curve was empirically determined. (Often, as an approximation, the effective charge of ions passing through thin targets at given velocities is taken to be the r.m.s. value of the measured components.) Data from Heckman et al[3] was chosen to represent the characteristics of heavy ions in this research.

---

[1] See, e.g. the review by W. Whaling, Encyclopedia of Physics, XXXIV, (Springer-Verlag, Berlin, Gottingen, Heidelberg, 1956), p. 194.

[2] M. A. Papineau, Comptes Rendus 242, 2933 (1956).

[3] H. H. Heckman, B. L. Perkins, W. G. Simon, F. M. Smith, and W. H. Barkas, Phys. Rev. 117, 544 (1960).

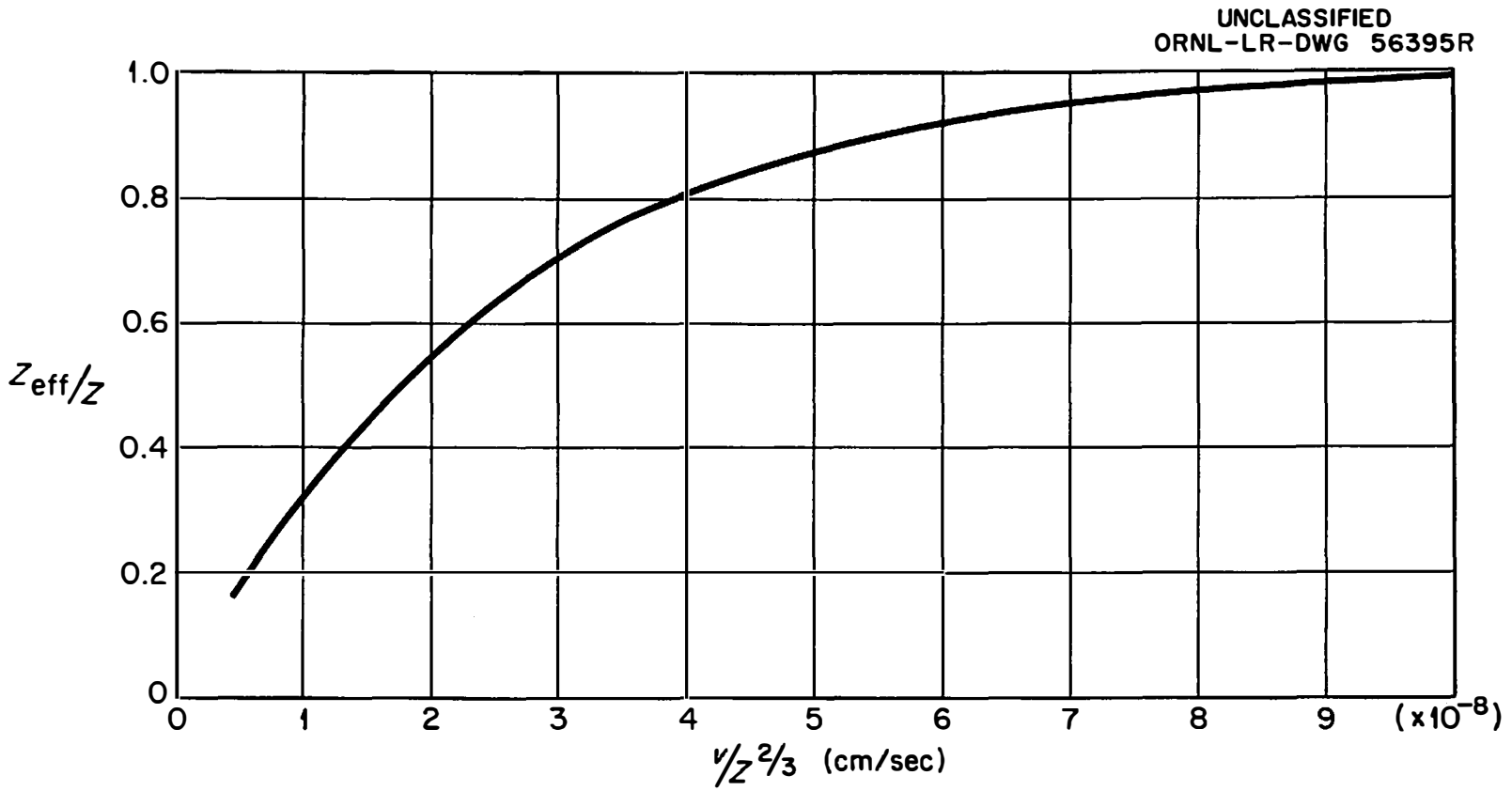

Fig. 37. Effective Charge of Ions as a Function of Their Characteristic Velocity.

In the use of the curve by the method of Papineau, the stopping powers of a given target material for two different ions H and P have the relation

$$\left(\frac{dE}{d\rho x}\right)_H Z_{eff_P}^2 = \left(\frac{dE}{d\rho x}\right)_P Z_{eff_H}^2 \quad . \tag{47}$$

The two effective charges must be obtained at the same (actual) velocities. Thus the relative energies to be used are in proportion to the masses. (For example, a 1 Mev proton is equivalent to a 20 Mev neon ion.)

The effective charge for protons is not always unity. A curve similar to Figure 37 was plotted from data for the stopping of protons in metals.[4] A different curve for protons is necessary because of a lack of complete universality of such curves, particularly with such light ions.

It is hard to estimate the accuracy of the method. With available heavy ion data[5] it was possible to make a limited test of the accuracy of this method. (This was, in fact, the basis for the particular choice of data for Figure 37.) When the errors in the data were extracted as well as was possible by statistical means, the remaining error was roughly ten per cent. This is assigned as the probable error in the values used for $\frac{dE}{d\rho x}$ in this work.

---

[4] T. A. Hall, Phys. Rev. 79, 509 (1950).

[5] Most of the data used were from reference 1 and 3.

APPENDIX B

ESTIMATION OF EXPERIMENTAL ERRORS

All of the quoted errors of a statistical nature in this thesis are intended to correspond to one standard deviation. Where combinations of errors were involved, the elementary algebra of propagation of variance was used.[1]

Unfortunately, in much of the work with accelerators, it is not possible to give a completely statistical estimate of the errors.

In the present work, the experimental errors of primary interest were those associated with the $\epsilon B(E2)$ and the angular distributions.

The errors in the $\epsilon B(E2)$ can be estimated[2] from equation (29). Only the errors in I' and the integral are significant. The experimental yield, I', had a standard error of about seven per cent except in the cases where the counting rate was especially poor. The factors involved in this estimate are given in equation (48) of Appendix C. Broken down, their standard errors are as follows:

N (counts in the peak)	3%
ϵ (efficiency, including geometrical error)	4%
R_γ (peak-to-totals ratio)	3%
A_γ (attenuation)	3%

---

[1] A. G. Worthing and J. Geffner, Treatment of Experimental Data, (John Wiley and Sons, Inc., New York, 1943).

[2] For a more complete discussion, see P. H. Stelson and F. K. McGowan, Phys. Rev. 110, 489 (1958).

η (number of incident particles)	1%
K_γ (iodine escape)	Negligible

The error in the integral is governed mainly by the uncertainty in $\frac{dE}{d\rho x}$. The estimated accuracy in the integral is 10 to 15 per cent. Thus, the estimated error in $\epsilon B(E2)$ is about 15 per cent. Special cases where a larger error seems likely were mentioned individually in the text.

For the angular distribution, the situation was less decisive. The significant routine sources of error in the ratio R are thought to be the following:

Decentering Error	1%
Background Error	0-3%
Statistical Counting Error	0-3%

The usual procedure was to evaluate each of the latter two of these types of errors for individual cases. Then the three results were combined in the usual statistical way and propagated in the equation for A_2. The effect of errors[3] in a_2 was small compared to the above errors. In several cases where the measurements of R were repeated enough times, a mean value was taken and a standard error calculated from the deviations, as a check on the first method. In the event of conflict, the latter result was used.

In the evaluation of errors for derived quantities, such as $\epsilon B(E2)$ and sometimes δ^2, it was often necessary to use quoted errors

---

[3]See F. K. McGowan and P. H. Stelson, Phys. Rev. 106, 522 (1957).

from other sources. Lacking these in some cases, the estimate of error was omitted. Due to the rather basic uncertainties in the single-particle estimates for B(M1) and B(E2), no error is quoted for the inhibition and enhancement factors F' and F. The listed values for these two quantities are rounded off to integral numbers or smooth fractions in the tables.

The standard errors for $B(E2)_{exc.}$ are thought to be generally only slightly larger than 15 per cent. This is because the standard error in $\epsilon B(E2)$ is about 15 per cent and the errors in ϵ are usually less than 5 per cent.

APPENDIX C

THE YIELD DETERMINATION AND THE THICK TARGET FORMULA

In determining the $\epsilon B(E2)$, the experimental quantity needed is the number of excitations per incident particle, I, of the nuclear state of interest. This is related to the observed gamma ray yield by $I' = \epsilon I$.

The determination of I' from scintillation pulse-height spectra was carried out in a standard way.[1] The relation used was

$$I' = \frac{1}{\eta}\left(\frac{N}{\epsilon R_\gamma A_\gamma K_\gamma} \right), \tag{48}$$

where η is the integrated number of projectiles in the beam during the taking of the spectrum, and the bracketed quantity is the number of gamma rays of the energy of interest emitted during this time. N is the number of counts in the Gaussian peak of the spectrum (the full-energy peak). $\epsilon R_\gamma A_\gamma K_\gamma$ converts these counts to the total number of gamma rays (of the proper energy) emitted by the target during the taking of the spectrum. ϵ is the total crystal efficiency.[2] It is a product of the fractional solid angle subtended by the crystal and the fractional absorption of the gamma rays of the desired energy which do

---

[1] For a more complete discussion, see P. H. Stelson and F. K. McGowan, Phys. Rev. 110, 489 (1958).

[2] See, e.g., J. B. Marion, Nuclear Data Tables, Part 3, (National Academy of Sciences, National Research Council, Washington, D. C., 1960).

strike the crystal. R_γ is defined as the ratio of the area in the full-energy peak to the total area in the spectrum. A_γ is an attenuation factor, and K_γ corrects for gamma rays which fail to fall in the full-energy peak because of iodine escape X-rays. It is nearly unity for gamma ray energies above 150 kev.

The derivation of the particular equation, (29), used in calculating $\epsilon B(E2)$ for this work is as follows. For a thick target

$$I = \int_{x=0}^{x \text{ at } E=0} I(x)dx = \int_{0}^{E_{incident}} \frac{I(E_x)}{dE_x/dx}\, dE_x \quad , \tag{49}$$

where x is the distance into the target that that projectile has travelled. E_x is the projectile energy at this point.

The number of excitations per incident particle, per unit energy loss, at the energy E_x is

$$I(E_x) = \sigma(E_x)\, \rho_n \tag{50}$$

where $\sigma(E_x)$ is the cross section, equation (28), and ρ_n is the density of target nuclei

$$\rho_n = \frac{\rho L n \eta}{A_2'} \left(\frac{\text{target nuclei}}{\text{cm}^3} \right) . \tag{51}$$

Here ρ is the target molecular density in gm/cm^3, L is Avagadros' number (6.03×10^{23} molecules per mole), A_2' is the molecular weight of the target, n is the number of target nuclei per molecule, and η is the isotopic fraction in the target.

For this work, the stopping power was used in the form $\frac{1}{\rho}\frac{dE_x}{dx} = \frac{dE_x}{d\rho x}$. With this, (50) and (51), equation (49) becomes

(dropping the subscript x)

$$I = \frac{Ln\eta}{A_2'} \int_0^E \frac{\sigma(E)dE}{dE/d\rho x} \quad . \tag{52}$$

Into this (28) is inserted. However, $g_{E2}(\xi) = 1.2665\ f_{E2}(\xi)$ was used in this work, as it has been tabulated for computation. Also the units of (28), barns, are converted to cm^2 and both sides of (52) are multiplied by ϵ. The resulting equation is solved for $\epsilon B(E2)$:

$$\epsilon B(E2) = \frac{436.9\ A_2'\ Z_2^2}{A_1 n\eta K^2} \quad \frac{\epsilon I}{\int_0^E \frac{E'g(\xi)dE}{dE/d\rho x}} \quad . \tag{29}$$